Instabilities in the Buoyant Convective Flows Subject to High Magnetic Fields

Hudoba, Agnieszka

Award date:
2015

Awarding institution:
Coventry University

.

Instabilities in the Buoyant Convective Flows Subject to High Magnetic Fields

AGNIESZKA HUDOBA

Ph. D.

April 2015

Instabilities in the Buoyant Convective Flows Subject to High Magnetic Fields

AGNIESZKA HUDOBA

A Thesis submitted in partial fulfilment
of the University's requirements for the degree of
Doctor of Philosophy

April 2015

To Christophe

Acknowledgements

I would like to express my deepest appreciation and special thanks to my supervisor, Sergei Molokov, for his patience, help and advise through the completion of this thesis.

Abstract

The present study is devoted to the problem of the onset of instability in time dependent convective flows of an electrically conducting fluid, subject to an externally applied magnetic field and to gravity forces. Linear stability theory is applied to investigate convective flows confined by two rigid walls and opposed by the magnetic field. These magnetohydrodynamic channel flows are studied for non-zero magnetic Prandtl numbers as well as in the inductionless approximation. The following configurations are considered: the Rayleigh-Bénard problem, the horizontal layer with longitudinal temperature gradient and the vertical channel with internal heating sources. The numerical results are obtained giving characteristic laws by critical values of parameters, beyond which the flows become unstable. The comparison is made between these problems for small, but non-zero Pr_m, with the inductionless approximation, in order to determine the validity of that approximation. The analysis of perturbations shows that the instabilities critically depend on the electrical and thermal boundary conditions and on the Prandtl (Pr), magnetic Prandtl (Pr_m), and Hartmann (Ha) numbers. The instabilities are driven by different mechanisms and set in either as two- or three-dimensional modes, stationary or oscillatory, depending on these parameters and on the orientation of magnetic field and gravity. New instability structures are observed in the horizontal layer heated for the side for small ranges of Pr_m. The MATLAB code created for the purpose of this thesis allows the study of convective flows in the presence of high magnetic fields up to $Ha = 10^5$ and the asymptotic relations are successfully reached for the critical values of parameters in most cases.

Contents

Chapter 1

Introduction

Magnetohydrodynamics (MHD) studies the interaction of the flow of an electrically conducting fluid with the magnetic field. This occurs owing to the Lorentz force $\mathbf{j} \times \mathbf{B}$, where $\mathbf{j}$ is the electric current density, and $\mathbf{B}$ is the magnetic field. The magnetic field may be either induced by the flow itself (the so-called dynamo problem), externally applied, which is more relevant to the industrial applications, or a combination of the two. Similarly, the electric current may be externally applied, induced by the flow, or both.

The driving force of the flow may be similar to ordinary hydrodynamics of non-conducting fluids, such as pressure gradient, motion of solid boundaries, gravity, buoyant convection, etc., or by the electromagnetic means, such as varying magnetic field with time (alternating, rotating, or traveling magnetic field). Typical electrically conducting media include liquid metals, plasmas, electrolytes, molten semiconductors, etc.

The focus here is on the flows driven by buoyant convection of liquid metals or molten semiconductors in the presence of a transverse magnetic field, which occurs in several industrial applications. Here the focus is on two such applications as described below. Instabilities, transition, and turbulence in such flows is of fundamental importance as they are known to strongly affect the quality of the materials produced or heat transfer characteristics of the devices in general. The successful understanding of these phenomena may be decisive on whether a particular device or facility is scientifically and commercially viable or not.

1.1 Applications

1.1.1 Semiconductor crystal growth

Solidification from the melt is the most common method of manufacturing crystals. Intensive theoretical, experimental and numerical studies have been carried over the years aimed at improving the crystal quality [1], [2], [3]. As the semiconductor crystal growth process needs careful control, a number of sophisticated techniques has been introduced [4], [5], [6].

The so-called Czochralski method (Fig. 1.1) is used to grow crystals from Gallium, Silicon, Arsenide and other semiconductors. The process takes place in a heated circular crucible, where the temperature is carefully adjusted for the centre of the liquid to be at its freezing point. A seed crystal, positioned axially above the crucible, is dipped into the melt. The pull rod is then slowly lifted as the solidification process continues. This method, simple in its concept and with relatively easily adjustable conditions, allows the growth of large dimension crystals. The main disadvantage here is a complex pulling mechanism, often involving rotation, as well as possible asymmetry and uneven dopand distribution, which is easily affected by flow instabilities and temperature gradients.

The Bridgman method [7] is used widely to grow crystals from semiconductors and metals, often for crystals grown from volatile materials and volatile dopants. Here the crucible containing melt is placed inside a gradient furnace. The growth is induced by moving the crucible through the furnace or by modifying the furnace temperature (gradient-freeze technique). With respect to gravity, the system can be either in a vertical or a horizontal configuration (Fig. 1.2). This method, with easily adjustable thermal gradient, allows good control of the experimental conditions.

The unsteady convection causes temperature fluctuations, which may lead to an oscillatory crystal growth and unwanted compositional inhomogenities. Several books on the subject [5], [6] give a detailed description of this processes. In order to avoid the nonuniform dopant distribution affecting the crystal quality, magnetic fields have been used extensively to suppress unwanted oscillations [8]. In the case of electrically conducting flows, an interaction between the field and

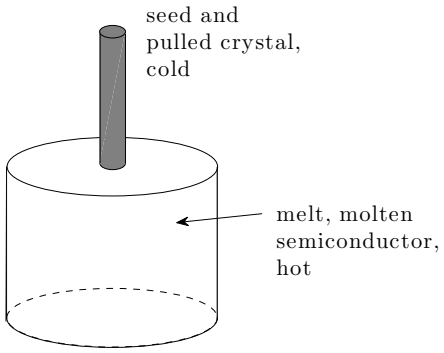

Figure 1.1: Schematic diagram of Czochralski semiconductor crystal growth

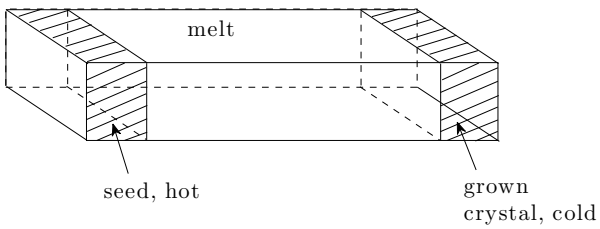

Figure 1.2: Schematic diagram of the horizontal Bridgman crystal growth

the induced electric currents affects the flow significantly, damping velocity and stabilizing temperature oscillations. Thus many attempts have been made to establish the most effective magnetic field orientation for damping convection.

Series and Hurle [9] reviewed the use of magnetic field in semiconductor crystal growth focussing on the Czochralski method. Several authors studied the horizontal Bridgman growth under different intensities of an axial magnetic field, both experimentally and numerically. Among them Bojarevics [10], Alboussiere et al. [11], Ben Hadid et al. [12], [13], Kadddeche et al. [14], Aleksandrova [15] and Molokov [16], etc.

1.1.2 Fusion reactor blankets

One of the most important magneto-fluid dynamics applications is liquid metal blankets for thermonuclear fusion reactors (Fig. 1.3). At temperatures above $10^8 K$ required for fusion reactors, the ionized fuel must be confined by strong magnetic fields. The magnetic fields considered here are the highest among all the engineering applications. The plasma-facing wall (the first wall) is designed to receive a high heat flux from the plasma, which has to be removed, as wall temperature must not exceed critical values.

A fusion blanket, situated between magnetic coils and plasma, shields the coils from high neutron radiation, absorbs the heat flux in the form of internal heating, and acts as a tritium breeder necessary for plasma production. Liquid metals, which can be operated at high temperatures, are widely used in blanket designs. Several concepts have been proposed [4] and tested. In a separately cooled blanket, liquid metal serves only as a breeder, while heat is removed by water or helium gas. In self-cooled blankets, liquid metal serves both as a coolant and a breeder. As all the heat released is removed here by liquid metal flow, high velocities must be considered. In the third concept of a fusion blanket, combining the ideas of self-cooled and separately-cooled blankets, the first wall is cooled by helium, while the breeding zone in cooled by the liquid metal flow.

A review of modeling requirements, existing experimental facilities and testing programs for fusion blankets magnetohydrodynamics has been presented by Buhler et al. [17]. The challenges of tritium breeding control have been addressed by Morgan and Pasley [18]. The problems of heat transfer in fusion blankets have been discussed by Barleon et al. [19].

1.2 Literature review

The early research of MHD convection due to nonuniform heating has been given by Chandrasekhar in his well-known monograph [20]; see also [21] for subsequent work. Most of this work has been devoted to a somewhat artificial model problem for free, perfectly electrically conducting boundaries, which is of little importance for industrial applications. The main conclusion was that the instability occurs

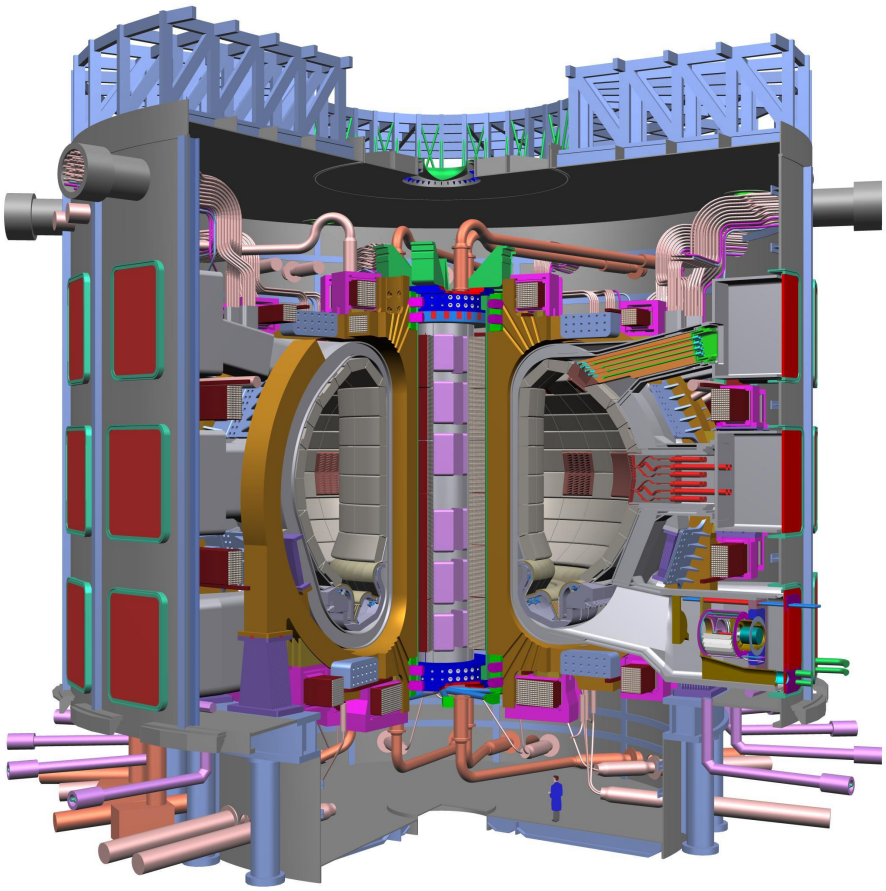

Figure 1.3: Schematic diagram of a thermonuclear reactor ITER; the size of the reactor can be appreciated by comparing with the height of human being shown at the bottom of the picture

in the form of stationary cells when the Prandtl number is less than its magnetic counterpart. The problem for solid, electrically insulating boundaries has been discussed in detail by Takashima [22] for various values of the Hartmann and conventional, Pr, and magnetic Prandtl numbers, Pr_m. In particular, he has shown that for sufficiently high Prandtl number, new, magnetic branches of oscillatory instability exist, and persist up to the values of $Ha < 10^3$ even for $Pr_m < Pr$.

The problem of stability of natural convection in a cavity with horizontal temperature gradient, without magnetic field, also received considerable attention and has been widely discussed by many authors. The main difference here with the Rayleigh-Bénard problem is that the equilibrium consists of a horizontal basic flow in the direction of temperature gradient. This flow is driven by pressure gradient induced by the necessity to balance the vertical buoyancy force by pressure. Hart [23] studied the stability problem in the astrophysical context by means of linear theory. He first identified a possibility of stationary transverse and oscillatory longitudinal disturbances, depending on the fluid properties. Gill [24] investigated theoretically the onset of longitudinal disturbances in liquid metals and semiconductors, while Hurle et al. [25], in a companion experimental research, observed the oscillatory instabilities in molten gallium. Later numerical work by Kuo and Korpela [26] showed that two-dimensional modes are usually less stable. They obtained critical values of parameters for longitudinal and transverse modes, supporting the linear theory calculations.

Laure and Roux [27] considered cavities with both rigid horizontal surfaces, as well as with an upper stress-free surface but without the magnetic field. The linear stability analysis results for different thermal boundary conditions showed the competition between disturbances for certain ranges of parameters.

The in-depth study of convection in the horizontal Bridgman configuration with a constant magnetic field was presented by Bojarevics [10], Alboussiere et al. [11], Ben Hadid et al. in [12], [13], and Aleksandrova and Molokov [16]. The instabilities in such flows have been studied first in a horizontal fluid layer by Ben Hadid et al. [12]. The authors performed numerical simulations for a cavity of finite dimensions with and without free surface. Both analytical and numerical results show strong dependence on boundary conditions and establish how magnetic field stabilizes the flow and changes its instabilities.

Then, the three-dimensional investigation for a parallelpiped cavity with constant horizontal temperature gradient was carried out [13]. Here the numerical solutions of a flow with distinguished core, Hartmann layers and sidewall regions have been obtained for three horizontal Bridgman cases: confined cavity, cavity with a stress-free boundary and a thermocapillary-driven flow with surface tension effects. The results show the effects of magnetic field, applied vertically and in the longitudinal direction, on the flow. Particularly, for the magnetic field strength exceeding a certain value, scaling for the Grashof number has been identified. Most of the investigations mentioned above, however, have been done for low-to-moderate values of the Hartmann number.

For high values of the Hartmann number, in general, very few investigations have been performed. For a parallellepiped cavity the only asymptotic analysis has been preformed by Aleksandrova and Molokov [16], who determined that for a vertical magnetic field there is a separate flow loop formed by high-velocity jets involving all the walls parallel to the magnetic field, and including face surfaces of both the seed and the crystal. These jets have first been observed in a duct flow relevant to the horizontal Bridgman crystal growth by Bojarevics [10].

To conclude the review, one may note that practically no results exist for the instability in high magnetic fields, especially when the magnetic Prandtl number is small but not equal to zero. This thesis may be considered as one of the first steps in this direction.

1.3 The aim and the structure of the thesis

Although the problem of MHD convection in various configurations has been studied in some detail by many authors, there are fundamental questions remaining, especially when high externally applied magnetic fields are concerned. The magnets available in industry become stronger every year, and the question remains whether the the so-called quasi-static approximation (almost exclusively used in modeling the MHD flows) remains to be valid when the magnetic field becomes very high. The aim of this thesis is to fill this gap and to understand how the buoyant flow behaves when the Hartmann number, Ha, which characterizes the intensity of the field, increases from zero to very high values. Therefore, the

problems considered here from the fundamental point of view involve an infinite fluid layer, being either horizontal or vertical, and the applied magnetic field is always transverse to the solid boundaries. This allows very accurate analysis of instabilities by pseudospectral methods, such as Chebyshev collocation.

In Chapter 2 the governing magnetohydrodynamic equations and the boundary conditions have been derived. The equations have been presented in the full formulation for non-zero magnetic Prandtl number, Pr_m. Then the inductionless (also called quasi-static) approximation of these equations has been derived.

The numerical method and its verification on known solutions has been given in Chapter 3.

Chapter 4 is devoted to the classical Rayleigh-Bénard problem in the presence of a transverse magnetic field for zero and for small but non-zero vales of the magnetic Prandtl number. The main aim here is to extend the range of the Hartmann numbers up to 10^5, which has never been done before, and to compare the results with the known asymptotic expressions for critical Grashof and wavenumbers.

Chapter 5 is concerned with the instabilities in convection in the horizontal layer owing to axial temperature gradient, which in the past has been considered only for small Hartmann number. Four combinations of possible electrical and thermal boundary conditions have been discussed.

Chapter 6 is devoted to a problem of instabilities in a vertical fluid layer owing to internal heat sources, which is of great importance to poloidal concepts of fusion reactor blankets.

Finally conclusions are drawn and the scope for future work is outlined.

Chapter 2

Governing equations

Consider a time-dependent, convective flow of a viscous, electrically conducting fluid in the presence of gravity $\mathbf{g}$. The flow occurs in the presence of a uniform externally applied magnetic field $\mathbf{B}_0$, material parameters of the fluid are defined by the density ρ, kinematic viscosity ν, thermal diffusivity κ, thermal expansion coefficient β and electric conductivity σ.

The behaviour of the flow is governed by the set of magnetohydrodynamic equations combining Navier-Stokes equations of motion of fluid substances, Maxwell electrodynamics equations and the energy equation. Detailed derivation of these equations has been presented in [28], [29], [30], [31].

2.1 Fluid dynamics

The general fluid dynamics equations are, from the continuum mechanics, the mass conservation and the momentum conservation equations. The change of mass in an arbitrary control volume is described by the continuity (mass conservation) equation, where at each point of fluid [30]:

$$\partial_t \rho + \nabla \cdot (\rho \mathbf{v}) = 0 \ , \tag{2.1}$$

where $\mathbf{v}$ denotes the fluid velocity and t is time. For incompressible fluids, such as liquid metals, the equation reduces to [31]:

$$\nabla \cdot \mathbf{v} = 0 \ , \tag{2.2}$$

as in such cases all changes of thermodynamic state variables through pressure variations are negligible and the velocity field becomes a solenoidal vector field.

The momentum conservation equation can be introduced as an application of Newton's second law to an arbitrary control volume [31] and in its general form may be written as:

$$\partial_t(\rho\mathbf{v}) + \mathbf{v}\nabla \cdot (\rho\mathbf{v}) + \rho(\mathbf{v} \cdot \nabla)\mathbf{v} = \nabla \cdot \pi + \mathbf{f} \ , \tag{2.3}$$

where π is the stress tensor and $\mathbf{f}$ represents the density of body forces applied to the fluid. The divergence of π for moving fluids reads [31], [32], [33]:

$$\nabla \cdot \pi = -\nabla p + \rho\nu\nabla^2\mathbf{v} + \frac{1}{3}\nabla(\nabla \cdot \mathbf{v}) \ , \tag{2.4}$$

where p denotes pressure and the last two terms correspond to the viscosity effects. The density of body forces $\mathbf{f}$ can be further decomposed into [31]:

$$\mathbf{f} = \rho\mathbf{f}_m + \mathbf{f}_V \ , \tag{2.5}$$

where $\mathbf{f}_m$ represents body forces per unit mass (later, gravity) and $\mathbf{f}_V$ represents body forces per unit volume (later, Lorentz force).

The fluid is called Newtonian when the stress tensor depends linearly on the velocity gradients [29]. For a Newtonian viscous fluid, the conservation of mass and momentum lead to the Navier-Stokes equation [28], [31], which for the case of $\nabla \cdot \mathbf{v} = 0$ can be presented in the form:

$$\rho\partial_t\mathbf{v} + \rho(\mathbf{v} \cdot \nabla)\mathbf{v} = -\nabla p + \rho\nu\nabla^2\mathbf{v} + \mathbf{j} \times \mathbf{B} + \rho\mathbf{g} \ . \tag{2.6}$$

The linear momentum evolution (composed of time dependent acceleration and the so-called convective acceleration of fluid with respect to space) is given here as

a balance between pressure forces, viscous friction, Lorentz forces and buoyancy force, respectively. The Lorentz force $\mathbf{j} \times \mathbf{B}$ is a consequence of an interaction between the induced electric current density $\mathbf{j}$ and the total magnetic field $\mathbf{B}$. The last term in Equation (2.6) is the gravity term.

2.1.1 Incompressible fluids and Boussinesq approximation

For liquid metals it is justified to assume incompressibility of fluid, i.e the density ρ is considered independent of the pressure p. The conservative description of the velocity field (2.2) is valid for small density variations, as these differences can be neglected except where they appear in terms multiplied by gravity, according to the Boussinesq approximation [30], [33], [34], [35]. The fluid density in the last term of (2.6) is assumed to be a linear function of temperature T, i.e.

$$\rho = \rho_0\{1 - \beta(T - T_0)\} \ , \tag{2.7}$$

where T_0 is a reference temperature and ρ_0 is the density of the fluid at T_0. The gravity is strong enough to make the specific weight of fluid particles different at different temperatures. Density differences due to gravity forces cause the buoyancy-induced convection [28], [30]. Then equation (2.6) takes the form:

$$\rho_0 \partial_t \mathbf{v} + \rho_0(\mathbf{v} \cdot \nabla)\mathbf{v} = -\nabla p + \rho_0 \nu \nabla^2 \mathbf{v} + \mathbf{j} \times \mathbf{B} + \rho_0\{1 - \beta(T - T_0)\}\mathbf{g} \ . \tag{2.8}$$

2.1.2 Temperature

The fluid flow timescales are very long compared to characteristic times of molecular interactions ($10^{10} - 10^{15}$ times) and the assumption of local thermodynamic equilibrium can be applied [29], [30]. That is, the following state variables can be assigned to each point of a continuum system: kinetic pressure p, density ρ_0, temperature T, and entropy per unit mass s.

The energy equation (the so-called convection-diffusion equation) is a direct consequence of the thermodynamic equation of heat conduction for moving fluids [29]:

$$\rho_0 T\{\partial_t s + \mathbf{v} \cdot \nabla s\} = -\nabla \cdot \mathbf{h} + \epsilon \ , \tag{2.9}$$

where $\mathbf{h}$ stands for the heat conduction vector defined as $\mathbf{h} = -\lambda_T \nabla T$ with λ_T being thermal conductivity. An additional term ϵ denotes possible volumetric internal heat sources such as chemical reactions, radioactivity, and also viscous and Ohmic dissipation.

The temperature equation can be derived assuming that the fluid is incompressible:

$$\frac{D\rho_0}{Dt} = 0 \ , \tag{2.10}$$

and applying standard thermodynamic relations between the entropy, density, temperature and pressure [29], [35], [36]:

$$\frac{Ds}{Dt} = \frac{c_p}{T}\frac{DT}{Dt} - \frac{\beta}{\rho_0}\frac{Dp}{Dt} \ , \tag{2.11}$$

$$\frac{D\rho_0}{Dt} = \frac{1}{a^2}\frac{Dp}{Dt} \ , \tag{2.12}$$

where c_p is the specific heat at constant pressure, a stands for the adiabatic speed of sound and for simplicity the material derivative $\frac{D}{Dt} = \partial_t + \mathbf{v} \cdot \nabla$ has been introduced. Then the temperature equation can be written as:

$$\rho_0 c_p \partial_t T + \rho_0 c_p (\mathbf{v} \cdot \nabla) T = \lambda_T \nabla^2 T \ + \epsilon \ , \tag{2.13}$$

where the ratio $\lambda_T / \rho_0 c_p$ defines the thermal diffusivity κ. The temperature equation describes the balance of the total energy in a volume element.

2.2 Electrodynamics

The fundamental equations governing electromagnetism are Maxwell equations, namely Maxwell-Coulomb equation, Gauss' divergence theorem, Faraday's and Ampere's laws [29], [30], [37], written as:

$$\nabla \cdot \mathbf{D} = q \ , \tag{2.14}$$

$$\nabla \cdot \mathbf{B} = 0 \ , \tag{2.15}$$

$$\nabla \times \mathbf{E} + \partial_t \mathbf{B} = 0 \ , \tag{2.16}$$

$$\nabla \times \mathbf{H} - \partial_t \mathbf{D} = \mathbf{j} \ , \tag{2.17}$$

respectively, where $\mathbf{D}$ is the electric induction, $\mathbf{E}$ is the electric field intensity, $\mathbf{H}$ is the magnetic field intensity and q stands for the charge density.

In vacuum the following relations hold:

$$\mathbf{D} = \varepsilon_0 \mathbf{E} \ , \tag{2.18}$$

$$\mathbf{H} = \frac{1}{\mu_0} \mathbf{B} \ , \tag{2.19}$$

where ε_0 is the vacuum electric permittivity and μ_0 stands for the vacuum magnetic permeability. For an electrically conducting medium, in general:

$$\mathbf{D} = \varepsilon \mathbf{E} \ , \tag{2.20}$$

$$\mathbf{H} = \frac{1}{\mu} \mathbf{B} \ , \tag{2.21}$$

with $\varepsilon = \varepsilon_r \varepsilon_0$ and $\mu = \mu_r \mu_0$, ε_r and μ_r being the relative permittivity and permeability of a material considered. For liquid metals, with a satisfying accuracy, it may be approximated that $\varepsilon_r = \mu_r = 1$ [29], [31].

In liquid metals and molten semiconductors the displacement current $\partial_t \mathbf{D}$ is negligible [30], [31], as the characteristic velocities are much lower than the velocity of light in vacuum $c = 1/\sqrt{\mu_0 \varepsilon_0}$, and Ampere's law (2.17) becomes

$$\nabla \times \mathbf{B} = \mu_0 \mathbf{j} \ . \tag{2.22}$$

The thermoelectric effects, namely the Thomson, Peltier, Seebeck, Soret and Dufour effects, discussed in details by [36] and [38], may be neglected in the context of problems considered here. The effects due to temperature dependence of density and magnetic field are very weak and the effect of mass transfer on

heat and charge transfer is negligible. Similarly the Joule heating effect, analyzed in the context of MHD channel flows by [36], [39], [40], may be neglected, as will be shown in the following subsections.

Here we assume that the fluid acts like a single species, the electron mass and the inertia of the electron fluid is neglected, thus the Hall effect may be omitted in this description [41].

Maxwell equations describe the electric and magnetic fields, $\mathbf{E}$ and $\mathbf{B}$, arising from varying distributions of electric charges and currents. The Navier-Stokes equations and the Maxwell equations are coupled by the Lorentz force in (2.8) and by the Ohm's law for electric currents in the fluid due to the electric field $\mathbf{E}$ and the induced electromotive force:

$$\mathbf{j} = \sigma(\mathbf{E} + \mathbf{v} \times \mathbf{B}) \ . \tag{2.23}$$

Here the term $\mathbf{v} \times \mathbf{B}$, called the back emf current [42], describes the deviation of the electric current by the hydrodynamic flow [31], which when interacting with $\mathbf{B}$ in (2.8), decelerates the flow.

In addition one needs to consider the charge conservation (obtained by taking the divergence of the Ampere's law):

$$\nabla \cdot \mathbf{j} = 0 \ . \tag{2.24}$$

2.2.1 Induction equation

In general, the external magnetic field influences the flow via the Lorentz force and the flow modifies the magnetic field inside the system [43]. The temporal evolution of the magnetic field may be derived by combining the Faraday's law (2.16), divergence theorem (2.15) and Ohm's law (2.23) to obtain the induction equation:

$$\partial_t \mathbf{B} = \nabla \times (\mathbf{v} \times \mathbf{B}) + \frac{1}{\mu_0 \sigma} \nabla^2 \mathbf{B} \ . \tag{2.25}$$

The magnetic field changes due to the two right-hand-side terms representing convection and diffusion. Using vector identities, mass conservation $\nabla \cdot \mathbf{v} = 0$ and the divergence theorem $\nabla \cdot \mathbf{B} = 0$, the convection term, representing the

interaction between the flow velocity and the magnetic field, can be rewritten as:

$$\nabla \times (\mathbf{v} \times \mathbf{B}) = (\mathbf{B} \cdot \nabla)\mathbf{v} - (\mathbf{v} \cdot \nabla)\mathbf{B}, \tag{2.26}$$

where the right-hand-side terms represent stretching along magnetic field lines and advection, respectively.

2.3 Scaling and dimensionless parameters

It is useful to transform the governing equations into a convenient dimensionless form by introducing re-scaled variables and dimensionless parameters. The variables are scaled by the characteristic length d, temperature difference ΔT and the applied magnetic field B_0 as follows:

$$\begin{aligned}
\mathbf{B} &\to B_0\mathbf{B} \ , \\
t &\to \frac{d^2}{\nu}t \ , \\
\mathbf{v} &\to \frac{\nu}{d}\mathbf{v} \ , \\
p &\to \rho_0\frac{\nu^2}{d^2}p \ , \\
T &\to (\Delta T)T \ , \\
\nabla &\to \frac{1}{d}\nabla \ , \\
\mathbf{j} &\to \frac{B_0}{\mu_0 d}\mathbf{j} \\
\epsilon &\to \frac{\rho_0 c_p \nu(\Delta T)}{d^2}Q \ .
\end{aligned} \tag{2.27}$$

Similar scales are used by other authors [28], [37], [44], [45], but other scalings

are also possible.

From the scales used above, one can construct the dimensionless parameters, which characterise convective fluid flow. These parameters are as follows:

$$Gr = g\beta\Delta T\frac{d^3}{\nu^2} \ , \tag{2.28}$$

$$Pr = \frac{\nu}{\kappa} \ , \tag{2.29}$$

$$Ra = PrGr = g\beta\Delta T\frac{d^3}{\nu\kappa} \ , \tag{2.30}$$

$$Ha = B_0 d\sqrt{\frac{\sigma}{\rho_0\nu}} \ , \tag{2.31}$$

$$Pr_m = \mu_0\sigma\nu \ , \tag{2.32}$$

$$Re_m = \mu_0\sigma v_0 d \ , \tag{2.33}$$

$$Lu = Ha\sqrt{Pr_m} = B_0 d\sigma\sqrt{\frac{\mu_0}{\rho_0}} \ . \tag{2.34}$$

The strength of buoyancy forces is characterized by the Grashof number Gr (2.28), the ratio of the electromagnetic to viscous forces is defined by the square of the Hartmann number Ha (2.31), while the Prandtl number Pr (2.29) measures the ratio of the kinematic viscosity, ν to the thermal diffusivity, κ. The Prandtl and the magnetic Prandtl numbers depend solely on the fluid properties. In such applications as fusion reactor blankets, semiconductor crystal growth or electromagnetic processing of materials, mainly low Prandtl number fluids, such as metals and semiconductors, are considered. In such fluids, heat diffuses very quickly compared to momentum (very effective heat conduction).

The magnetic Prandtl number Pr_m (2.32) is defined as the ratio of the kinematic viscosity ν to the magnetic diffusivity $\eta = (\mu_0\sigma)^{-1}$, while the magnetic Reynolds number Re_m (2.33) gives the relative importance of the magnetic ad-

vection compared to the magnetic diffusion (here v_0 is a characteristic velocity).

The Lundquist number Lu (2.34), combining both Hartmann and magnetic Prandtl numbers, determines the importance of the resistive diffusion time. In the parameters introduced above, the Rayleigh number (2.30), combining the Grashof and Prandtl numbers, can be recovered.

The dimensionless parameters and scales introduced above allow to conclude the insignificance of the Joule heating effect. For a flow of Indium Phosphide ($Pr = 0.015$, $\beta = 13.8 \cdot 10^{-6}$ K^{-1}, $c_p = 310$ Jkg^{-1}K^{-1}) in a channel of width $d = 0.05$ m, the ratio of the Joule heating ($\mathbf{j}^2/\sigma$) to the internal heating effects, scaled according to (2.27), is of the order $10^{-8} \cdot Ha^2/Gr$. Thus the effects of the Joule heating may be neglected in the problems considered here.

2.3.1 Summary

The resulting set of nondimensional equations governing the motion of the electrically conducting fluid, which will be used below, is:

$$\partial_t \mathbf{v} + (\mathbf{v} \cdot \nabla)\mathbf{v} = -\nabla p + \nabla^2 \mathbf{v} + \frac{Ha^2}{Pr_m}(\nabla \times \mathbf{B}) \times \mathbf{B} - GrT\hat{\mathbf{e}}_g \ , \tag{2.35}$$

$$\partial_t \mathbf{B} + (\mathbf{v} \cdot \nabla)\mathbf{B} = \frac{1}{Pr_m}\nabla^2 \mathbf{B} + (\mathbf{B} \cdot \nabla)\mathbf{v} \ , \tag{2.36}$$

$$\partial_t T + (\mathbf{v} \cdot \nabla)T = \frac{1}{Pr}\nabla^2 T + Q \ , \tag{2.37}$$

$$\nabla \cdot \mathbf{B} = 0 \ , \tag{2.38}$$

$$\nabla \cdot \mathbf{v} = 0 \ . \tag{2.39}$$

and additionally:

$$\mathbf{j} = \frac{1}{Pr_m}\nabla \times \mathbf{B} \ , \tag{2.40}$$

$$\nabla \cdot \mathbf{j} = 0 \ , \tag{2.41}$$

Here $\hat{\mathbf{e}}_g$ is the direction of gravity forces and Q stands for the dimensionless internal heat sources.

2.3.2 Inductionless approximation

The magnetic field can be split into two components, namely $\mathbf{B} = \mathbf{B}_0 + \mathbf{b}_0$, where $\mathbf{B}_0$ is the externally applied magnetic field, and $\mathbf{b}_0$ is the induced magnetic field due to fluid flow.

If the problem is considered in the inductionless approximation, the flow disturbances of the imposed magnetic field are very small. This assumption holds in applications where the magnetic Reynolds number is very low $Re_m << 1$. The induced magnetic field value b_0 is proportional to the magnetic Reynolds number $b_0 \simeq Re_m B$, therefore it may be considered negligible compared to the applied field [28], [44].

Since the magnetic induction is constant and equal to the applied external magnetic field $\mathbf{B} = \mathbf{B}_0$ and $\partial_t \mathbf{B} = 0$, then according to the Faraday's law (2.16), the irrotational electric field can be expressed as the gradient of the electric potential ϕ, and the Ohm's law can be written as

$$\mathbf{j} = \sigma(-\nabla\phi + \mathbf{v} \times \mathbf{B}_0) \ . \tag{2.42}$$

The resulting set of nondimensional equations, in terms of the velocity $\mathbf{v}$, the electric potential ϕ and the temperature T, writes here:

$$\partial_t \mathbf{v} + (\mathbf{v} \cdot \nabla)\mathbf{v} = -\nabla p + \nabla^2 \mathbf{v} + Ha^2(-\nabla\phi + \mathbf{v} \times \mathbf{B}_0) \times \mathbf{B}_0 - GrT\hat{\mathbf{e}}_g \ , \tag{2.43}$$

$$\partial_t T + (\mathbf{v} \cdot \nabla)T = \frac{1}{Pr}\nabla^2 T + Q \ , \tag{2.44}$$

$$\nabla \cdot \mathbf{v} = 0 \ , \tag{2.45}$$

$$\nabla^2 \phi = \mathbf{B}_0 \cdot (\nabla \times \mathbf{v}). \tag{2.46}$$

2.4 Boundary conditions

In many technological applications the flow is confined by rigid walls and boundary conditions must be applied at an interface. For a viscous fluid in a hydrodynamically closed system (no fluid can enter or escape through the boundaries) all the velocity components must vanish at the walls (the so-called 'no-slip' hydrodynamic boundary conditions):

$$\mathbf{v} = 0 \ . \tag{2.47}$$

Mathematically this is the case of the homogeneous Dirichlet boundary conditions [29], [31].

Additionally, electromagnetic and thermal boundary conditions need to be introduced. In the case of thermal and electromagnetic boundary conditions, limit cases are here considered here: perfectly conducting or perfectly insulating.

2.4.1 Thermal boundary conditions

In the case of thermally conducting boundaries, where the temperature can adjust immediately to the temperature at which the walls are held T_w, the boundary conditions read:

$$T = T_w \ . \tag{2.48}$$

If the walls are thermally insulating, no heat flows across them and the temperature gradient must be zero:

$$\partial_n T = 0 \ , \tag{2.49}$$

where $\mathbf{n}$ is the unit vector normal to the wall.

2.4.2 Electromagnetic boundary conditions

In the case of an electrically conducting fluid flow bounded by rigid boundaries, the continuity of normal and tangential components of the magnetic field $\mathbf{B}$ at

interfaces needs to be assumed:

$$\mathbf{n} \cdot (\mathbf{B} - \mathbf{B}_w) = 0 \ , \tag{2.50}$$

$$\mathbf{n} \times (\mathbf{B} - \mathbf{B}_w) = 0 \ , \tag{2.51}$$

where $\mathbf{B}_w$ is the magnetic field inside a solid wall. The continuity of tangential components of the magnetic field implies the lack of surface currents, which may be neglected in the timescales considered [29].

For the electrically insulating boundaries, no current may enter a wall and the boundary condition reads

$$\mathbf{n} \cdot \mathbf{j} = 0 \ . \tag{2.52}$$

For the electrically perfectly conducting boundaries, in general:

$$\tau \cdot \mathbf{j} = 0 \ , \tag{2.53}$$

where τ is the tangential unit vector to the boundaries. Specific equations governing electrodynamics inside a conducting wall need to be considered for a given geometry.

In cases considered below insulating and perfectly conducting boundaries are considered only.

2.4.2.1 Inductionless approximation, $Pr_m = 0$ case

In the inductionless approximation the electromagnetic boundary conditions are introduced through the electric potential ϕ. Since, according to the no-slip condition (2.47), $\mathbf{v} = 0$, the Ohm's law (2.42) reduces at the boundaries to $\mathbf{j} = -\sigma \nabla \phi$.

For the electrically insulating boundaries, according to (2.52), the boundary condition for the electric potential writes:

$$\partial_n \phi = 0 \ . \tag{2.54}$$

For the electrically conducting boundaries the wall potential is uniform and can be set to a constant:

$$\phi = constant \ . \tag{2.55}$$

Chapter 3

Stability analysis, numerical methods and verification

3.1 Stability analysis

We will be interested here in the stability of a convective flow. In order to perform the stability analysis of a system, first the possibility of equilibrium needs to be established. Stability is defined as the ability of a system to be immune to small disturbances [46].

3.1.1 Steady base flow solution

A flow is said to be in equilibrium when it is not accelerated due to the balance of forces [31], [46]. A base flow solution can be determined by solving steady equations for a given geometry, together with applied boundary conditions. In general, a problem for the basic velocity $\mathbf{u}_0$, pressure p_0, magnetic field $\mathbf{B}_0 + \mathbf{b}_0$ and temperature T_0 is governed, according to (2.35)-(2.37), by the following set of equations:

$$(\mathbf{u}_0 \cdot \nabla)\mathbf{u}_0 = -\nabla p_0 + \nabla^2 \mathbf{u}_0 + \frac{Ha^2}{Pr_m}(\nabla \times \mathbf{b}_0) \times (\mathbf{B}_0 + \mathbf{b}_0) - GrT_0\hat{\mathbf{e}}_g \ , \tag{3.1}$$

$$(\mathbf{u}_0 \cdot \nabla)\mathbf{b}_0 = \frac{1}{Pr_m}\nabla^2 \mathbf{b}_0 + (\mathbf{B}_0 \cdot \nabla)\mathbf{u}_0 + (\mathbf{b}_0 \cdot \nabla)\mathbf{u}_0 \ , \tag{3.2}$$

$$(\mathbf{u}_0 \cdot \nabla)T_0 = \frac{1}{Pr}\nabla^2 T_0 + Q \ . \tag{3.3}$$

Hereafter only channel flows, confined by two rigid walls and with the velocity profile being either zero or unchanged in the flow direction will be considered. If there is a base flow in an equilibrium state, such flows are characterised by one-component velocity profiles, which can only be functions of the coordinate across the boundaries [28], [46]. For the sake of deriving the general form of disturbance equations, applicable to different geometries, layers and channels considered hereafter will be bounded by rigid boundaries situated at finite values of $z-$ direction and all the body forces will be acting in the $(x-z)$ plane. Here (x, y, z) are Cartesian coordinates (Figure 3.1). Notice that the externally applied magnetic field is always in the $z-$ direction, and axis y points into the spanwize direction.

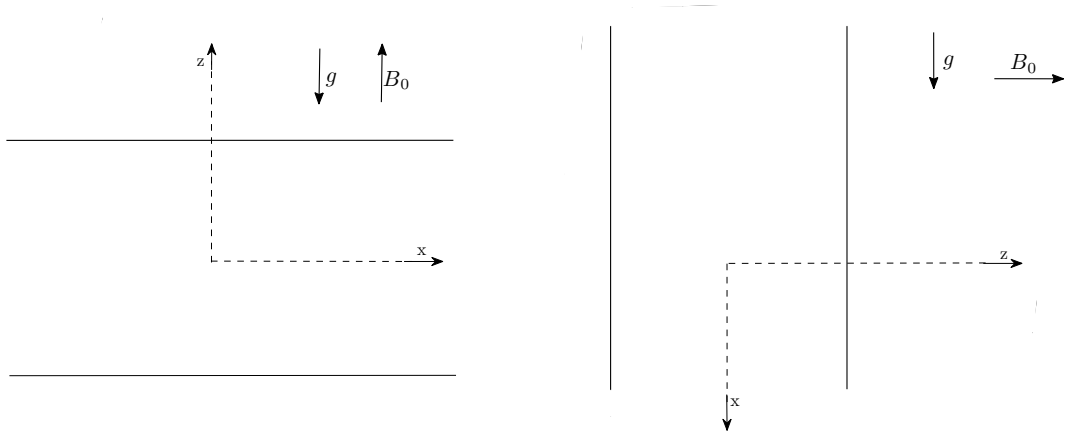

Figure 3.1: Geometries considered: a horizontal layer and a vertical channel

For such flows, which are time-independent, incompressible and parallel, the steady base flow solution is:

$$\mathbf{u}_0 = [u_0(z), 0, 0] \ . \tag{3.4}$$

The assumptions given above lead to further restrictions on the basic profiles of electrically conducting flows subject to a uniform external magnetic field. For the flow to be parallel and fully developed, the induced magnetic field must be, like the basic velocity, independent of the $x-$ and $y-$ coordinates. This gives the following basic induced magnetic field profile:

$$\mathbf{b}_0 = [b_0(z), 0, 0] \ , \tag{3.5}$$

in addition the the externally applied uniform field $\mathbf{B}_0$.

3.1.2 Perturbations

In order to test whether the equilibrium state is stable, reaction of the system to small perturbations needs to be examined. The stability is investigated here by linear analysis. Assuming that disturbances to the flow are fully three-dimensional, the flow can be decomposed into the base flow and the fluctuating component in the following way:

$$F = F_0 + \tilde{f}(x, y, z, t) \ , \tag{3.6}$$

where functions F, F_0 and $\tilde{f}$ are any scalar or vector flow quantities. The superscript tilde ($\sim$) indicates a small perturbation component and the zero subscript stands for the base flow.

Assuming that the introduced perturbation is infinitisemally small one can linearize the problem (2.35)-(2.37) at the vicinity of the steady state (3.1)-(3.3), neglecting in further calculations all products of perturbations in comparison with the other terms. These products result in an order of magnitude smaller terms and cannot influence other terms to this order of approximation [31]. Thus the stability can be studied on the linearized system:

$$\begin{aligned}\partial_t \tilde{\mathbf{v}} + (\mathbf{u}_0 \cdot \nabla)\tilde{\mathbf{v}} + (\tilde{\mathbf{v}} \cdot \nabla)\mathbf{u}_0 = -\nabla(p_0 + \tilde{p}) + \nabla^2 \tilde{\mathbf{v}} + \frac{Ha^2}{Pr_m}(\nabla \times \mathbf{b}_0) \times \tilde{\mathbf{b}} \\ + \frac{Ha^2}{Pr_m}(\nabla \times \tilde{\mathbf{b}}) \times \mathbf{b}_0 + \frac{Ha^2}{Pr_m}(\nabla \times \tilde{\mathbf{b}}) \times \mathbf{B}_0 - Gr\tilde{\theta}\hat{\mathbf{e}}_g\end{aligned} \tag{3.7}$$

$$\partial_t \tilde{\mathbf{b}} + (\mathbf{u}_0 \cdot \nabla)\tilde{\mathbf{b}} + (\tilde{\mathbf{v}} \cdot \nabla)\mathbf{b}_0 = \frac{1}{Pr_m}\nabla^2 \tilde{\mathbf{b}} + (\tilde{\mathbf{b}} \cdot \nabla)\mathbf{u}_0 + (\mathbf{B}_0 \cdot \nabla)\tilde{\mathbf{v}} + (\mathbf{b}_0 \cdot \nabla)\tilde{\mathbf{v}} \tag{3.8}$$

$$\partial_t \tilde{\theta} + (\mathbf{u}_0 \cdot \nabla)\tilde{\theta} + (\tilde{\mathbf{v}} \cdot \nabla)T_0 = \frac{1}{Pr}\nabla^2 \tilde{\theta} \tag{3.9}$$

3.1.3 Disturbance equations

The classical method for solving such a problem is by modal expansion (normal modes method) [46]. In this case the perturbations can be expressed with Fourier expansions in the $x-$ and $y-$ directions. This is justified since the extent of the planes perpendicular to z (defined by x and y) is assumed to be doubly infinite. Additionally assuming that the time dependence can be separated, the problem is to find solutions of the type:

$$\tilde{f}(x, y, z, t) = \hat{f}(z) \exp\{ixk_x + iyk_y + \lambda t\} \ , \tag{3.10}$$

where k_x and k_y are the wavenumbers in the $x-$ and $y-$ directions, respectively, and $\lambda = \lambda_r + i\lambda_i$ is the eigenvalue. Its real part λ_r is the disturbance growth rate and λ_i is the angular oscillation frequency. In general the flow is stable if for given values of the characteristic numbers, λ_r is non-positive for all the possible values of the wavenumbers.

It is convenient to introduce vorticity $\tilde{\underline{\omega}} = \nabla \times \tilde{\mathbf{v}}$ into the problem in order to reduce the number of variables in the resulting disturbance problem, as will be shown below.

Substituting the expression (3.10) into the system of equations (3.7)-(3.10) leads to a generalised eigenvalue problem:

$$\{\mathbf{D}^4 - u_0 ik_x \mathbf{D}^2 + u_0'' ik_x\}\hat{w} + \frac{Ha^2}{Pr_m}\{b_0 ik_x \mathbf{D}^2 - b_0'' ik_x + \mathbf{D}^2 \partial_z\}\hat{b}_z$$

$$+ Grik_x(\partial_z \hat{\theta})e_g \delta_{xg} + Grk^2 \hat{\theta} e_g \delta_{zg} = \lambda \mathbf{D}^2 \hat{w} \ , \tag{3.11}$$

$$\{\mathbf{D}^2 - u_0 ik_x\}\hat{\omega}_z + u_0' ik_y \hat{w} - \frac{Ha^2}{Pr_m} b_0' ik_y \hat{b}_z$$

$$+Ha^2\{\partial_z + b_0 ik_x\}\hat{j}_z + Gr ik_y \hat{\theta} e_g \delta_{xg} = \lambda \hat{\omega}_z \ , \tag{3.12}$$

$$\{\frac{1}{Pr_m}\mathbf{D}^2 - u_0 ik_x\}\hat{b}_z + \{b_0 ik_x + \partial_z\}\hat{w} = \lambda \hat{b}_z \ , \tag{3.13}$$

$$\{\mathbf{D}^2 - Pr_m u_0 ik_x\}\hat{j}_z + \{b_0 ik_x + \partial_z\}\hat{\omega}_z + b_0' ik_y \hat{w} - u_0' ik_y \hat{b}_z = \lambda Pr_m \hat{j}_z \ , \tag{3.14}$$

$$\{\frac{1}{Pr}\mathbf{D}^2 - u_0 ik_x\}\hat{\theta} - i(\partial_x T_0)\frac{k_y}{k^2}\hat{\omega}_z - \{\partial_z T_0 + i(\partial_x T_0)\frac{k_x}{k^2}\partial_z\}\hat{w} = \lambda \hat{\theta} \ , \tag{3.15}$$

where $\hat{\theta}$ is the disturbed temperature and $\hat{w}$, $\hat{\omega}_z$, $\hat{b}_z$ and $\hat{j}_z$ are the $z-$components of disturbed velocity, vorticity, magnetic field and electric current density, respectively. The prime symbol ($'$) denotes derivative with respect to z. For simplicity the operator $\mathbf{D} = i\mathbf{k} + [0, 0, \frac{d}{dz}]$ has been introduced, with the wavenumber $\mathbf{k} = [k_x, k_y, 0]$. Additionally $e_g = \pm 1$ and δ_{xg} and δ_{zg}, being classic Kronecker deltas, define the direction of gravity.

Specifically, equations (3.11) and (3.12) have been obtained from the momentum equation (2.35), equations (3.13) and (3.14) from the induction equation (2.36) and the equation (3.15) from the temperature equation (2.37) in the following ways. The velocity disturbance equation (3.11) is a result of comparison between the $z-$derivative of the gradient of momentum equation with the Laplacian of its $z-$component. The vorticity disturbance equation (3.12) is the $z-$component of the curl of momentum equation. The magnetic field disturbance equation (3.13) is simply the $z-$component of the induction equation, while the disturbed current equation (3.14) have been obtained by taking the $z-$component of the curl of induction equation. The disturbed temperature equation (3.15) is a direct result of the governing temperature equation.

The equations (3.11)-(3.15) fully define the stability problem for all geometries considered below.

3.2 Boundary conditions for disturbances

With the geometry assumptions made above, the boundary conditions for disturbances can be derived from the general boundary conditions presented in the section 2.4.

From the no-slip velocity condition (2.47) and the conservation law (2.39), the mechanical boundary conditions are:

$$\hat{w} = \partial_z \hat{w} = 0 \qquad \text{at } z = \pm 0.5 \ . \tag{3.16}$$

$$\hat{\omega}_z = 0 \qquad \text{at } z = \pm 0.5 \ , \tag{3.17}$$

Following the reasoning presented in the section 2.4.1, the thermal boundary conditions for disturbances are:

$$\hat{\theta} = 0 \qquad \text{at } z = \pm 0.5 \text{ for thermally conducting walls} \ , \tag{3.18}$$

$$\partial_z \hat{\theta} = 0 \qquad \text{at } z = \pm 0.5 \text{ for thermally insulating walls} \ . \tag{3.19}$$

Concerning the electrical boundary conditions, for the case of the electrically conducting walls, from the conservation law (2.41) it follows that:

$$\partial_z \hat{j}_z = 0 \qquad \text{at } z = \pm 0.5 \text{ for electrically conducting walls} \ , \tag{3.20}$$

which is valid with the assumption of tangential components of currents disappearing at the boundaries. Since $\hat{b}_z$ must be continuous and finite in the wall:

$$\hat{b}_z = 0 \qquad \text{at } z = \pm 0.5 \text{ for electrically conducting walls} \ . \tag{3.21}$$

In the case of the electrically insulating boundaries, no current enters the wall from the fluid side:

$$\hat{j}_z = 0 \qquad \text{at } z = \pm 0.5 \text{ for electrically insulating walls} \ . \tag{3.22}$$

Equations governing the magnetic induction inside the walls, according to (2.35)

and (2.37), are:

$$\nabla \cdot \mathbf{B}_w = 0 \ , \tag{3.23}$$

$$\nabla^2 \mathbf{B}_w = 0 \ , \tag{3.24}$$

here the subscript $'w'$ stands for the wall properties. The boundary conditions, following[22] and [29], can be written as:

$$\frac{1}{\mu} B_x = \frac{1}{\mu_w} B_{xw} \ , \tag{3.25}$$

$$\frac{1}{\mu} B_y = \frac{1}{\mu_w} B_{yw} \ , \tag{3.26}$$

$$B_z = B_{zw} \ , \tag{3.27}$$

here the total magnetic field in the flow and inside the wall are $\mathbf{B} = [B_x, B_y, B_z]$ and $\mathbf{B}_w = [B_{xw}, B_{yw}, B_{zw}]$, respectively. The assumption $\mu = \mu_w$, leads to the following disturbance equation:

$$\mathbf{D}^2 \hat{b}_{zw} = 0 \ , \tag{3.28}$$

with the general solution:

$$\hat{b}_{zw} = C_1 e^{kz} + C_2 e^{-kz} \ , \tag{3.29}$$

here C_1 and C_2 are constants and $k = \sqrt{k_x^2 + k_y^2}$. Since b_{zw} must be finite,

$$\hat{b}_{zw} = C_2 e^{-kz} \qquad \text{at } z = 0.5 \ , \tag{3.30}$$

$$\hat{b}_{zw} = C_1 e^{kz} \qquad \text{at } z = -0.5 \ , \tag{3.31}$$

and according to (3.27), the final boundary conditions for the disturbed magnetic field read:

$$\{\partial_z + k\}\hat{b}_3 = 0 \qquad \text{at } z = 0.5 \text{ for electrically insulating walls} \ , \tag{3.32}$$

$$\{\partial_z - k\}\hat{b}_3 = 0 \qquad \text{at } z = -0.5 \text{ for electrically insulating walls .} \tag{3.33}$$

3.3 Perturbation energy considerations

The perturbation energy analysis is performed for a better understanding of the instability mechanisms. The energy equations can be derived from the governing equations: the fluctuating kinetic energy from the momentum equation (2.35), the fluctuating magnetic energy from the induction equation (2.36) and the fluctuating thermal energy from the temperature equation (2.37). These equations are studied in order to establish different energetic contributions corresponding to specific instabilities.

Following the approach in [44], the governing perturbation equations (3.7)-(3.9) are multiplied by the corresponding complex conjugates and integrated along the z-direction. The real parts of the resulting equations, with the perturbations satisfying (3.10), give the desired energy balances.

The rate of change of the fluctuation kinetic energy K:

$$Re(\partial_t K) = \lambda \int_z \hat{\mathbf{v}} \cdot \hat{\mathbf{v}}^* dz = K_d + K_f + K_b + K_m \ , \tag{3.34}$$

with the viscous dissipation of fluctuating kinetic energy K_d :

$$K_d = Re\left(\int_z \nabla^2 \hat{\mathbf{v}} \cdot \hat{\mathbf{v}}^* dz\right) \ , \tag{3.35}$$

the production of fluctuating kinetic energy by shear of mean flow K_f :

$$K_f = -Re\left(\int_z u_0' \hat{w}\hat{u}^* dz\right) \ , \tag{3.36}$$

the work done by buoyancy forces K_b :

$$K_b = -Re\left(\int_z Gr\hat{\theta}(\hat{\mathbf{e}}_g \cdot \hat{\mathbf{v}}^*) dz\right) \ , \tag{3.37}$$

the dissipation of fluctuating kinetic energy by magnetic forces K_m :

$$K_m = Re\left(\int_z \frac{Ha^2}{Pr_m}\left(-ik_y\hat{b}_z\hat{v}^* + (\partial_z\hat{b}_y)\hat{v}^* + ik_x b_0\hat{b}_z\hat{w}^* - ik_y b_0\hat{b}_x\hat{v}^* - ik_y\hat{b}_z\hat{v}^*\right)dz\right)$$

$$+Re\left(\int_z \frac{Ha^2}{Pr_m}\left((\partial_z\hat{b}_y)\hat{v}^* + ik_x b_0\hat{b}_z\hat{w}^* - b_0(\partial_z\hat{b}_x)\hat{w}^* - b_0'\hat{b}_x\hat{w}^*\right)dz\right) \ . \qquad (3.38)$$

In the inductionless approximation, the dissipation of fluctuating kinetic energy by magnetic forces simplifies to K_{m0}:

$$K_{m0} = Re\left(\int_z Ha^2(ik_x\hat{\phi}\hat{v}^* - ik_y\hat{\phi}\hat{u}^* - \hat{u}\hat{u}^* - \hat{v}\hat{v}^*)dz\right) \ . \qquad (3.39)$$

The rate of change of the fluctuation magnetic energy M:

$$Re(\partial_t M) = \lambda\int_z \hat{\mathbf{b}}\cdot\hat{\mathbf{b}}^* dz = M_d + M_{ad} + M_{s1} + M_{s2} + M_{s3} \ , \qquad (3.40)$$

with the dissipation of fluctuating magnetic energy M_d :

$$M_d = Re\left(\int_z \frac{1}{Pr_m}\nabla^2\hat{\mathbf{b}}\cdot\hat{\mathbf{b}}^* dz\right) \ , \qquad (3.41)$$

the production of fluctuating magnetic energy by advection M_{ad} :

$$M_{ad} = -Re\left(\int_z b_0'\hat{w}\hat{b}_x^* dz\right) \ , \qquad (3.42)$$

the dissipation of fluctuating magnetic energy by stretching of magnetic field lines by shear of mean flow M_{s1} :

$$M_{s1} = Re\left(\int_z u_0'\hat{b}_z\hat{b}_x^* dz\right) \ , \qquad (3.43)$$

the dissipation of fluctuating magnetic energy by stretching of magnetic field lines

along the flow M_{s2} :

$$M_{s2} = Re\left(\int_z ik_x b_0 \hat{\mathbf{v}} \cdot \hat{\mathbf{b}}^* dz\right) \ , \tag{3.44}$$

the dissipation of fluctuating magnetic energy by stretching of magnetic field lines along magnetic field lines M_{s3} :

$$M_{s3} = Re\left(\int_z (\partial_z \hat{\mathbf{v}}) \cdot \hat{\mathbf{b}}^* dz\right) \ , \tag{3.45}$$

The rate of change of the fluctuation thermal energy Θ:

$$Re(\partial_t \Theta) = \lambda \int_z \hat{\theta} \cdot \hat{\theta}^* dz = \Theta_d + \Theta_1 + \Theta_2 \ , \tag{3.46}$$

with the dissipation of fluctuating thermal energy Θ_d :

$$\Theta_d = Re\left(\int_z \frac{1}{Pr} \nabla^2 \hat{\theta} \cdot \hat{\theta}^* dz\right) \ , \tag{3.47}$$

the production of fluctuating thermal energy by vertical transport of temperature Θ_1:

$$\Theta_1 = -Re\left(\int_z (\partial_z T_0) \hat{w} \hat{\theta}^* dz\right) \ , \tag{3.48}$$

the production of fluctuating thermal energy by horizontal transport of temperature Θ_2:

$$\Theta_2 = -Re\left(\int_z (\partial_x T_0) \hat{u} \hat{\theta}^* dz\right) \ . \tag{3.49}$$

The negative values of energy contributions characterise stabilizing dissipative terms, while the positive contributions are by nature destabilizing.

In the problems considered here the energy analysis results are given at the critical thresholds. Since the critical eigenvectors are defined to within a multiplicative constant, the energy equations specific terms also can be given to within a multiplicative constant. In order to present well-defined energy balances, the energy equations are scaled by the corresponding dissipation terms:

$$\bar{K}_d = \bar{K}_f + \bar{K}_b + \bar{K}_m = 1 \ , \tag{3.50}$$

$$\bar{M}_d = \bar{M}_{ad} + \bar{M}_{s1} + \bar{M}_{s2} + \bar{M}_{s3} = 1 \ , \tag{3.51}$$

$$\bar{\Theta}_d = \bar{\Theta}_1 + \bar{\Theta}_2 = 1 \ , \tag{3.52}$$

here the scaled terms are denoted with an overbar.

To compare the kinetic, magnetic and thermal energy contributions, the following dimensionless ratios are given:

$$R_{dt} = \frac{1}{Gr}\frac{K_d}{\Theta_d} \ , \tag{3.53}$$

comparing the kinetic energy to the thermal energy contributions,

$$R_{dm} = \frac{Pr_m}{Ha^2}\frac{K_d}{M_d} \ , \tag{3.54}$$

comparing the kinetic energy to the magnetic energy contributions,

$$R_{tm} = \frac{R_{dm}}{R_{dt}} \ , \tag{3.55}$$

comparing the thermal energy to the magnetic energy contributions.

3.4 Numerical methods

The problem of numerical solutions of ordinary and partial differential equations has been extensively studied and several techniques for the disturbance problems are known and widely used, namely spectral methods [47], [48], finite element and finite difference methods [49].

The spectral methods give higher accuracy with an error decreasing exponentially with the number of trial functions introduced and in that sense are superior over the finite difference and finite elements methods. The detailed comparison is given in [48].

In the problems considered here, the spectral collocation method based on Chebyshev interpolants, presented in [50], [51], has been applied. The approach taken follows these references closely.

In general, in the spectral collocation method and interpolant $p_{N-1}(x)$ of the function $f(x)$ is given by:

$$f(x_k) = p_{N-1}(x_k) \ , \qquad k = 1, ..., N \ , \tag{3.56}$$

where $\{x_j\}_{j=1}^N$ is a set of interpolation nodes. The interpolant is further defined with interpolating functions $\{\phi_j(x)\}_{j=1}^N$ and the weight function $\alpha(x)$ as:

$$f(x) \approx p_{N-1}(x) = \sum_{j=1}^{N} \frac{\alpha(x)}{\alpha(x_j)} \phi_j(x) f(x_j) \ . \tag{3.57}$$

The numerical derivatives are given by collocation derivative operators and the differentiation process can be represented as the matrix-vector operation:

$$\mathbf{f}^{(l)} = \mathbf{D}^{(l)} \mathbf{f} \ , \tag{3.58}$$

namely:

$$f^{(l)}(x_k) = \sum_{j=1}^{N} D_{k,j}^{(l)} f(x_j) \ . \tag{3.59}$$

It has been shown that Chebyshev methods, with their constant weight function:

$$\alpha(x) = 1 \ , \tag{3.60}$$

are most suitable for solving hydrodynamic stability problems [51]. The grid points, given here on the interval $[-1, 1]$, are distributed in a minimal-energy configuration, clustering near the boundaries $x = \pm 1$, defined as:

$$x_k = \cos \frac{(k-1)\pi}{N-1} \ . \tag{3.61}$$

Note that a finite interval $[a, b]$ can always be rescaled to $[-1, 1]$ via a linear transformation, making the Chebyshev nodes applicable to various problems.

The interpolating function $\phi_j(x)$ is defined here as:

$$\phi_j(x) = \frac{(-1)^j}{c_j} \frac{1 - x^2}{(N-1)^2} \frac{T'_{N-1}(x)}{x - x_j} \ , \tag{3.62}$$

where $c_1 = c_N = 2$, $c_2 = ... = c_{N-1} = 1$, the prime ($'$) symbol represents the first derivative and $T_n(x)$ are Chebyshev polynomials defined as follows:

$$T_0(x) = 1 \ ,$$

$$T_1(x) = x \ ,$$

$$T_2(x) = 2x^2 - 1 \ ,$$

$$T_3(x) = 4x^3 - 3x \ ,$$

$$T_{n+1}(x) = 2xT_n(x) - T_{n-1}(x) \ . \tag{3.63}$$

Thus the Chebyshev differentiation matrices may be written as:

$$D^{(l)}_{k,j} = \phi^{(l)}_j(x_k) \ . \tag{3.64}$$

The main complication while solving a differential equation with the spectral collocation methods arises from incorporating appropriate boundary conditions.

In the case of the homogeneous Dirichlet conditions $f(\pm 1) = 0$, the first and last columns, and the first and last rows of the differentiation matrices (3.64) may be multiplied by zero, as the function simply vanishes at the boundaries.

If the required boundary conditions involve derivatives, then the appropriate differentiation matrices must be derived through the interpolant, which satisfies both the interpolation conditions (3.57) and the boundary conditions, defined in general as:

$$a_+ f(1) + b_+ f'(1) = c_+ \ , \quad a_- f(-1) + b_- f'(-1) = c_- \ , \tag{3.65}$$

where $a_\pm$, $b_\pm$ and $c_\pm$ are given constants.

The interpolant here, being a polynomial of degree $N+1$, is given in [51] as:

$$p_{N+1}(x) = \tilde{\phi}_+(x) + \tilde{\phi}_-(x) + \sum_{j=1}^{N} f(x_j)\tilde{\phi}_j(x) \ , \tag{3.66}$$

with :

$$\tilde{\phi}_+(x) = \left(\frac{c_+}{b_+}\right)\frac{(x^2-1)}{2}\phi_1(x) \ ,$$

$$\tilde{\phi}_-(x) = \left(\frac{c_-}{b_-}\right)\frac{(1-x^2)}{2}\phi_N(x) \ ,$$

$$\tilde{\phi}_1(x) = \left\{\frac{1+x}{2} + \left(\frac{1}{2} + \phi_1'(1) + \frac{a_+}{b_+}\right)\left(\frac{1-x^2}{2}\right)\right\}\phi_1(x) \ ,$$

$$\tilde{\phi}_j(x) = \left(\frac{1-x^2}{1-x_j^2}\right)\phi_j(x) \ , \quad j = 2, ..., N-1 \ ,$$

$$\tilde{\phi}_N(x) = \left\{\frac{1-x}{2} + \left(\frac{1}{2} - \phi_N'(-1) - \frac{a_-}{b_-}\right)\left(\frac{1-x^2}{2}\right)\right\}\phi_N(x) \ .$$

Thus the differentiation matrices with the boundary conditions incorporated writes:

$$\tilde{D}_{k,j}^{(l)} = \tilde{\phi}_j^{(l)}(x_k) \ . \tag{3.67}$$

Application of the spectral collocation method to the equations (3.8)-(3.12) leads to the matrix eigenvalue problem:

$$\mathbf{AV} = \lambda\mathbf{BV} \ , \tag{3.68}$$

where $\mathbf{V} = [\hat{w}, \hat{\omega}_z, \hat{b}_z, \hat{j}_z, \hat{\theta}]^T$.

3.4.1 Matlab implementation and verification

With matrix as a basic unit, Matlab is a very convenient tool for solving ordinary and partial differential equations with the use of differentiation matrices. The additional advantages are its high level commands for such operations as polynomial interpolation, and treatment of operations on matrices, such as matrix inversion. The Matlab code created for the purpose of this thesis is provided in the appendix A. It has been tested on simplified problems, presented below, for which the numerical results have already been obtained by a number of authors and are commonly accepted.

3.4.1.1 Simplified problem: The Poiseuille flow

The isothermal, non-magnetic flow confined by two walls and driven by a constant pressure gradient with a parabolic basic velocity profile $u_0 = z^2 - 1$, is called the Poiseuille flow [46], [52], [53]. Here the governing equations are scaled by the Reynolds number:

$$\partial_t \mathbf{v} + (\mathbf{v} \cdot \nabla)\mathbf{v} = -\nabla p + \frac{1}{Re}\nabla^2 \mathbf{v} \ , \tag{3.69}$$

$$\nabla \cdot \mathbf{v} = 0 \ . \tag{3.70}$$

Normal modes analysis leads to well-known Orr-Sommerfeld equation of stability theory:

$$\left\{ \frac{1}{Re}\mathbf{D}^4 + u_0'' i k_x - u_0 i k_x \mathbf{D}^2 \right\} \hat{v}_z = \lambda \mathbf{D}^2 \hat{v}_z \ . \tag{3.71}$$

The critical Reynolds number for which the flow becomes unstable has been found previously by several authors and the accepted value is $Re_{crit} = 5772.22$ with corresponding critical wavenumber $k_{crit} = 1.02056$. Results computed while testing the code developed here are:

$$Re_{crit} = 5772.22345 \ ,$$

$$k_{crit} = 1.020553 \ .$$

The convergences of these results with the increasing number of Chebyshev grid points N (and degree of Chebyshev polynomials) are shown in Figure 3.2.

The comparison has also been made for the plane Poiseuille flow with $Re = 10^4$ and $k_x = 1$. Obtained result for the most unstable eigenmode is in perfect agreement with the eigenvalue computed in [52]:

$$\lambda = 0.00373967 - 0.23752649i \ .$$

3.4.1.2 Simplified problem: Thermogravitational convection, the Hadley flow

The convective flow confined between two horizontal walls (located at $z = \pm\frac{1}{2}$) with perpendicular gravity, governed by the Navier-Stokes and energy equations [27], [28], [54]:

$$\partial_t \mathbf{v} + (\mathbf{v} \cdot \nabla)\mathbf{v} = -\nabla p + \nabla^2 \mathbf{v} + GrT\mathbf{e_z} \ , \tag{3.72}$$

$$\nabla \cdot \mathbf{v} = 0 \ , \tag{3.73}$$

$$\partial_t T + \mathbf{v} \cdot \nabla T = \frac{1}{Pr}\nabla^2 T \ . \tag{3.74}$$

There exists an exact basic state solution with the velocity $\mathbf{u_0} = [u_0(z), 0, 0]$ and temperature $T_0(x, z)$ profiles:

$$u_0(z) = \frac{Gr}{6}\left\{\frac{1}{4}z - z^3\right\} \ , \tag{3.75}$$

$$T_0(x, z) = -x + \frac{Ra}{120}\left\{z^5 - \frac{5}{6}z^3 + Sz\right\} \ , \tag{3.76}$$

with $S = 7/48$ for thermally conducting boundaries and $S = 5/16$ for thermally insulating boundaries. Normal modes analysis again leads to a generalised eigenvalue problem:

$$\{u_0 ik_x - \mathbf{D}^2\}\hat{\omega}_z - (\partial_z u_0) ik_y \hat{w} = -\lambda\hat{\omega}_z \ , \tag{3.77}$$

$$\{(\partial_z^2 u_0) ik_x + \mathbf{D}^4 - u_0 ik_x \mathbf{D}^2\}\hat{w} - Grk^2\hat{\theta} = \lambda\mathbf{D}^2\hat{w} \ , \tag{3.78}$$

$$\{u_0 ik_x - \frac{1}{Pr}\mathbf{D}^2\}\hat{\theta} + \{\partial_z T_0 + i(\partial_x T_0)\frac{k_x}{k^2}\partial_z\}\hat{w} + i(\partial_x T_0)\frac{k_y}{k^2}\hat{\omega}_z = -\lambda\hat{\theta} \ . \tag{3.79}$$

Here the comparison has been made for transverse modes ($k_y = 0$) at the low-Prandtl-number ($Pr < 0.01$). For both thermally conducting and thermally insulating cases the critical Grashof number is asymptotically reaching the value

$Gr_{crit} = 7930$ with decreasing Pr. Obtained results again are in an agreement with the literature [5], [7], [9].

Further comparisons for known solutions for magnetic cases will be made in the following chapters.

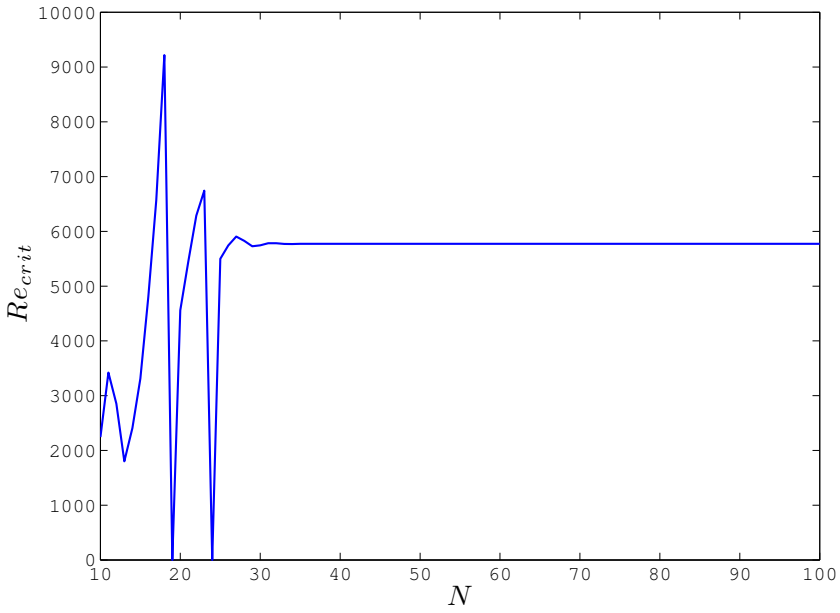

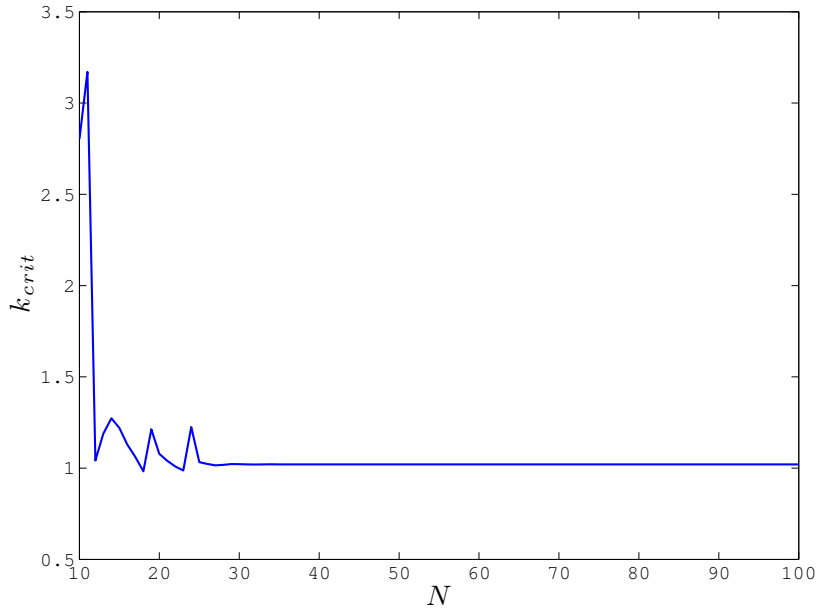

Figure 3.2: Convergence of the critical parameters values for the Poiseuille flow with increasing N

Chapter 4

Horizontal layer with vertical temperature gradient (Rayleigh-Bénard problem)

4.1 Problem formulation

Consider the problem of linear stability of an infinite horizontal fluid layer heated from below, as shown in Fig. 4.1. This is the case of Rayleigh-Bénard convection with an additional stabilizing effect of vertical magnetic field [20], [22], [34], [55]. The flow, subject to a uniform externally applied magnetic field $\mathbf{B}_0 = \mathbf{e}_z$ is studied in the presence of gravity $\mathbf{g} = -\mathbf{e}_z$ and with the assumption of no internal heat sources $Q = 0$. The applied vertical temperature gradient reads here $\partial_z T_0 = -1$.

In a laboratory implementation, the top and bottom thermally insulating boundaries are maintained at constant dimensional temperatures, T_t and $T_b > T_t$, respectively, so that $\Delta T = T_b - T_t$. To approximate the ideal infinite layer, the horizontal extent of the system is assumed to be large compared with the layer thickness, as the sidewalls vicinity strongly modifies the problem [34].

The thermally stratified fluid layer is maintained at its steady state by viscous forces, thermal diffusion and stabilizing effects of the applied magnetic field. Once the temperature difference between the walls is increased and exceeds a critical value, the stabilizing forces can no longer dissipate perturbations and the

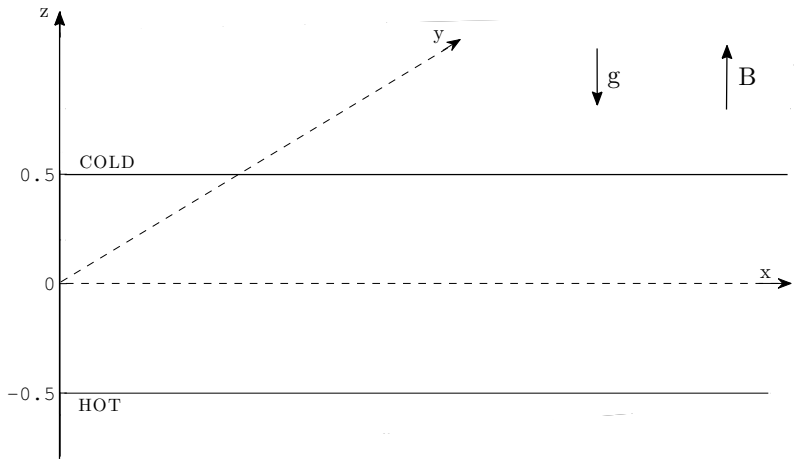

Figure 4.1: Schematic diagram of the Rayleigh-Bénard problem with a vertical magnetic field

buoyancy effects cause the fluid motion, driving the heavy fluid downward and the lighter fluid upward, alternately [20], [28], [55].

Although the Rayleigh-Bénard convection has been studied by many authors, we extend the calculations to very high values of the Hatmann number, $\sim 10^5$. The main aims are to compare the results with the first terms of the asymptotic expansions for $Ha \gg 1$, and to study the modes at high Ha for both $Pr_m = 0$ and $Pr_m \neq 0$.

The problem admits a static steady state solution $\mathbf{v}_0 = \mathbf{j}_0 = \mathbf{b}_0 = 0$, governed by the following set of equations:

$$\nabla p_0 = GrT_0\hat{e}_z \ , \tag{4.1}$$

$$\nabla^2 T_0 = 0 \ . \tag{4.2}$$

The analytical expressions for basic temperature, $T_0(z)$, and pressure, $p_0(z)$, profiles, similar to those obtained in [22] are:

$$T_0 = \frac{1}{2} - z \ , \tag{4.3}$$

$$p_0 = Gr\left\{\frac{1}{2}z - \frac{1}{2}z^2\right\} \ . \tag{4.4}$$

Here we take $T_0 = 1$ at $z = -\frac{1}{2}$ and $T_0 = 0$ at $z = +\frac{1}{2}$.

The motionless steady state is possible only in a geometry, where the applied temperature gradient and the gravity vector are aligned [30], [37]. It is apparent when the problem is interpreted in terms of the vorticity:

$$\partial_t \underline{\omega} + (\mathbf{v}\cdot\nabla)\underline{\omega} - (\underline{\omega}\cdot\nabla)\mathbf{v} = \nabla^2\underline{\omega} + Ha^2(\mathbf{B}\cdot\nabla)\mathbf{j} + Ha^2(\mathbf{j}\cdot\nabla)\mathbf{B} \ . \tag{4.5}$$

The vorticity equation has been obtained by taking the curl of the governing momentum equation (2.35). Both the pressure and the buoyancy terms disappear here: $\nabla\times\nabla p = 0$ and $\nabla\times(T_0\hat{e}_z) = 0$, allowing the motionless basic state.

The disturbance equations derived in Chapter 3 are reduced here to a simplified form:

$$\mathbf{D}^4\hat{w} + \mathbf{D}^2\partial_z\hat{b}_z - Grk^2\hat{\theta} = \lambda\mathbf{D}^2\hat{w} \ , \tag{4.6}$$

$$\mathbf{D}^2\hat{\omega}_z + \partial_z\hat{j}_z = \lambda\hat{\omega}_z \ , \tag{4.7}$$

$$\mathbf{D}^2\hat{b}_z + Ha^2\partial_z\hat{w} = \lambda Pr_m\hat{b}_z \ , \tag{4.8}$$

$$\mathbf{D}^2\hat{j}_z + Ha^2\partial_z\hat{\omega}_z = \lambda Pr_m\hat{j}_z \ , \tag{4.9}$$

$$\frac{1}{Pr}\mathbf{D}^2\hat{\theta} - (\partial_z T_0)\hat{w} = \lambda\hat{\theta} \ , \tag{4.10}$$

here, for simplicity, the following additional rescaling has been introduced:

$$\hat{b}_z \to \frac{Pr_m}{Ha^2}\hat{b}_z \quad \text{and} \quad \hat{j}_z \to \frac{1}{Ha^2}\hat{j}_z \tag{4.11}$$

The governing disturbance equations clearly decouple and two independent sets can be solved separately. Equations (4.7) and (4.9), involving disturbed

vorticity $\hat{\omega}_z$ and electric current density $\hat{j}_z$, respectively, can be neglected as these variables are functionally related to disturbed velocity $\hat{w}$ and magnetic field $\hat{b}_z$, respectively. This leads to the final set:

$$\mathbf{D}^4\hat{w} + \mathbf{D}^2\partial_z\hat{b}_z - Grk^2\hat{\theta} = \lambda\mathbf{D}^2\hat{w} \ , \tag{4.12}$$

$$\mathbf{D}^2\hat{b}_z + Ha^2\partial_z\hat{w} = \lambda Pr_m\hat{b}_z \ , \tag{4.13}$$

$$\frac{1}{Pr}\mathbf{D}^2\hat{\theta} - (\partial_z T_0)\hat{w} = \lambda\hat{\theta} \ . \tag{4.14}$$

In the above disturbance equations, the wavenumber appears only in (4.11) as k^2 which in general reads $k^2 = k_x^2 + k_y^2$. The problem, with the motionless steady state and all the basic quantities: $\mathbf{B}_0$, $\mathbf{g}$ and the applied temperature gradient, aligned along the $z-$ direction, is perfectly symmetrical in the $x-$ and $y-$ directions. However, for simplicity and in order to clearly present the result in a well-defined cross-section, we will assume here that the wavenumber lies along the $x-$ direction, $k^2 = k_x^2$ and $k_y = 0$.

In order to examine the effect of a uniform vertical magnetic field on the stability of the system considered here, the numerical linear stability results have been obtained. Characteristic laws are given by the critical Grashof number, Gr_{crit}, as a function of various parameters. Beyond those critical values, the system loses its stability. Such neutral stability results have been calculated for $Pr = 0.015$, and for each combination of parameters Pr_m and Ha. The procedure is in defining Gr_{crit} for which an eigenvalue has a real part equal to zero, by minimisation along the wavenumber k_x.

The appropriate boundary conditions, specified in Section 3.2, are applied at the top and bottom rigid boundaries.

The energy analysis is performed to establish different energy balances corresponding to specific disturbances. Energy balances obtained here confirm the thermal origin of instabilities in this problem.

In the fluctuating magnetic energy balances, for all the cases considered below, there is only one remaining contribution balancing the dissipation, corresponding

to stretching of magnetic field lines along the field: $\bar{M}_{s3} = \bar{M}_d = 1$. Due to the motionless basic state, terms in general corresponding to the energy production by advection and energy dissipation by stretching of magnetic field lines (by the shear of mean flow and along the flow) do not exist.

Similarly, in the fluctuating thermal energy balances, the only remaining contribution balancing the dissipation is the energy production by vertical transport of temperature: $\bar{\Theta}_1 = \bar{\Theta}_d = 1$.

Therefore in the following subsections, only the fluctuating kinetic energy balances are presented, where only the term corresponding to the energy production by shear of mean flow disappear, and $\bar{K}_d = \bar{K}_b + \bar{K}_m = 1$. In all the cases considered, the fluctuating kinetic energy balances show clearly that the magnetic contribution $\bar{K}_m$ always serves as a stabilizing term, and the buoyancy forces term $\bar{K}_b$ is always destabilizing.

4.2 Linear stability results: thermally conducting and electrically insulating walls

It has been already shown by other authors [22], [55], that in the case of thermally conducting and electrically insulating boundary conditions, for given values of Prandtl and for a range of magnetic Prandtl numbers, the instability sets in a stationary mode for the Hartmann numbers lower than a certain value $Ha < Ha^*$. Above that value, for $Ha > Ha^*$, the instability sets in an oscillatory mode. Obtained linear stability results are in agreement with these findings.

The neutral stability curves, calculated for $Pr = 0.015$, are shown in Fig. 4.3, giving values of the critical Grashof number, Gr_{crit}, critical wavenumber, k_{crit}, and the critical frequency, f_{crit}, as functions of Ha, for different values of Pr_m. These results have been compared with the findings in [22] for $Pr = 0.01$, as illustrated in Fig. 4.3. The numerical method applied here (presented in detail in Section 3) allowed to extend the range of considered Hartmann number up to 10^5.

The results show, that for a given value of Pr_m, the critical values of wavenumber and Grashof number increase with increasing Ha, until a transition value

$Ha*$, where an oscillatory mode takes over.

At the lowest values of Ha, the stationary instability, identical for all the magnetic Prandtl numbers considered, tends to a unique limit $Gr_{crit} = 1.139 \cdot 10^5$ and $k_{crit} = 3.115$, which is in good agreement with the results obtained by other authors [28] for $Ha = 0$. The transition to the oscillatory mode occurs at higher Hartmann numbers for decreasing Pr_m.

At the highest values of Ha, the stationary mode critical values reach asymptotic relations $Gr_{crit} = 655Ha^2$ and $k_{crit} = 1.91Ha^{1/3}$. These numerical results are in good agreement with the findings in [20], [21], [56] for $k_{crit} \gg 1$:

$$Ra_{stat} = PrGr_{crit} \simeq \pi^2 Ha^2 \ , \tag{4.15}$$

$$k_{crit} \simeq \frac{\pi^{2/3}}{2^{1/6}} Ha^{1/3} \ . \tag{4.16}$$

The transition to the oscillatory modes is accompanied by a drop in the critical wavenumber. Further increase of the Hartmann number Ha shifts the oscillatory instability onset to higher values of Gr. The wavenumber further increases above the transition point, the increase is slower for the higher values of Pr_m. The critical frequency values increase rapidly for $Ha > Ha*$, showing the dependence $f_{crit} \sim Ha$ at the highest values of the Hartman numbers considered. The asymptotic relations for the oscillatory mode for $Pr_m = 10^{-1}$ are: $Gr_{crit} = 18Ha^2$ and $k_{crit} = 0.97Ha^{1/3}$. These numerical results are again in good agreement with the findings in [21] and [57]:

$$Ra_{osc} = PrGr_{crit} \simeq \frac{Pr^2(1+Pr_m)}{Pr_m^2(1+Pr)} \pi^2 Ha^2 \ , \tag{4.17}$$

$$k_{crit} \simeq \frac{2^{1/3}\pi^{2/3}(Pr_m - Pr)^{1/3}}{(1+Pr)^{1/3}(2+Pr)^{1/3}} Ha^{1/3} \ . \tag{4.18}$$

For the higher values of magnetic Prandtl number, $Pr_m \geq 10^0$, the numerical results obtained do not allow to establish any asymptotic relations.

The process of transition from stationary to oscillatory mode is presented in Fig. 4.2, where the minimization along the wavenumber for different Hartmann

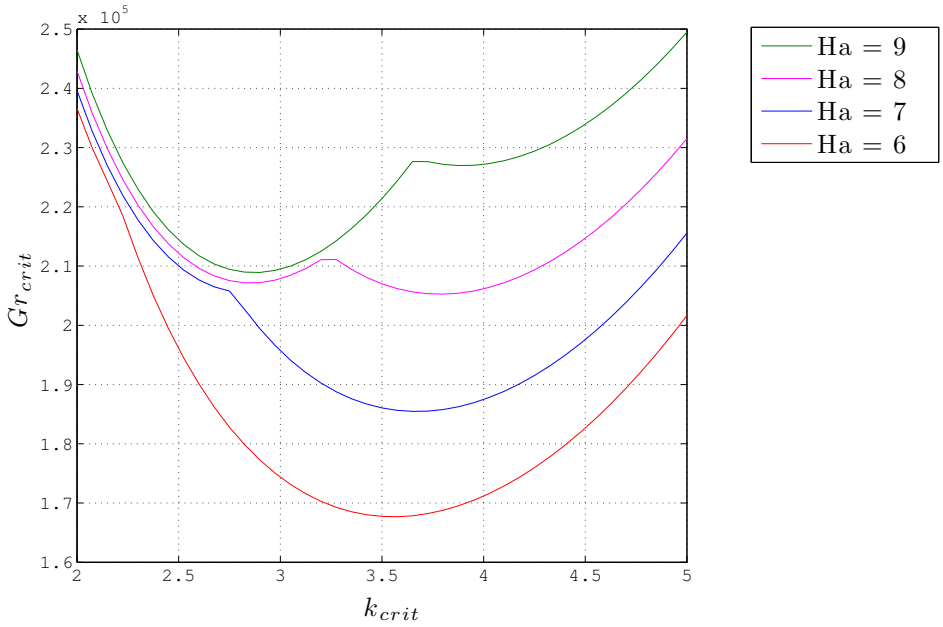

Figure 4.2: Transition process from the stationary (higher k_{crit}) to oscillatory (lower k_{crit}) mode for $Pr_m = 10^0$

number values in the vicinity of a transition point is shown. The values of Hartmann numbers, at which the transitions take place (denoted with the * symbol), are given for different magnetic Prandtl numbers in Tables 4.1-4.5.

The decrease of the Prandtl number (from $Pr = 0.015$ to $Pr = 0.01$ in Fig. 4.3) shifts the stationary instability onset, as well as the transition to the oscillatory modes, toward higher Grashof numbers. The onset of convection occurs here at $Gr_{crit} = 1.708 \cdot 10^5$, which is again in the agreement with [55], where $Ra_{crit} = 1707.8$. The stationary wavenumbers remain unchanged, while the wavenumbers of the oscillatory modes decrease slightly. The Prandtl number decrease does not affect the oscillatory modes frequencies.

The energy analysis results (Tables 4.1-4.5) shows that, for all the instabilities studied here, the ratios R_{dt} and R_{dm} decrease with the increasing Hartmann number Ha, indicating increasing importance of the thermal and magnetic effects and decreasing importance of the dynamic effects.

The kinetic energy balance is most influenced by the magnetic field at the lowest values of Pr_m ($Pr_m = 10^{-2}$ in Table 4.1). At the lowest values of the Hartmann number, the thermal and dynamic effects dominate. With the increasing magnetic field strength, the magnetic contributions quickly take over the dynamic ones. At the highest Hartmann number values, $Ha > 100$, thermal and magnetic effects dominate, while the dynamic contributions are negligible.

With the increasing values of magnetic Prandtl number, for $Pr_m = 10^{-1}$ and $Pr_m = 10^{0}$ (Tables 4.2 and 4.3, respectively), similar relations occur, with the energy balances being less influenced by the increased Ha values.

For the higher magnetic Prandtl numbers, $Pr_m \geq 10^{1}$ (Tables 4.4-4.5), the energy balances are not significantly modified by the magnetic field and the magnetic effects are the least important contributions in the energy balances for all Hartmann numbers considered.

Additionally to the neutral stability curves and the energy analysis, contour plots illustrating side views of temperature disturbance isotherms, disturbed velocity streamlines and disturbed magnetic field lines at critical conditions for different Pr_m and frequencies f are presented in Fig. 4.4-4.6. For the lowest values of Pr_m considered ($Pr_m = 10^{-2}$ in Fig. 4.4), the cell size decreases with increasing Ha, which corresponds to the wavenumber increase. With the increasing Pr_m, the cell size is less affected by the magnetic field strength.

For the stationary modes, disturbances isotherms, streamlines and magnetic field lines are symmetric with respect to a vertical centre axis of a cell. For the oscillatory modes, there is no such axis of symmetry.

Ha	frequency	$\bar{K}_b$	$\bar{K}_m$	R_{dt}	R_{dm}	R_{tm}
2	0	1.06	-0.06	0.95	17.9	18.8
10	0	1.95	-0.95	0.51	1.05	2.06
100	0	11.7	-10.7	0.09	0.09	1.00
500	0	38.8	-37.8	0.03	0.03	1.00
1000	0	63.9	-62.9	0.02	0.02	1.00

Table 4.1: Energy balances for the thermally conducting and electrically insulating walls, $Pr_m = 10^{-2}$

Ha	frequency	$\bar{K}_b$	$\bar{K}_m$	R_{dt}	R_{dm}	R_{tm}
2	0	1.06	-0.06	0.95	17.9	18.8
10	0	1.95	-0.95	0.51	1.05	2.06
*33.5	0	4.99	-3.99	0.20	0.25	1.25
*33.5	236.3	7.14	-6.14	0.14	0.16	1.16
100	969.4	7.04	-6.04	0.14	0.17	1.21
500	4922	8.60	-7.60	0.12	0.13	1.08
1000	9736	9.67	-8.67	0.10	0.12	1.20

Table 4.2: Energy balances for the thermally conducting and electrically insulating walls, $Pr_m = 10^{-1}$

Ha	frequency	$\bar{K}_b$	$\bar{K}_m$	R_{dt}	R_{dm}	R_{tm}
2	0	1.06	-0.06	0.95	17.9	18.8
*8.1	0	1.69	-0.69	0.59	1.44	2.44
*8.1	14.02	1.77	-0.77	0.57	1.30	2.30
10	25.9	1.78	-0.78	0.56	1.28	2.29
100	369.2	2.02	-1.02	0.49	0.98	2.00
500	1752.6	2.11	-1.11	0.47	0.91	1.94
1000	3424.9	2.15	-1.15	0.47	0.89	1.89

Table 4.3: Energy balances for the thermally conducting and electrically insulating walls, $Pr_m = 10^{0}$

Ha	frequency	$\bar{K}_b$	$\bar{K}_m$	R_{dt}	R_{dm}	R_{tm}
2	0	1.06	-0.06	0.95	17.9	18.8
*2.4	0	1.08	-0.08	0.92	12.2	13.2
*2.4	0.54	1.08	-0.08	0.92	12.08	13.08
10	12.4	1.13	-0.13	0.88	7.61	8.65
100	136.7	1.41	-0.41	0.71	2.44	3.44
500	614.2	1.65	-0.65	0.61	1.55	2.54
1000	1161.2	1.69	-0.69	0.59	1.47	2.49

Table 4.4: Energy balances for the thermally conducting and electrically insulating walls, $Pr_m = 10^1$

Ha	frequency	$\bar{K}_b$	$\bar{K}_m$	R_{dt}	R_{dm}	R_{tm}
2	0.7	1.01	-0.01	0.99	90.0	91.0
10	4.5	1.03	-0.03	0.97	36.2	37.4
100	50.1	1.09	-0.09	0.92	11.2	12.1
500	250.2	1.27	-0.27	0.79	3.70	4.68
1000	485.4	1.43	-0.43	0.70	2.38	3.40

Table 4.5: Energy balances for the thermally conducting and electrically insulating walls, $Pr_m = 10^2$

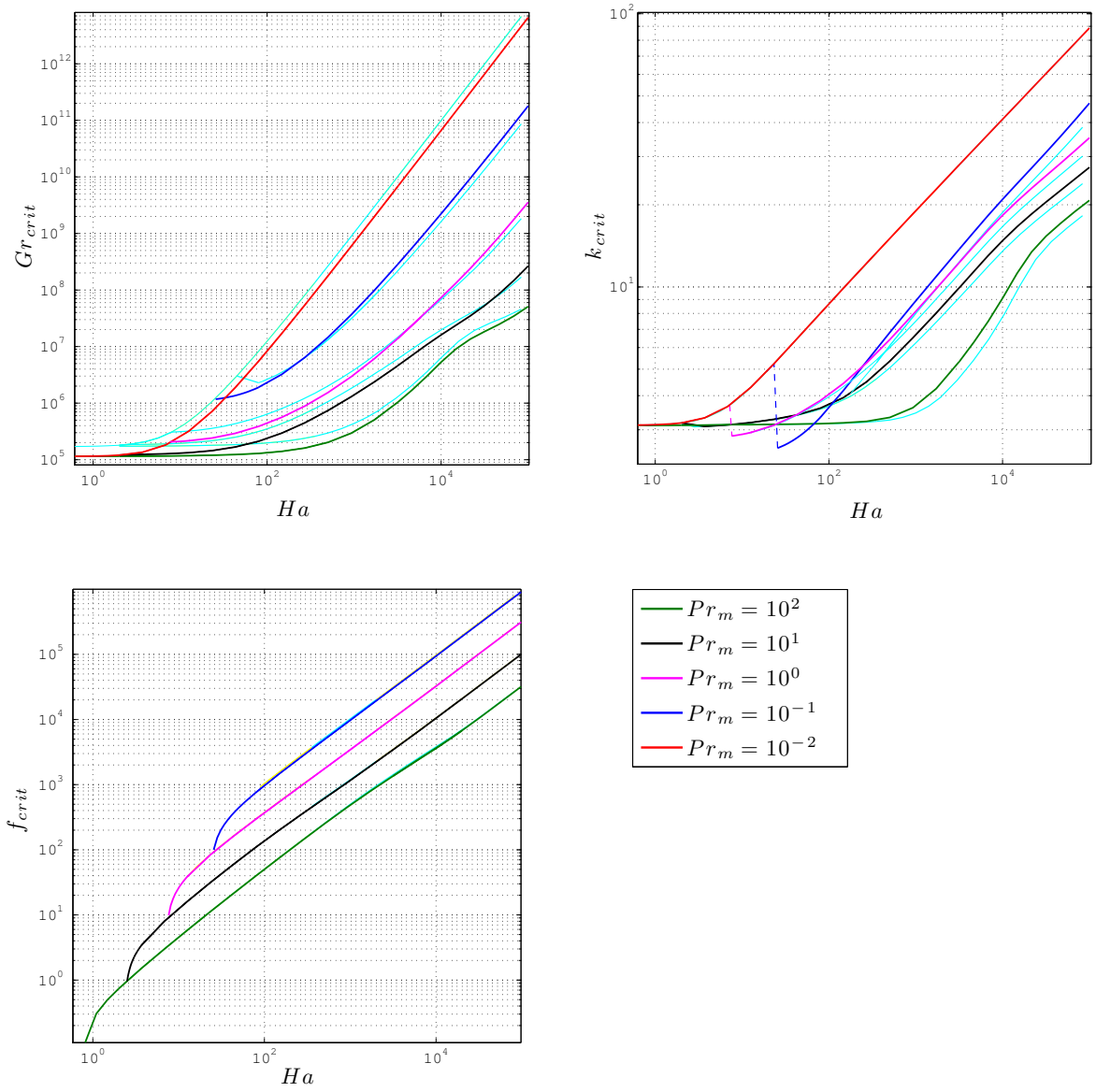

Figure 4.3: Critical values of parameters for $Pr = 0.015$. Thermally conducting and electrically insulating walls. Additional cyan lines represent respective curves for $Pr = 0.01$.

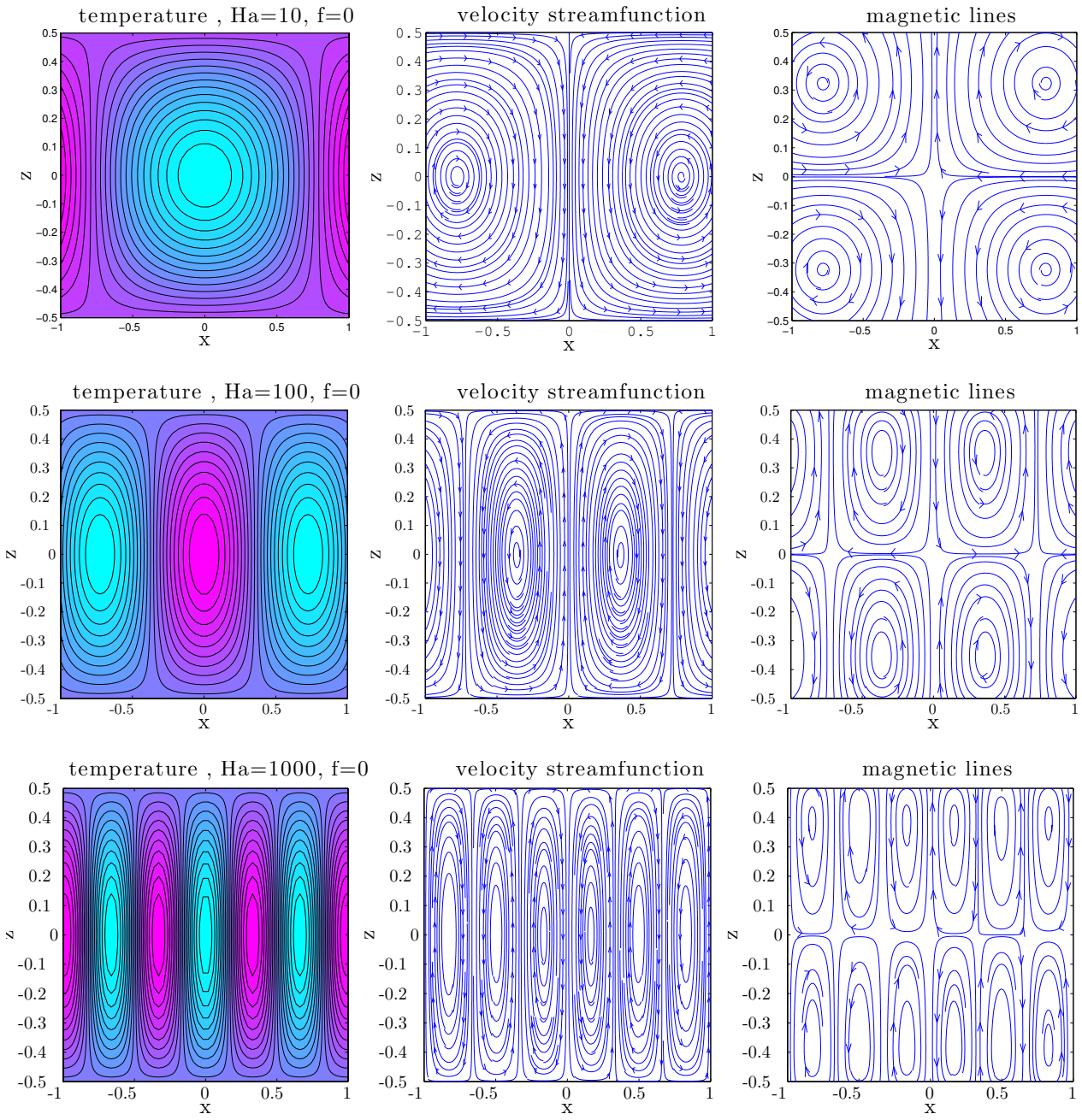

Figure 4.4: Contour plots of disturbance isotherms (left), disturbed velocity streamlines (center) and disturbed magnetic field lines (right) for the thermally conducting and electrically insulating walls, $Pr_m = 10^{-2}$

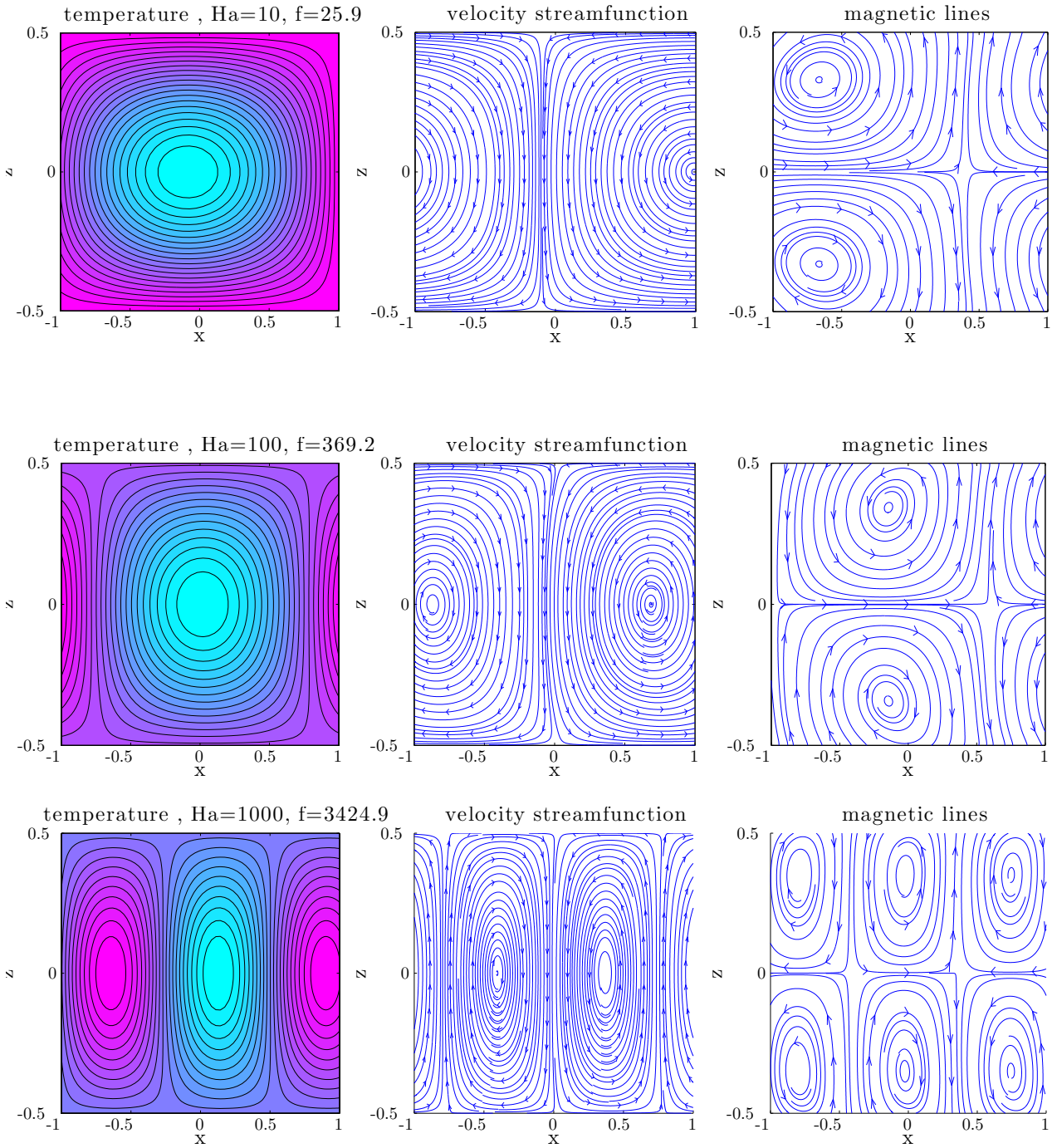

Figure 4.5: Contour plots of disturbance isotherms (left), disturbed velocity streamlines (center) and disturbed magnetic field lines (right) for the thermally conducting and electrically insulating walls, $Pr_m = 10^0$

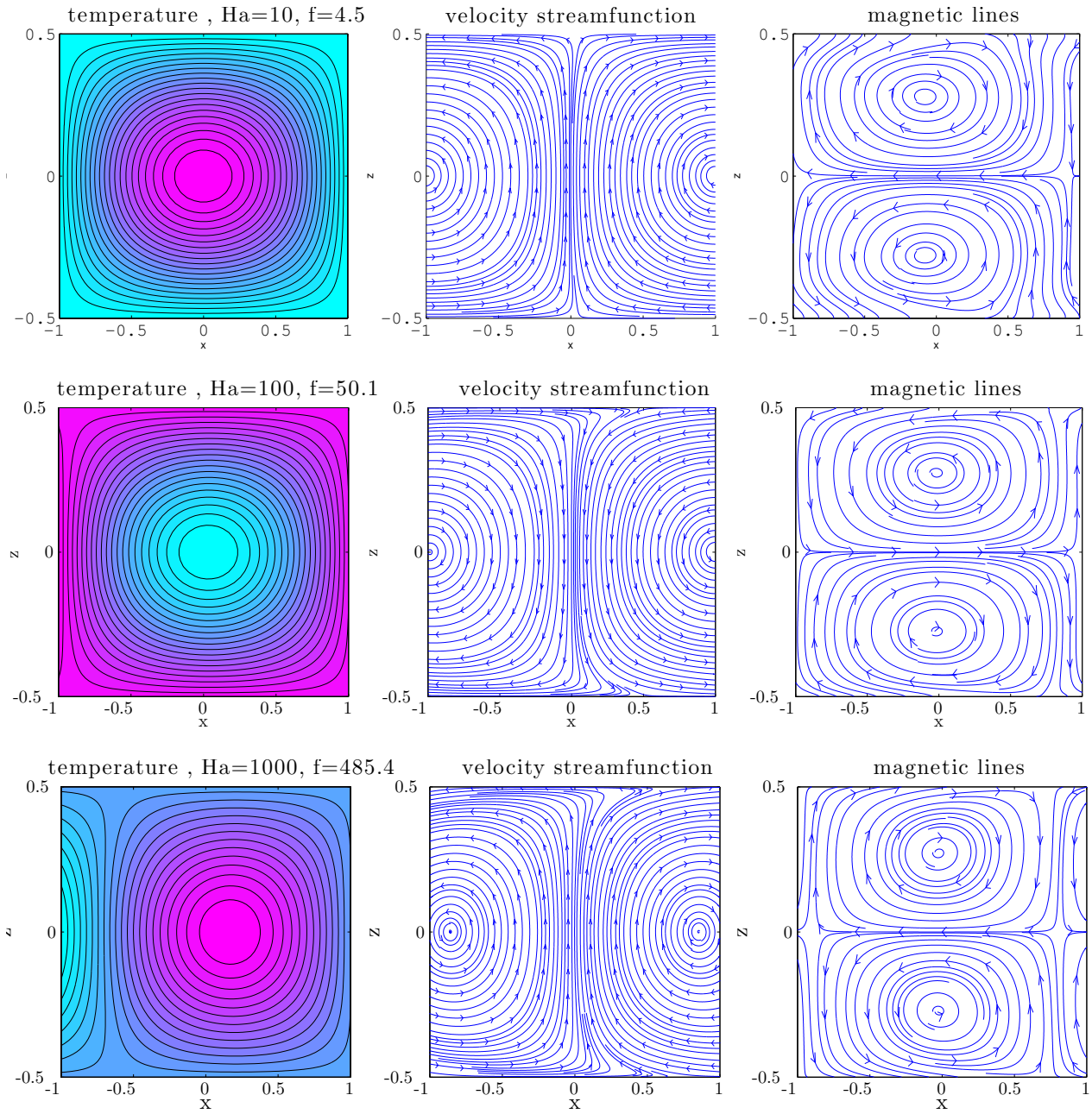

Figure 4.6: Contour plots of disturbance isotherms (left), disturbed velocity streamlines (center) and disturbed magnetic field lines (right) for the thermally conducting and electrically insulating walls, $Pr_m = 10^2$

4.3 Linear stability results: thermally conducting and electrically conducting walls

The problem of buoyancy driven instability in the presence of a vertical magnetic field have been extended to the case of thermally conducting and electrically conducting walls. The neutral stability curves, calculated again for $Pr = 0.015$, are shown in Fig. 4.7. in comparison to the case of thermally conducting and electrically insulating boundaries.

The results show, that the flow experience very similar behavior for both cases of electromagnetic boundary conditions. For low Ha, the instability sets in a stationary mode, identical with the electrically insulating walls case. The transition from stationary to oscillatory mode is observed here at higher Hartmann number values for all the considered magnetic Prandtl numbers (Tables 4.6-4.10).

For $Pr_m = 10^{-1}$ both the critical frequency and the critical Grashof number curves of the oscillatory mode lie above the respective electrically insulating boundaries case curves.

For the higher magnetic Prandtl numbers, $Pr_m \geq 10^0$, the critical frequency and the critical Grashof numbers are lower than in the case of electrically insulating boundaries, until a possible crossing point and high Hartmann numbers.

The main difference between the two cases is an asymptotic behavior of the oscillatory modes in the case of electrically conducting walls, while for the electrically insulating boundaries such regularities can be observed only for a small range of magnetic Prandtl numbers, $Pr_m < 10^0$. For the electrically conducting boundaries the following asymptotic relations have been concluded: $Gr_{crit} \simeq 20Ha^2$ and $k_{crit} \simeq 1.15Ha^{1/3}$ for $Pr_m = 10^{-1}$, $Gr_{crit} \simeq 0.37Ha^2$ and $k_{crit} \simeq 0.73Ha^{1/3}$ for $Pr_m = 10^0$, $Gr_{crit} \simeq 0.02Ha^2$ and $k_{crit} \simeq 0.45Ha^{1/3}$ for $Pr_m = 10^1$.

The results show that for $Pr_m \leq 10^{-2}$ and for $Pr = 0.015$, the oscillatory magnetic mode does not appear for the values of Ha up to 10^5. This means that for liquid metals, for which $Pr_m \sim 10^{-5} - 10^{-7}$ the mode of instability is always stationary for all boundary conditions considered here.

The energy analysis results (Tables 4.6-4.10) show, that, while the stationary modes energy balances remain almost identical for both cases of electromagnetic boundary conditions, the oscillatory modes energy balances are much less affected

by the increasing magnetic field strength in the case of electrically conducting walls.

The side views of temperature disturbance isotherms, disturbed velocity streamlines and disturbed magnetic field lines are presented in Fig. 4.8-4.10, showing the magnetic Prandtl number influence on the instability cross-sections. These results show, that for the oscillatory modes in the case of electrically conducting boundaries, the symmetry with respect to a vertical centre axis of a cell is less disturbed with the increased values of Pr_m and Ha than for the case of electrically insulating walls (Fig. 4.4-4.6).

Ha	frequency	$\bar{K}_b$	$\bar{K}_m$	R_{dt}	R_{dm}	R_{tm}
2	0	1.06	-0.06	0.95	17.9	18.9
10	0	1.95	-0.95	0.51	1.06	2.06
100	0	11.7	-10.7	0.09	0.09	1.10
500	0	38.5	-37.5	0.03	0.03	1.04
1000	0	62.5	-61.5	0.02	0.02	1.03

Table 4.6: Energy balances for the thermally conducting and electrically conducting walls, $Pr_m = 10^{-2}$

Ha	frequency	$\bar{K}_b$	$\bar{K}_m$	R_{dt}	R_{dm}	R_{tm}
2	0	1.06	-0.06	0.95	17.9	18.9
10	0	1.95	-0.95	0.51	1.06	2.06
*61.2	0	8.02	-7.02	0.12	0.14	1.15
*61.2	435.2	17.9	-16.9	0.06	0.06	1.07
100	1023.5	20.5	-19.5	0.05	0.05	1.06
500	5523.7	20.7	-19.7	0.05	0.05	1.06
1000	10713.8	19.3	-18.3	0.05	0.06	1.08

Table 4.7: Energy balances for the thermally conducting and electrically conducting walls $Pr_m = 10^{-1}$

Ha	frequency	$\bar{K}_b$	$\bar{K}_m$	R_{dt}	R_{dm}	R_{tm}
2	0	1.06	-0.06	0.95	17.9	18.9
10	0	1.95	-0.95	0.51	1.06	2.06
*11	0	2.09	-1.09	0.48	0.92	1.93
*11	25.2	2.33	-1.33	0.43	0.75	1.75
100	502.6	2.49	-1.49	0.40	0.68	1.68
500	2257.4	2.62	-1.62	0.38	0.62	1.63
1000	4234.5	2.61	-1.61	0.38	0.63	1.66

Table 4.8: Energy balances for the thermally conducting and electrically conducting walls $Pr_m = 10^0$

Ha	frequency	$\bar{K}_b$	$\bar{K}_m$	R_{dt}	R_{dm}	R_{tm}
2	0	1.06	-0.06	0.95	17.9	18.9
*3.1	0	1.13	-0.13	0.88	7.71	8.71
*3.1	0.91	1.13	-0.13	0.88	7.50	8.51
10	15.6	1.14	-0.14	0.88	7.06	8.06
100	164.5	1.14	-0.14	0.88	7.04	8.05
500	789.1	1.15	-0.15	0.87	6.74	7.75
1000	1502.5	1.16	-0.16	0.87	6.55	7.57

Table 4.9: Energy balances for the thermally conducting and electrically conducting walls $Pr_m = 10^1$

Ha	frequency	$\bar{K}_b$	$\bar{K}_m$	R_{dt}	R_{dm}	R_{tm}
2	0.9	1.01	-0.01	0.99	72.6	73.6
10	5.2	1.02	-0.02	0.99	64.4	65.4
100	52.3	1.02	-0.02	0.99	67.1	68.1
500	258.9	1.01	-0.01	0.99	70.5	71.5
1000	509.6	1.01	-0.01	0.99	69.4	70.4

Table 4.10: Energy balances for the thermally conducting and electrically conducting walls $Pr_m = 10^2$

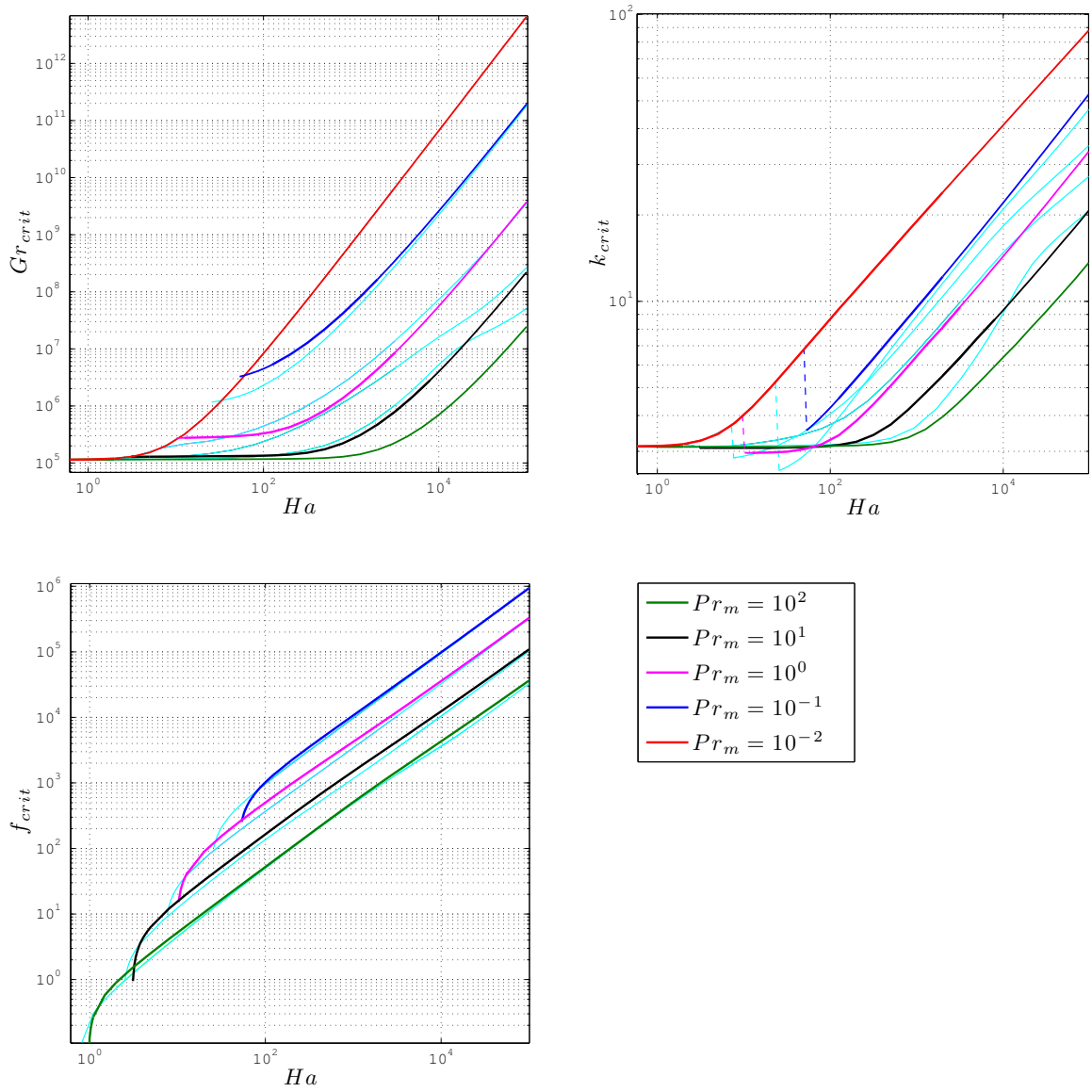

Figure 4.7: Critical values of parameters for $Pr = 0.015$. Thermally conducting and electrically conducting walls. Additional cyan lines represent respective curves for electrically insulating boundaries.

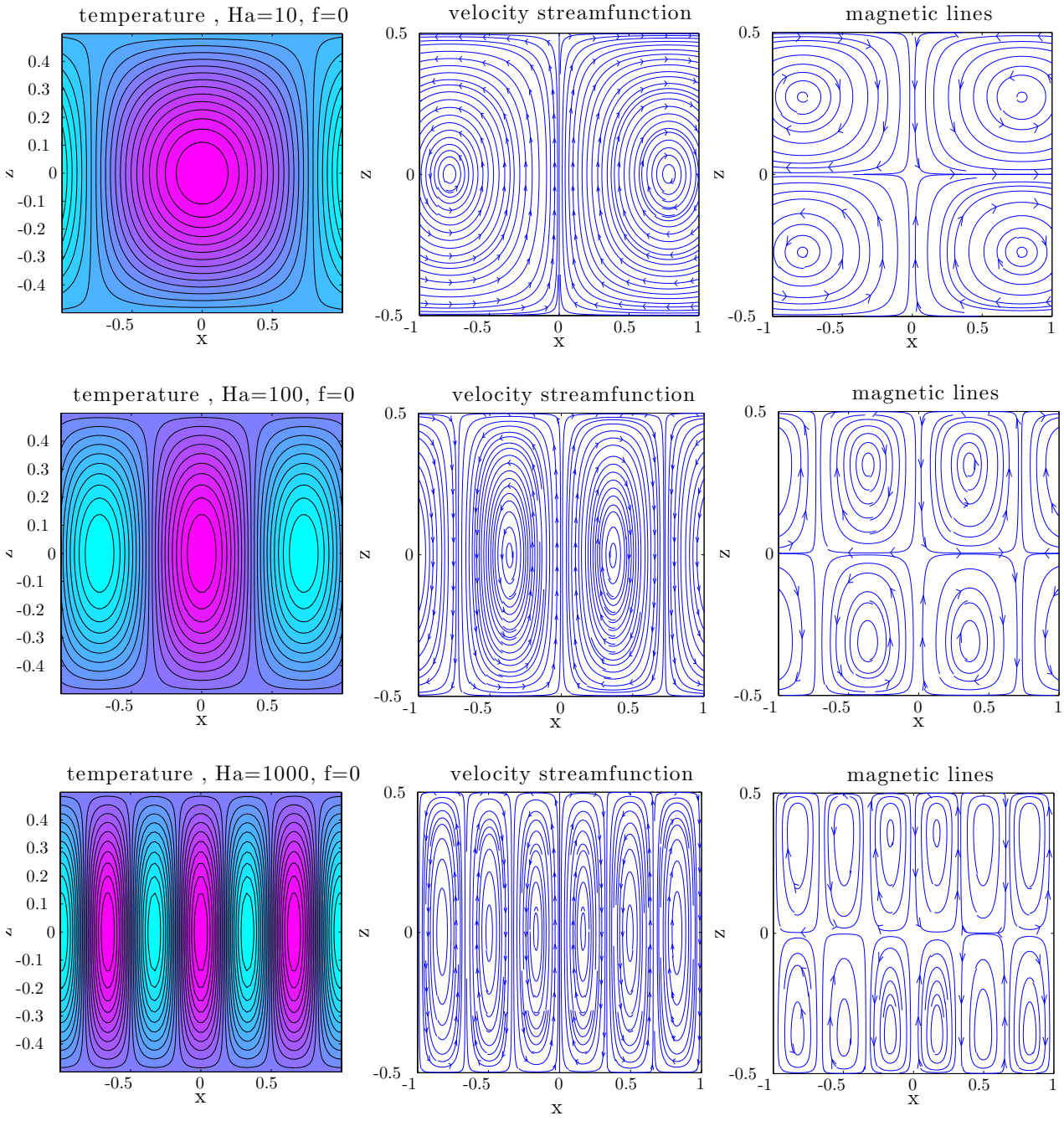

Figure 4.8: Contour plots of disturbance isotherms (left), disturbed velocity streamlines (center) and disturbed magnetic field lines (right) for the thermally conducting and electrically conducting walls, $Pr_m = 10^{-2}$

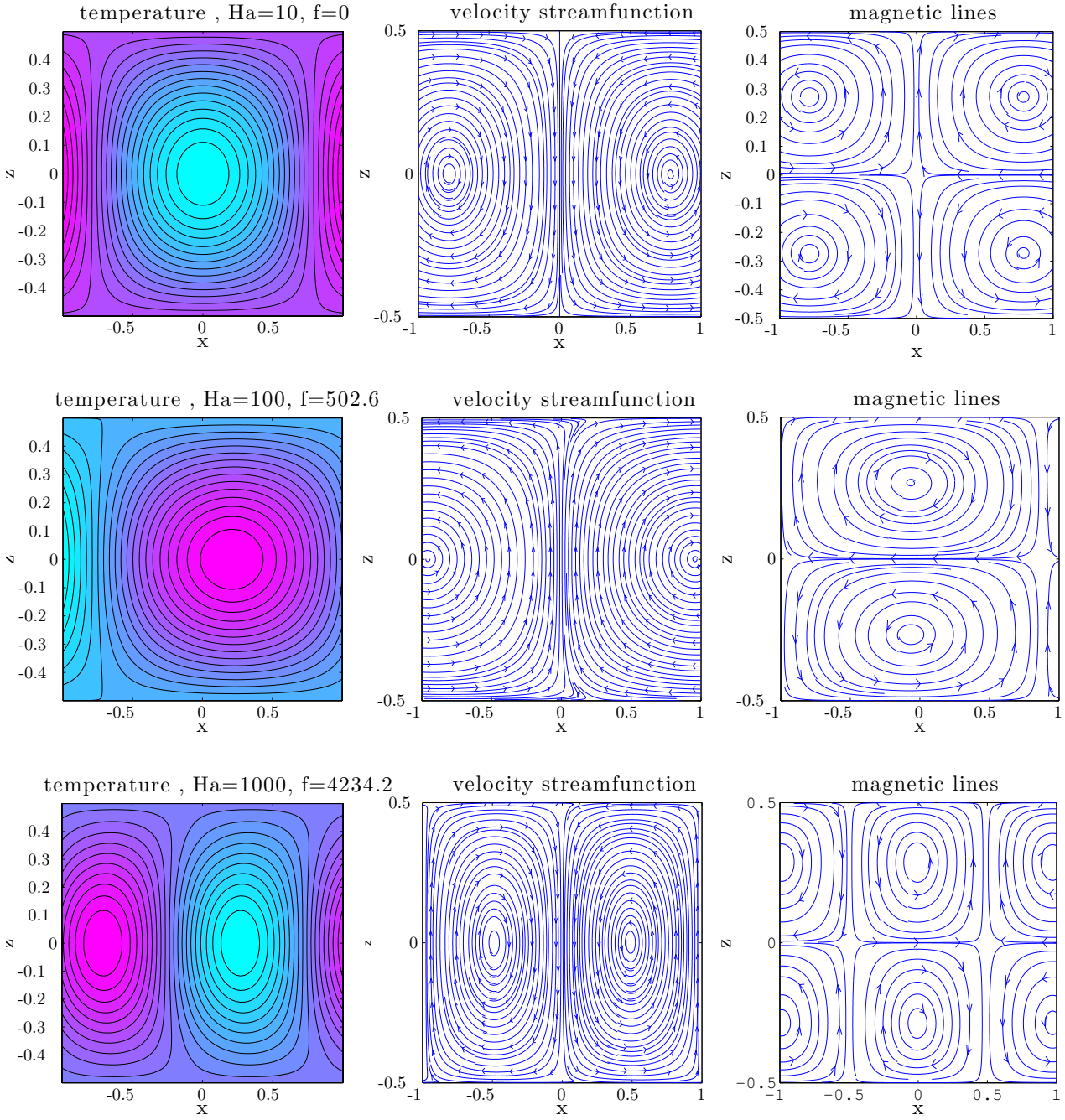

Figure 4.9: Contour plots of disturbance isotherms (left), disturbed velocity streamlines (center) and disturbed magnetic field lines (right) for the thermally conducting and electrically conducting walls, $Pr_m = 10^0$

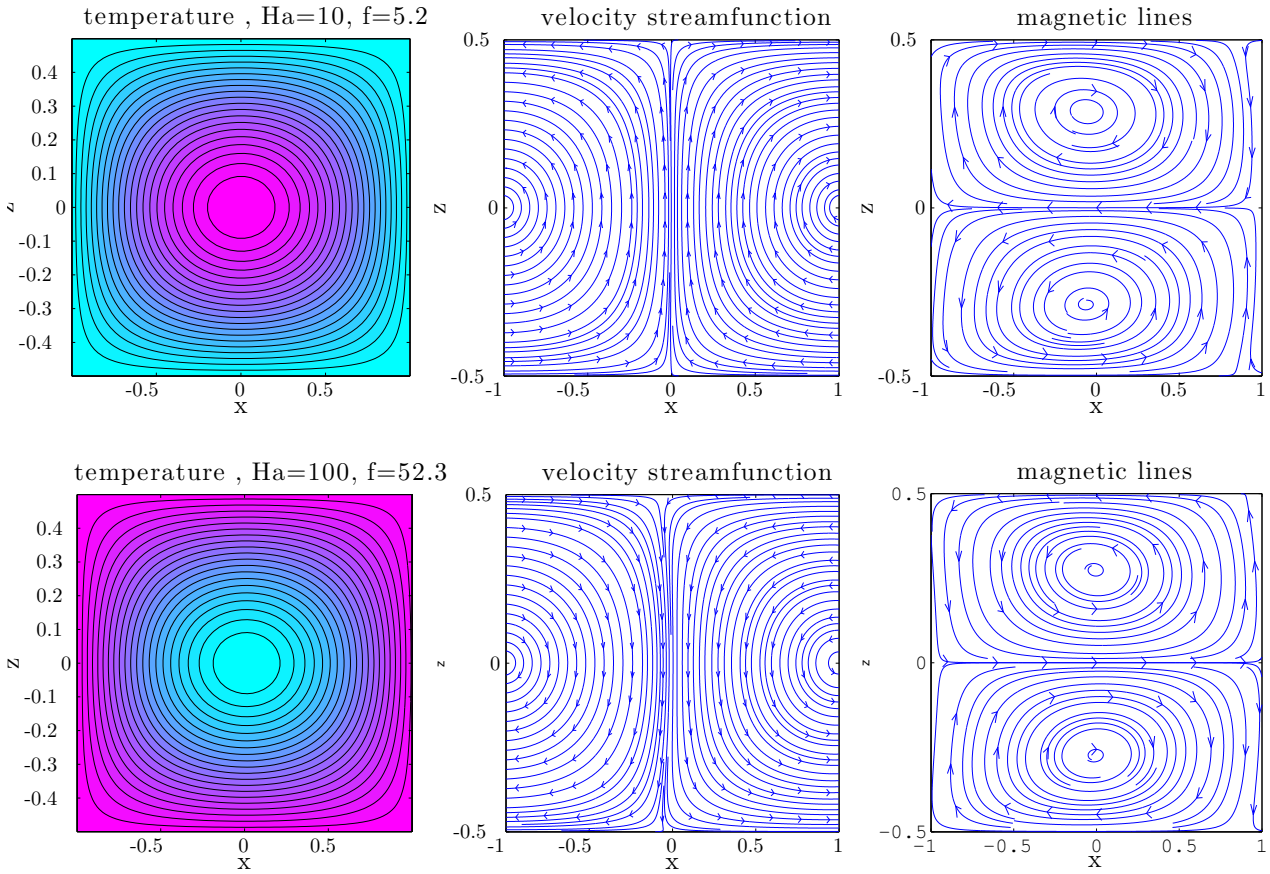

Figure 4.10: Contour plots of disturbance isotherms (left), disturbed velocity streamlines (center) and disturbed magnetic field lines (right) for the thermally conducting and electrically conducting walls, $Pr_m = 10^2$

Chapter 5

Horizontal layer with longitudinal temperature gradient

5.1 Problem formulation

Consider the problem of linear stability of buoyancy-driven convection in a horizontal layer. The flow is induced by axial heating in a fluid layer bounded by infinite horizontal rigid surfaces, as shown in Fig. 5.1. The flow, subject to a uniform, vertical magnetic field $\mathbf{B}_0 = \mathbf{e}_z$ is studied in the presence of gravity $\mathbf{g} = -\mathbf{e}_z$ and with the assumption of no internal heat sources $Q = 0$.

Constant horizontal temperature gradient $\partial_x T_0 = -1$, which induces a steady circulation, is applied. In a laboratory implementation, two opposite vertical boundaries are set at different temperatures and the horizontal gradient drives the fluid upward near the hot and downward near the cold wall.

The problem has a steady flow solution (Fig. 5.2) whereby $\mathbf{u}_0 = [u_0(z), 0, 0]$, $\mathbf{b}_0 = [b_0, 0, 0]$ and $T_0 = -x + \theta_0$. Then the problem for u_0, b_0, p_0 and T_0 is, as follows from (3.1)-(3.3), governed by the following set of equations:

$$\partial_x p_0 = u_0'' + \frac{Ha^2}{Pr_m} b_0' \ , \tag{5.1}$$

$$\partial_z p_0 = GrT_0 - \frac{Ha^2}{Pr_m} b_0 b_0' \ , \tag{5.2}$$

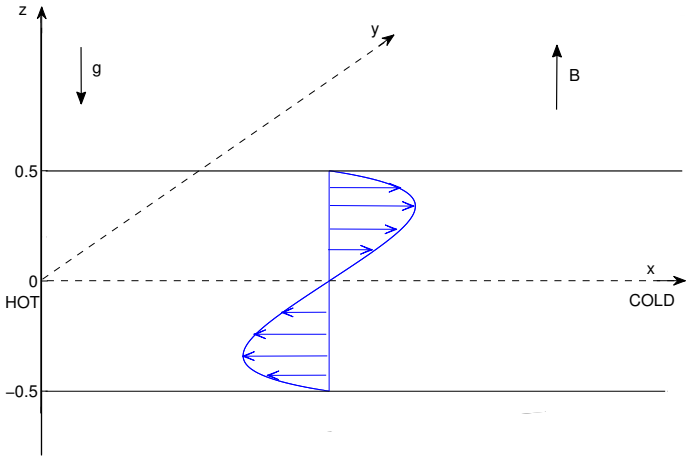

Figure 5.1: Schematic diagram of the buoyant convective flow with horizontal temperature gradient and a vertical magnetic field

$$b_0'' = -Pr_m u_0' \ , \tag{5.3}$$

$$-u_0 = \frac{1}{Pr}\partial_z^2 T_0 \ . \tag{5.4}$$

The analytical expressions for the basic velocity $u_0(z)$, magnetic field $b_0(z)$ and temperature $T_0(x,z)$ profiles, obtained first in [58] are:

$$u_0 = \frac{Gr}{Ha^2}\left\{z - \frac{\sinh(Haz)}{2\sinh(0.5Ha)}\right\} \ , \tag{5.5}$$

$$b_0 = \frac{Pr_m Gr}{Ha^2}\left\{\frac{\cosh(Haz)}{2Ha\sinh(0.5Ha)} - \frac{1}{2}z^2 + \frac{1}{8} - \frac{\cosh(0.5Ha)}{2Ha\sinh(0.5Ha)}\right\} \ , \tag{5.6}$$

$$T_0 = -x + \frac{Ra}{Ha^2}\left\{\frac{\sinh(Haz)}{2Ha^2\sinh(0.5Ha)} - \frac{1}{6}z^3 + Dz\right\} \ , \tag{5.7}$$

where the constant D is:

$D = \frac{1}{24} - \frac{1}{Ha^2}$ for thermally conducting walls

$D = \frac{1}{8} - \frac{\cosh(0.5Ha)}{2Ha\sinh(0.5Ha)}$ for thermally insulating walls

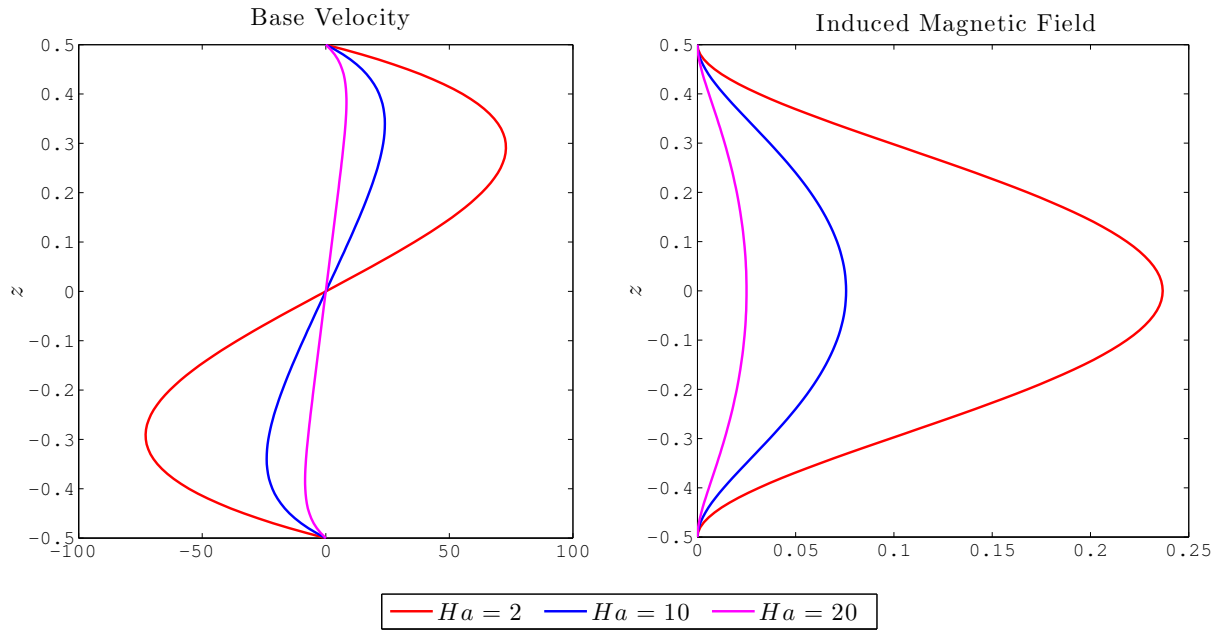

Figure 5.2: Steady mean flow profiles for $Pr = 0.1$ and $Gr = 10^4$

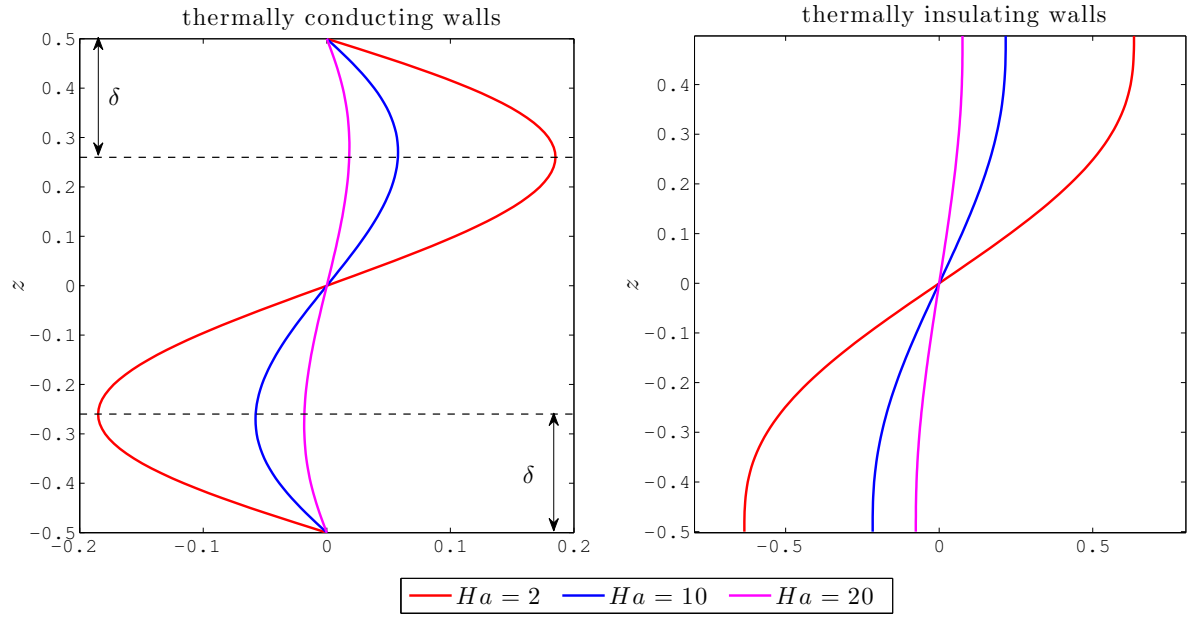

Figure 5.3: Steady mean flow temperature profiles for $Pr = 0.1$ and $Gr = 10^4$. For the thermally conducting boundaries (left), unstable thermal stratification zones near the horizontal boundaries are denoted by δ

At high values of the Hartmann number, $Ha \gg 1$, since $e^{-Ha} \to 0$, the full basic profiles (5.5)-(5.7) can be replaced by the following asymptotic profiles:

$$u_0 \simeq \frac{Gr}{Ha^2}\left\{z - \frac{1}{2}\Big(e^{Ha(z-0.5)} - e^{-Ha(z+0.5)}\Big)\right\} , \tag{5.8}$$

$$b_0 \simeq \frac{Pr_m Gr}{Ha^2}\left\{\frac{1}{2Ha}\Big(e^{Ha(z-0.5)} + e^{-Ha(z+0.5)}\Big) - \frac{1}{2}z^2 + \frac{1}{8} - \frac{1}{2Ha}\right\} , \tag{5.9}$$

$$T_0 \simeq -x + \frac{Ra}{Ha^2}\left\{\frac{1}{2Ha^2}\Big(e^{Ha(z-0.5)} - e^{-Ha(z+0.5)}\Big) - \frac{1}{6}z^3 + Dz\right\} , \tag{5.10}$$

with:
$D = \frac{1}{24} - \frac{1}{Ha^2}$ for thermally conducting walls
$D = \frac{1}{8} - \frac{1}{2Ha}$ for thermally insulating walls

The velocity and temperature profiles do not depend on the magnetic Prandtl number and thus are identical for the case of inductionless approximation and for the case of the non-zero magnetic Prandtl number.

The disturbance equations derived in Chapter 3 apply here with a number of simplifications, and are:

$$\{\mathbf{D}^4 - u_0 ik_x \mathbf{D}^2 + u_0'' ik_x\}\hat{w}$$
$$+\frac{Ha^2}{Pr_m}\{b_0 ik_x \mathbf{D}^2 - b_0'' ik_x + \mathbf{D}^2\partial_z\}\hat{b}_z - Grk^2\hat{\theta} = \lambda \mathbf{D}^2\hat{w} , \tag{5.11}$$

$$\{\mathbf{D}^2 - u_0 ik_x\}\hat{\omega}_z + u_0' ik_y\hat{w} - \frac{Ha^2}{Pr_m}b_0' ik_y\hat{b}_z + Ha^2\{\partial_z + b_0 ik_x\}\hat{j}_z = \lambda\hat{\omega}_z , \tag{5.12}$$

$$\{\frac{1}{Pr_m}\mathbf{D}^2 - u_0 ik_x\}\hat{b}_z + \{b_0 ik_x + \partial_z\}\hat{w} = \lambda\hat{b}_z , \tag{5.13}$$

$$\{\mathbf{D}^2 - Pr_m u_0 ik_x\}\hat{j}_z + \{b_0 ik_x + \partial_z\}\hat{\omega}_z + b_0' ik_y \hat{w}$$
$$-u_0' ik_y \hat{b}_z = \lambda Pr_m \hat{j}_z \ , \tag{5.14}$$

$$\{\frac{1}{Pr}\mathbf{D}^2 - u_0 ik_x\}\hat{\theta} - i(\partial_x T_0)\frac{k_y}{k^2}\hat{\omega}_z - \{\partial_z T_0 + i(\partial_x T_0)\frac{k_x}{k^2}\partial_z\}\hat{w} = \lambda\hat{\theta} \ , \tag{5.15}$$

In order to examine the effect of a uniform vertical magnetic field on the stability of buoyant flows for different boundary conditions, the numerical linear stability results have been obtained for $Pr = 0.015$. As in Chapter 4, the critical Grashof number, for which an eigenvalue has a real part equal to zero is defined by minimization along either k_x and k_y, depending on either transverse or longitudinal rolls are considered.

The appropriate boundary conditions, specified in Section 3.2, are applied at the top and bottom rigid boundaries.

5.2 $Pr_m = 0$ linear stability results

The inductionless approximation leads to further simplification of the governing disturbance equations, reducing the system to:

$$\{\mathbf{D}^4 - u_0 ik_x\mathbf{D}^2 + u_0'' ik_x - Ha^2\partial_z^2\}\hat{w} - Grk^2\hat{\theta} = \lambda\mathbf{D}^2\hat{w} \ , \tag{5.16}$$

$$\{\mathbf{D}^2 - u_0 ik_x - Ha^2\}\hat{\omega}_z + u_0' ik_y\hat{w} - Ha^2k^2\hat{\phi} = \lambda\hat{\omega}_z \ , \tag{5.17}$$

$$\{\frac{1}{Pr}\mathbf{D}^2 - u_0 ik_x\}\hat{\theta} + i\frac{k_y}{k^2}\hat{\omega}_z - \{\theta_0' - i\frac{k_x}{k^2}\partial_z\}\hat{w} = \lambda\hat{\theta} \ . \tag{5.18}$$

Here the electric potential ϕ is related to the vorticity $\underline{\omega}$ through (2.46), which leads to the following disturbance equation:

$$\hat{\omega}_z = \mathbf{D}^2\hat{\phi} \ , \tag{5.19}$$

with the following boundary conditions for the disturbed electric potential:

$\hat{\phi} = 0$ at $z = \pm 0.5$ for electrically conducting walls,
$\partial_z \hat{\phi} = 0$ at $z = \pm 0.5$ for electrically insulating walls.

It has been shown by a number of authors [44], [45], that the two major branches of instability at relatively low values of Hartmann numbers are stationary transverse and oscillatory longitudinal rolls. Transverse rolls have their axes perpendicular to the main flow and in this case the two-dimensional flow structure persists. In the case of the longitudinal rolls, with their axes parallel to the base flow, a global three-dimensional flow structure is observed. The origin of these two modes is explained as the Prandtl number is decreased [28]. For $Pr \to 0$, the momentum an temperature equations can be decoupled, with the latter taking the form $\nabla^2 T = 0$. The two-dimensional stationary mode tends then to a unique limit indicating a hydrodynamic origin of the disturbance, which appears at the inflection point of the basic velocity profile between the streams in the $x-$ and $-x-$ directions. The three-dimensional oscillatory mode disappears as a result of its thermal origin.

In the following, together with the numerical stability results, the influence of the magnetic field strength and boundary conditions on the thermal and kinetic energy balances are considered. The dimensionless ratio of the respective dissipation terms R_{dt} indicating the origin of instabilities clearly shows that the stationary modes at low Hartmann numbers, both transverse and longitudinal, have always dynamical origin while all the instabilities occurring at higher Hartmann numbers ($Ha \geq 60$) for thermally conducting walls are of thermal origin.

The kinetic energy balances for all the instabilities considered show that the magnetic energy contributions are always serving as stabilizing terms, regardless of the instability type or the boundary conditions. The stronger the magnetic field applied, the stronger stabilizing effect is observed.

For all the instabilities of the thermal origin considered here, the ratio R_d decreases with the increase of the Hartmann number, indicating the increasing influence of thermal effects.

5.2.1 Transverse modes

5.2.1.1 Transverse modes, thermally conducting boundaries

The results show that the electrical boundary conditions have no effect on the transverse instabilities. As has been shown in [44], it is confirmed here that the transverse stationary two-dimensional mode is the most dangerous at low Hartman numbers, remaining a dominant instability for the values up to $Ha \simeq 9$ (Fig. 5.4), where the longitudinal mode becomes more unstable (Fig. 5.8). The magnetic field stabilises this mode very efficiently by eliminating the inflection point in the velocity profile and by creating a constant shear in the core, similar to the Couette flow [46]. Thus the critical Grashof number increases rapidly before the instability disappearance at $Ha \simeq 16$, while the wavenumber in this case is slowly decreasing with the increasing Ha until reaching the minimum $k_x \simeq 0.96$ at $Ha \simeq 12.5$.

The side views of temperature disturbance isotherms and disturbed velocity streamlines, shown in Fig. 5.5, illustrate clearly the dynamical origin of the instabilities, located at the basic velocity inflection point.

The thermal mode of the transverse oscillatory instability appears at the higher value of the Hartmann number $Ha \simeq 29$ (Fig. 5.4), as a result of unstable thermal stratification zones (Fig. 5.3). Contour plots of disturbed temperature isotherms and velocity streamlines (Fig. 5.6) show clearly, that these instabilities are located near the horizontal boundaries, indicating their thermal origin.

For the thermal oscillatory modes, after a short decrease of Gr_{crit} with the increasing Ha, the further increase of the magnetic field strength shifts the instability onset to high Grashof numbers. The wavenumbers rapidly increase up to high values, indicating a strong decrease of the size of the marginal cells.

The transverse mode of the thermal origin occurs at high frequency, which first rapidly decreases before reaching its minimum at $Ha \simeq 91.4$ and then increases with increasing Ha.

The critical values of parameters reach asymptotic relations at the highest values of the Hartmann number $Ha > 10^4$, namely: $Gr_{crit} = 4155Ha^2$, $k_{crit} = 4.45Ha^{1/3}$ and $f = 7395Ha^{1/3}$.

In the kinetic energy balances for the low-Hartmann number stationary trans-

verse instabilities (Table 5.1), the shear of mean flow contribution $\bar{K}_f$ is the only positive term corresponding to destabilizing effects. Both magnetic $\bar{K}_m$ and buoyancy forces $\bar{K}_b$ terms serve here as stabilizing contributions.

The thermal energy balances are strongly modified by the increasing magnetic field strength. Both terms corresponding to the production of fluctuating thermal energy by vertical and horizontal transport of temperatures are positive, indicating destabilizing effects. For the lowest values of the Hartmann number, the horizontal transport of temperature contribution is the dominant destabilizing term. At higher values of Ha, just before the disappearances of these stationary instabilities, the vertical transport of temperature contribution becomes the main destabilizing term.

The thermal energy balance, dominant for high Hartmann number instabilities, is not strongly modified by the increasing magnetic field strength. The vertical transport of temperature term $\bar{\Theta}_1$ is the main destabilizing contribution while the destabilizing effects of the horizontal transport of temperature are very weak $\bar{\Theta}_2 \ll \bar{\Theta}_1$.

Ha	$\bar{K}_f$	$\bar{K}_b$	$\bar{K}_m$	$\bar{\Theta}_1$	$\bar{\Theta}_2$	R_{dt}
stationary instabilities						
2	1.08	-0.03	-0.05	0.06	0.94	25.48
6	1.48	-0.11	-0.37	0.14	0.86	6.67
10	1.87	-0.54	-0.33	0.73	0.27	0.53
oscillatory instabilities						
60	-0.90	4.36	-2.46	0.99	0.01	0.05
100	-1.63	9.19	-6.56	0.93	0.07	0.03
200	-1.16	16.21	-14.05	0.92	0.08	0.02
500	-0.32	23.91	-22.59	0.96	0.04	0.01
1000	-0.10	30.87	-29.77	0.97	0.03	0.01

Table 5.1: Transverse modes, energy balances for the thermally conducting walls

In the kinetic energy balance the only destabilizing contribution comes from the buoyancy forces effects. The term $\bar{K}_b$ increases with the increasing Hartmann number, while the dissipation of fluctuating kinetic energy by magnetic forces $\bar{K}_m$ is a dominant stabilizing contribution.

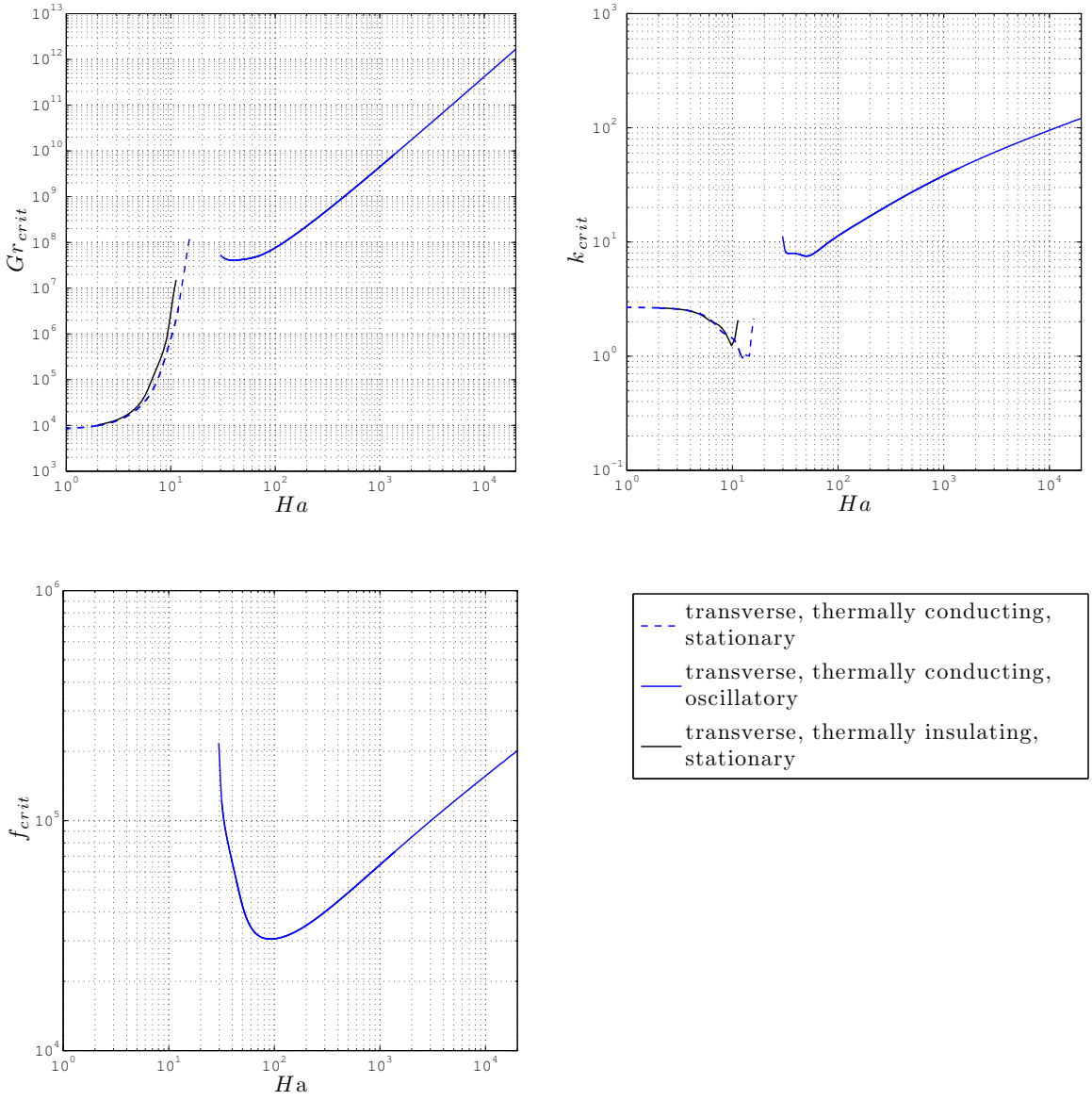

Figure 5.4: Critical values of parameters for the transverse modes

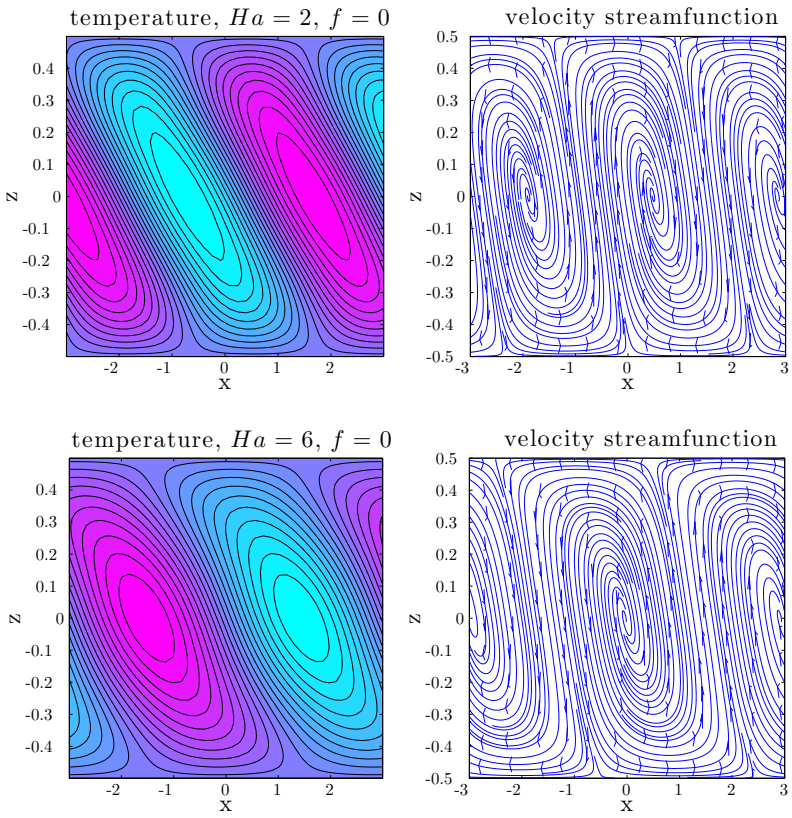

Figure 5.5: Transverse modes contour plots of disturbance isotherms (left) and disturbed velocity streamlines (right) for the thermally conducting walls; low Hartmann numbers

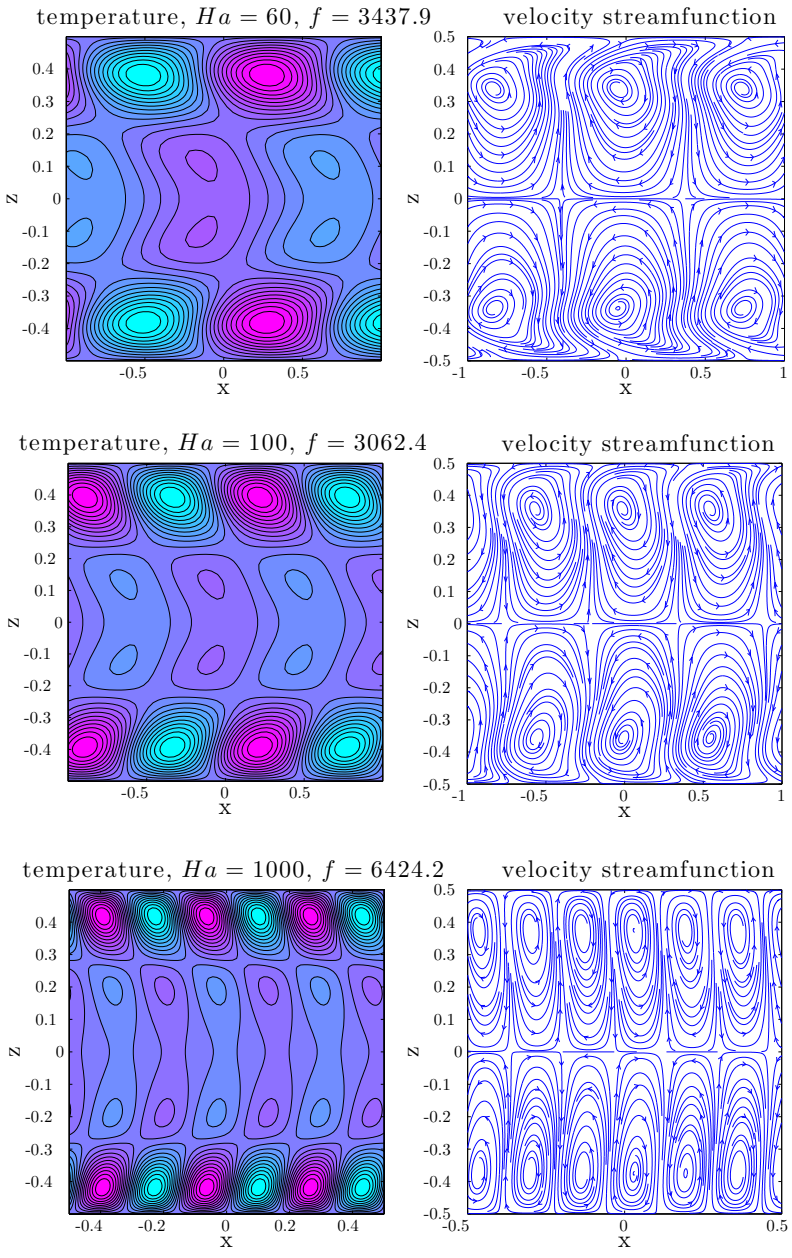

Figure 5.6: Transverse modes contour plots of disturbance isotherms (left) and disturbed velocity streamlines (right) for the thermally conducting walls; high Hartmann numbers

5.2.1.2 Transverse modes, thermally insulating boundaries

In the case of thermally insulating horizontal walls, modes of instability for relatively low applied magnetic field, exhibit similar behavior as with the thermally conducting boundaries (Fig. 5.4, 5.7).

The transverse stationary mode is more quickly stabilized here by the magnetic field and while following closely the instability of the thermally conducting boundaries case, remains less dangerous and disappears at $Ha \simeq 11.5$.

The main difference occurs at larger values of the Hartmann number, where the thermal modes of instability do not exist for thermally insulating boundaries as the temperature profile is here stably stratified (Fig. 5.3).

The energy balances for the low-Hartmann number stationary transverse instabilities are very similar for both cases of thermal boundary conditions. In the case of thermally insulating boundaries (Table 5.2), the only destabilizing contribution $\bar{K}_f$ is slightly stronger and balanced by the stronger buoyancy term $\bar{K}_b$. In the thermal fluctuating energy balance, the contribution corresponding to vertical transport of temperature is here stronger than in the case of thermally conducting boundary conditions.

Ha	$\bar{K}_f$	$\bar{K}_b$	$\bar{K}_m$	$\bar{\Theta}_1$	$\bar{\Theta}_2$	R_{dt}
stationary instabilities						
2	1.11	-0.06	-0.06	0.17	0.83	10.9
6	1.73	-0.42	-0.31	0.65	0.35	1.70
10	2.11	-0.91	-0.20	0.88	0.12	0.03

Table 5.2: Transverse modes, energy balances for the thermally insulating walls

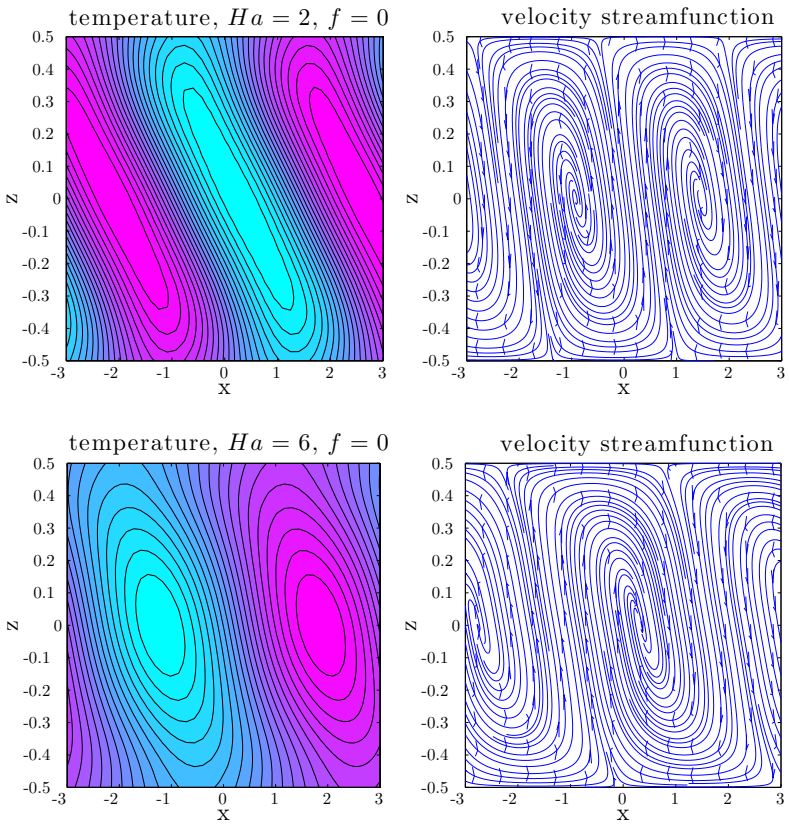

Figure 5.7: Transverse modes contour plots of disturbance isotherms (left) and disturbed velocity streamlines (right) for the thermally insulating walls

5.2.2 Longitudinal modes, thermally conducting boundaries

5.2.2.1 Longitudinal modes, thermally conducting and electrically insulating boundaries

As has been shown in [45], it is confirmed here that also in the case of the three-dimensional oscillatory longitudinal rolls, increasing the magnetic field strength shifts the onset of the instabilities to higher Grashof numbers very rapidly (Fig. 5.8). At $Ha \simeq 38$ the first branch of the oscillatory longitudinal mode reaches its limiting value of the Hartmann number before its disappearance. The wavenumber remains almost constant, insignificantly increasing and reaching its maximum $k_y \simeq 2.75$ at $Ha \simeq 31.7$.

The stationary longitudinal mode is shown to be more stable at the lowest Hartmann number values but for $38 < Ha < 46$ it becomes a dominating instability, located very closely to the thermal branch of the longitudinal oscillatory mode.

The oscillatory mode of the thermal origin first appears at $Ha \simeq 33$ and at $Ha > 46$ it becomes the main instability for longitudinal rolls, with its critical parameter values increasing with the increasing Ha.

The frequency of the first branch of the longitudinal oscillatory mode is shown to increase rapidly before its disappearance. For the second branch, after a slight decrease, the critical frequency increases asymptotically with increasing Ha.

At $Ha \simeq 2350$, a dramatical decrease of frequency is observed and the previously oscillatory mode becomes stationary. This is accompanied by a drop in the value of the wavenumber from $k_y \simeq 51$ to $k_y \simeq 47.8$.

For the highest values of the Hartmann number, $Ha > 10^4$, the asymptotic relation for the critical Grashof number is $Gr_{crit} = 4175 Ha^{1.98}$. Obtained numerical results did not allow to draw a definite conclusion regarding the critical wavenumber asymptotic relation. For $10^4 < Ha < 2 \cdot 10^4$, the wavenumber neutral stability curve behaves like $k_{crit} = 2.35 Ha^{0.39}$. This means, that for the higher Hartmann number, it is still far from an asymptotic relation of the type $k_{crit} \sim Ha^{1/3}$, observed for the case of Rayleigh-Bénard problem in Chapter 4.

The contour plots with side views of disturbed temperature isotherms, veloc-

ity streamlines and electric current streamlines at critical conditions are presented in Figs. 5.9-5.10, showing the location and the origin of different types of instabilities.

Ha	$\bar{K}_f$	$\bar{K}_b$	$\bar{K}_m$	$\bar{\Theta}_1$	$\bar{\Theta}_2$	R_{dt}
oscillatory instabilities						
2	1.02	0.04	-0.06	-0.01	1.01	0.42
10	2.01	0.35	-1.36	-0.04	1.04	0.14
25	3.09	2.71	-4.80	-0.15	1.15	0.06
stationary instabilities						
2	1.01	0.00	-0.01	0.10	0.90	8.69
10	1.12	0.01	-0.13	0.19	0.81	5.43
25	1.29	0.02	-0.31	0.44	0.56	3.17
60	1.64	0.09	-0.73	0.98	0.02	1.21
oscillatory instabilities						
60	2.79	0.60	-2.39	0.67	0.33	0.20
100	2.26	1.83	-3.09	0.84	0.16	0.11
200	1.31	5.16	-5.47	1.02	-0.02	0.06
500	0.57	14.96	-14.53	1.06	-0.06	0.02
1000	0.29	27.58	-26.87	1.05	-0.05	0.01
stationary instabilities						
3000	0.09	78.86	-77.95	1.03	-0.03	0.005
5000	0.04	101.42	-100.46	1.02	-0.02	0.004

Table 5.3: Longitudinal modes, energy balances for the thermally conducting and electrically insulating walls.

For the low Hartmann number oscillatory longitudinal instabilities of thermal origin, the dominant thermal energy balance is not strongly modified by the magnetic field (Table 5.3). The production of fluctuating thermal energy by the horizontal transport of temperature $\bar{\Theta}_2$ is here the only positive contribution corresponding to its destabilizing effects, while the small vertical temperature transport contribution $\bar{\Theta}_1$ weakly stabilizes the flow.

In the kinetic energy balances, the production of fluctuating energy by shear of mean flow $\bar{K}_f$ is the main destabilizing contribution, while the buoyancy forces contribution $\bar{K}_b$ serves here as a secondary destabilizing effect.

In both the thermal and kinetic energy balances, all the stabilizing and destabilizing effects are stronger with the increased values of Ha.

For the high Hartmann number oscillatory longitudinal instabilities, the dominant thermal energy balance is clearly affected by the magnetic field. The production of fluctuating thermal energy by the vertical transport of temperature $\bar{\Theta}_1$ is here the main destabilizing effect. The production of energy by the horizontal transport of temperature $\bar{\Theta}_2$ serves as a secondary destabilizing contribution at the appearance of the instability, quickly decreasing with the increasing Hartmann number and $Ha \simeq 200$, becomes a weak stabilizing contribution.

In the kinetic energy balance, again both effects due to shear of mean flow $\bar{K}_f$ and buoyancy forces $\bar{K}_b$ are destabilizing. Here the first contribution, $\bar{K}_f$, decreases quickly with the increasing Ha and the buoyancy term $\bar{K}_b$ become the main destabilizing contribution, growing quickly with Ha.

For the low-Hartmann number stationary longitudinal instabilities, in the dominant kinetic energy balance, the production of fluctuating energy by shear of mean flow $\bar{K}_f$ serves as the main destabilizing contribution, which grows with the increased values of Ha. The energy production due to buoyancy forces serves here as the secondary, very weak stabilizing effect $\bar{K}_b \ll \bar{K}_f$.

In the thermal energy balance both contributions due to temperature transport are destabilizing. At the lowest values of Hartmann number, the horizontal temperature transport $\bar{\Theta}_2$ term is dominant and decreases with the increasing Ha, while previously secondary vertical temperature transport $\bar{\Theta}_1$ contribution increases and takes over as a main destabilizing term.

The ratio R_{dt} decreases with the increasing magnetic field strength, indicating the decreasing influence of dynamical effects.

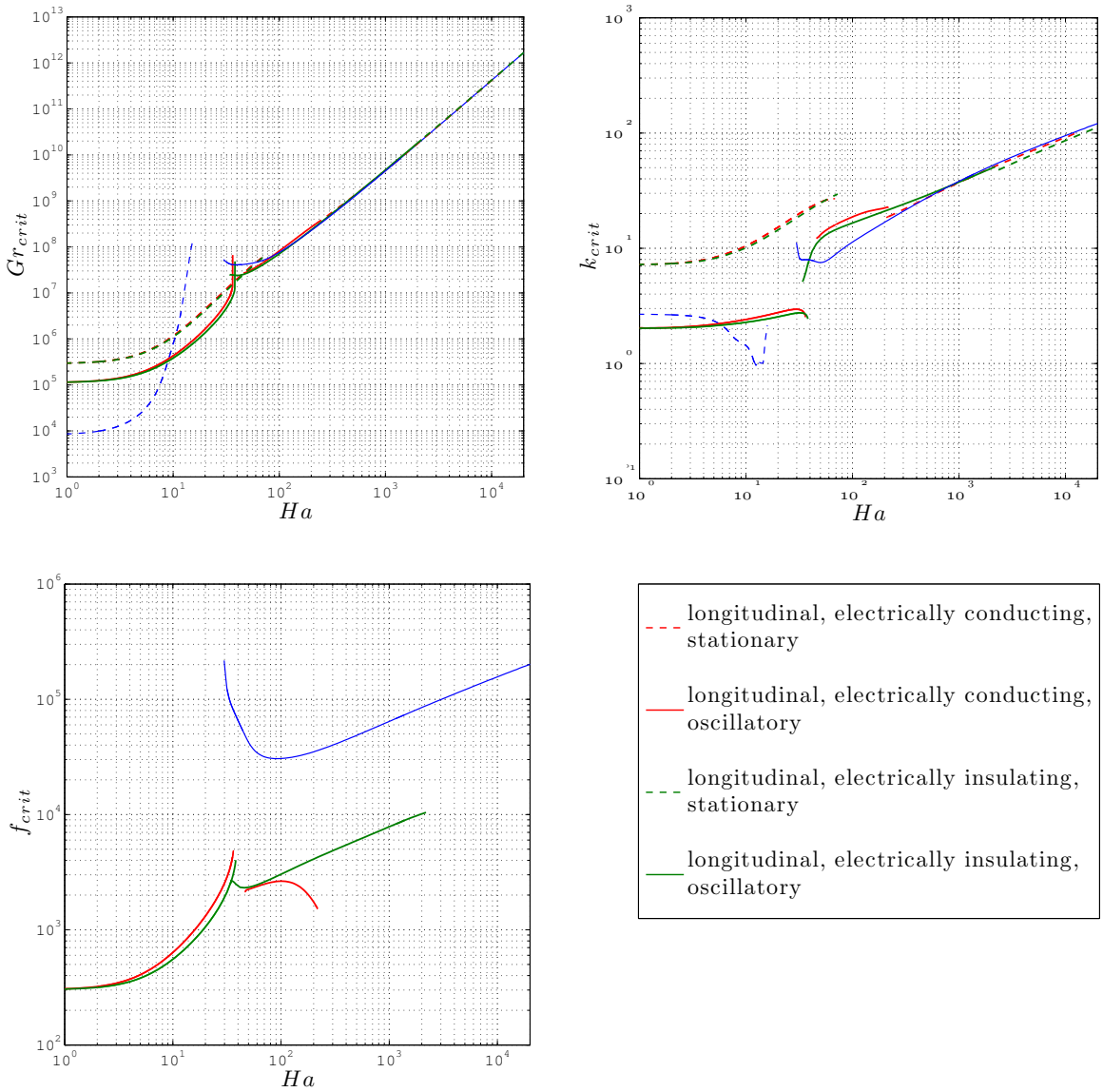

Figure 5.8: Longitudinal modes critical values of parameters for the thermally conducting boundaries; additional blue lines represent respective curves for transverse modes

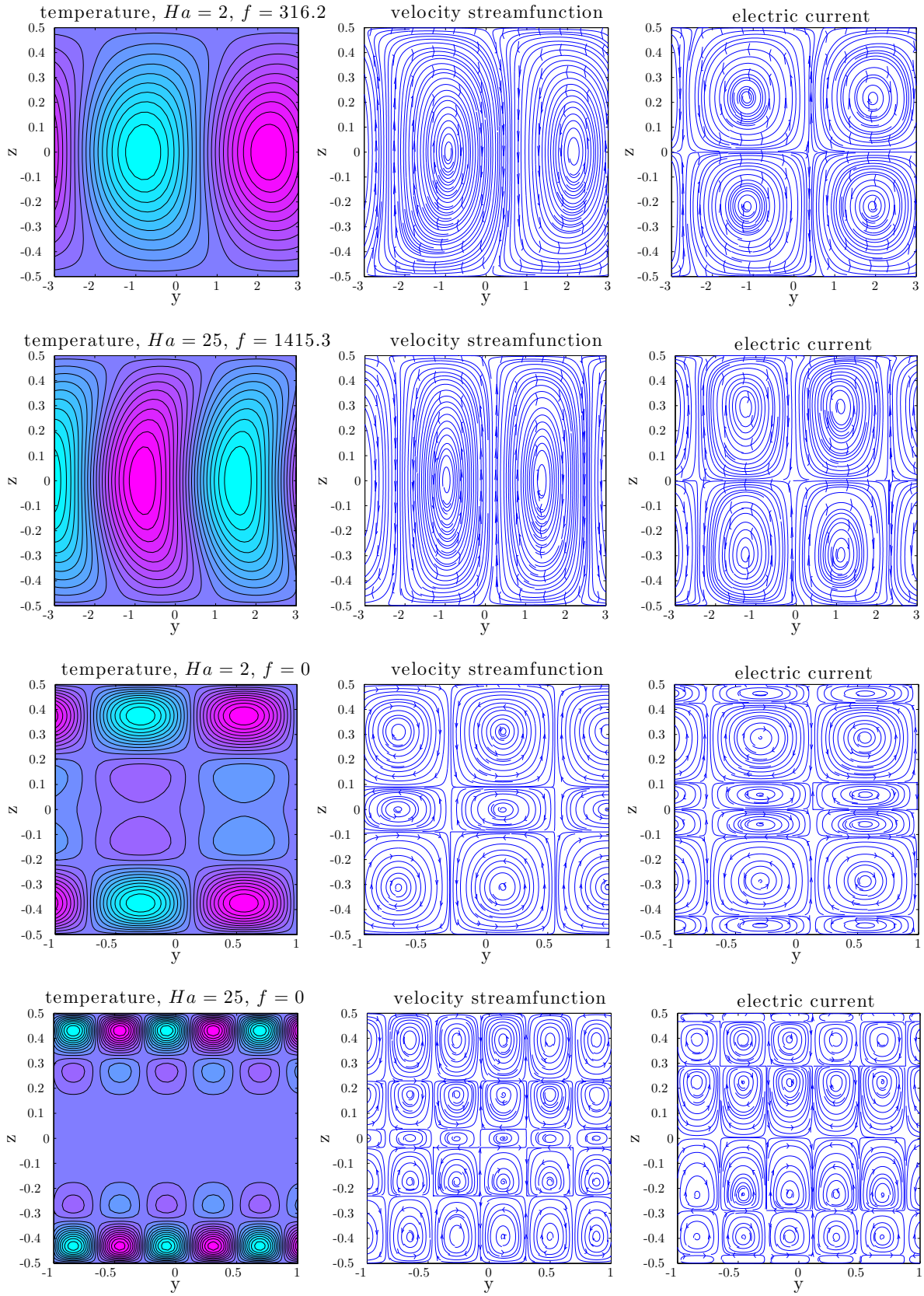

Figure 5.9: Longitudinal modes contour plots of disturbance isotherms (left), disturbed velocity streamlines (center) and electric current streamlines (right) for the thermally conducting and electrically insulating walls; low Hartmann numbers

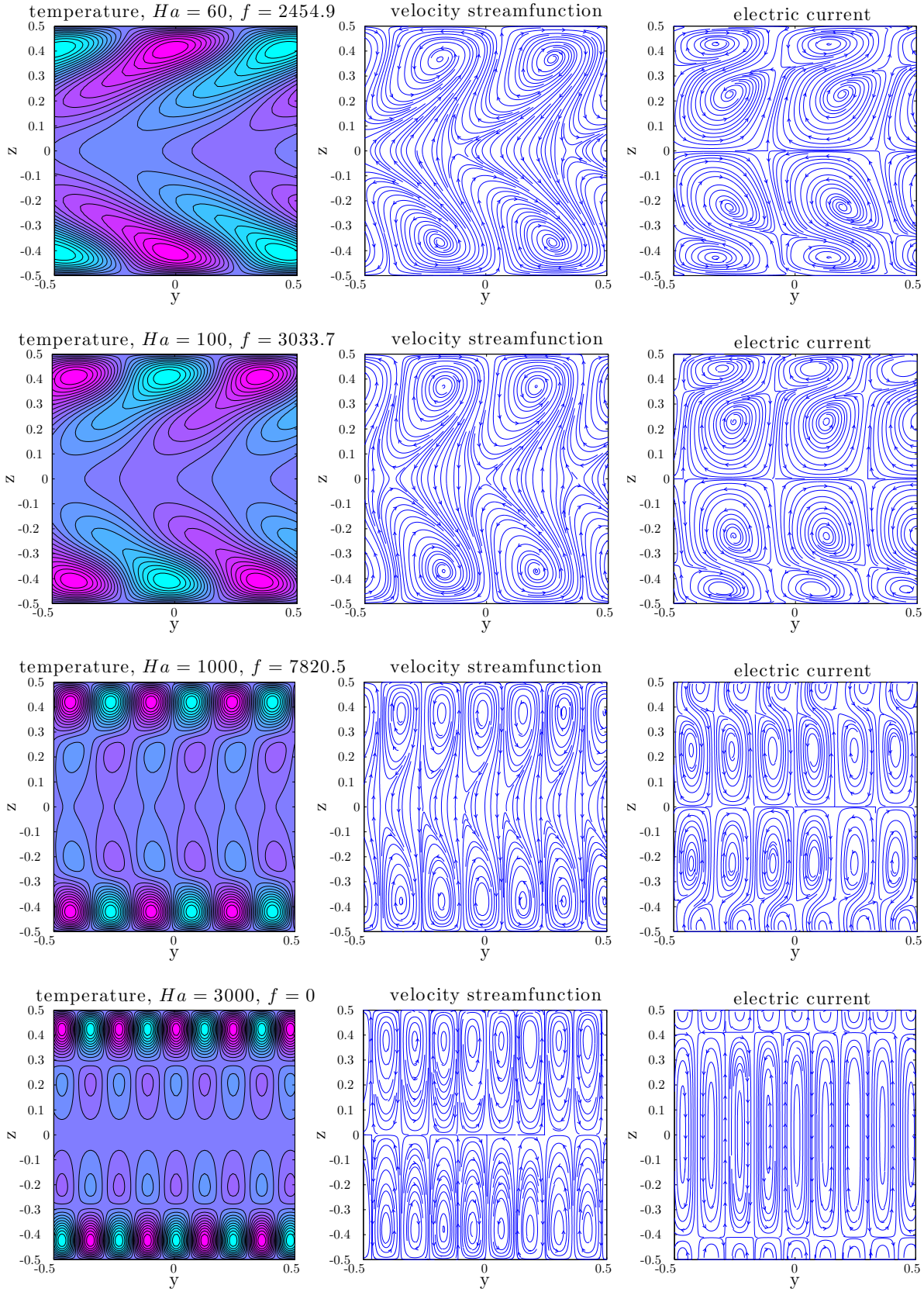

Figure 5.10: Longitudinal modes contour plots of disturbance isotherms (left), disturbed velocity streamlines (center) and electric current streamlines (right) for the thermally conducting and electrically insulating walls; high Ha

5.2.2.2 Longitudinal modes, thermally conducting and electrically conducting boundaries

Electrically conducting boundaries have slightly more stabilizing effect on the first branch of the longitudinal oscillatory mode (Fig. 5.8). The most dangerous instability in this case disappears at $Ha \simeq 36.5$. The wavenumber curve for the first branch of the three-dimensional mode lies slightly above the analogous electrically insulating boundaries case curve, reaching its maximum $k_y \simeq 2.95$ at $Ha \simeq 29.6$. This mode of instability occurs at slightly higher frequencies for the electrically conducting boundaries than in the case of electrically insulating walls.

The longitudinal stationary modes, for both cases of electrical boundary conditions, lie very closely to one another, with the electrically conducting case critical Grashof number and wavenumber curves slightly above the electrically insulating case (Fig. 5.8).

The thermal mode of the longitudinal oscillatory instability, appearing very closely to the analogous one in the electrically insulating case, exhibit similar frequency drop, becoming a stationary mode at just $Ha \simeq 218.2$. The corresponding drop in the value of the wavenumber reads here from $k_y \simeq 22.8$ to $k_y \simeq 18.85$.

For the highest values of Hartmann number, $Ha > 10^4$, the asymptotic relation for the critical Grashof number is $Gr_{crit} = 4185 Ha^{1.98}$. Similarly as for the electrically insulating boundary conditions, an asymptotic relation for the critical wavenumber has not yet been reached. It is likely that an asymptotic relation of the type $k_{crit} \sim Ha^{1/3}$ could be found for the higher Hartmann numbers.

The contour plots with side views of disturbed temperature isotherms, velocity streamlines and electric current streamlines for the thermally and electrically conducting boundaries are presented in Figs. 5.11-5.12, showing the location and the origin of different types of instabilities.

For the low Hartmann number oscillatory longitudinal instabilities of thermal origin (Table 5.4), the dominant thermal energy balance is very similar for both cases of electromagnetic boundary conditions, with the destabilizing effects of thermal fluctuating energy production by the horizontal transport of temperature $\bar{\Theta}_2$.

Ha	$\bar{K}_f$	$\bar{K}_b$	$\bar{K}_m$	$\bar{\Theta}_1$	$\bar{\Theta}_2$	R_{dt}
oscillatory instabilities						
2	1.04	0.04	-0.08	-0.01	1.01	0.42
10	2.61	0.33	-1.94	-0.04	1.04	0.13
25	5.90	2.49	-7.39	-0.12	1.12	0.05
stationary instabilities						
2	1.01	0.00	-0.01	0.10	0.90	8.79
10	1.16	0.01	-0.17	0.20	0.80	5.47
25	1.39	0.02	-0.41	0.47	0.53	3.11
60	1.73	0.09	-0.82	1.03	-0.03	1.14
oscillatory instabilities						
60	2.82	0.44	-0.26	0.72	0.28	0.26
100	3.17	1.33	-3.50	0.99	0.01	0.15
200	2.76	5.51	-7.27	1.16	-0.16	0.05
stationary instabilities						
300	2.10	15.7	-16.8	1.10	-0.10	0.02
500	0.90	22.9	-22.8	1.06	-0.06	0.01
1000	0.30	33.2	-32.5	1.03	-0.03	0.01

Table 5.4: Longitudinal modes, energy balances for the thermally conducting and electrically conducting walls.

The kinetic energy balance, similar for both cases of electromagnetic boundary conditions, is slightly less affected by the magnetic field for the electrically conducting walls.

For the high Hartmann number instabilities of thermal origin, the dominant thermal fluctuating energy balance is here again very similar with the case of electrically insulating boundary conditions, while the kinetic energy balance is less affected by the magnetic field.

For the low-Hartmann number stationary longitudinal instabilities, the dominant kinetic energy balance strongly depends on the electromagnetic boundary conditions.

In the case of electrically conducting walls, the kinetic balance is not significantly modified by the magnetic field and remains almost constant for all the values of Ha. The production of fluctuating energy by shear of mean flow, $\bar{K}_f$, is the main destabilizing effect, while the buoyancy and magnetic forces contributions remain weak, $\bar{K}_b$ slightly destabilizing and $\bar{K}_m$ stabilizing the flow.

The thermal energy balances are again very similar for both cases of electromagnetic boundary conditions.

The ratio R_{dt} decreases here with the increasing magnetic field strength, for all the instabilities considered, indicating the decreasing influence of dynamical effects.

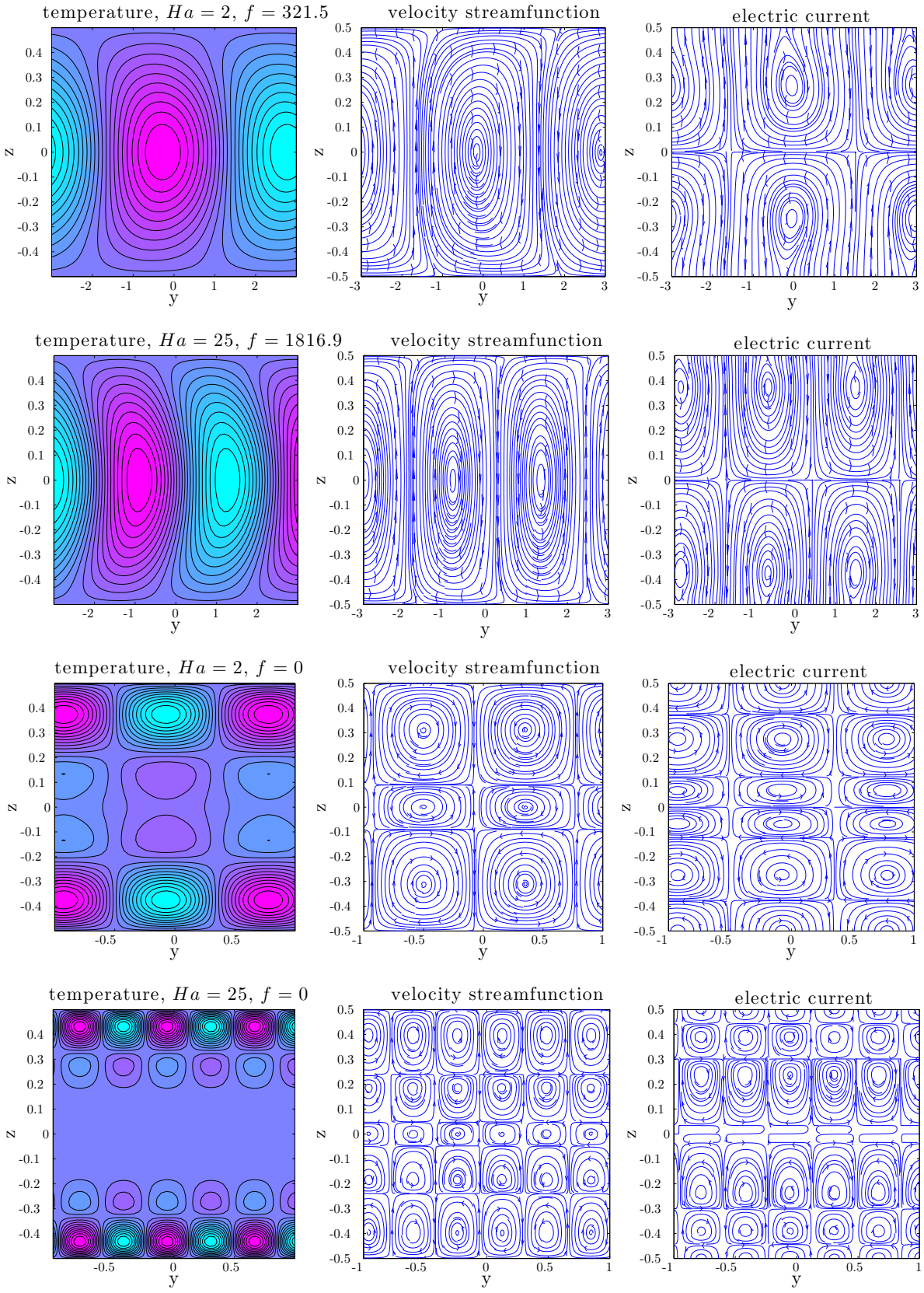

Figure 5.11: Longitudinal modes contour plots of disturbance isotherms (left), disturbed velocity streamlines (center) and electric current streamlines (right) for the thermally and electrically conducting walls; low Hartmann numbers

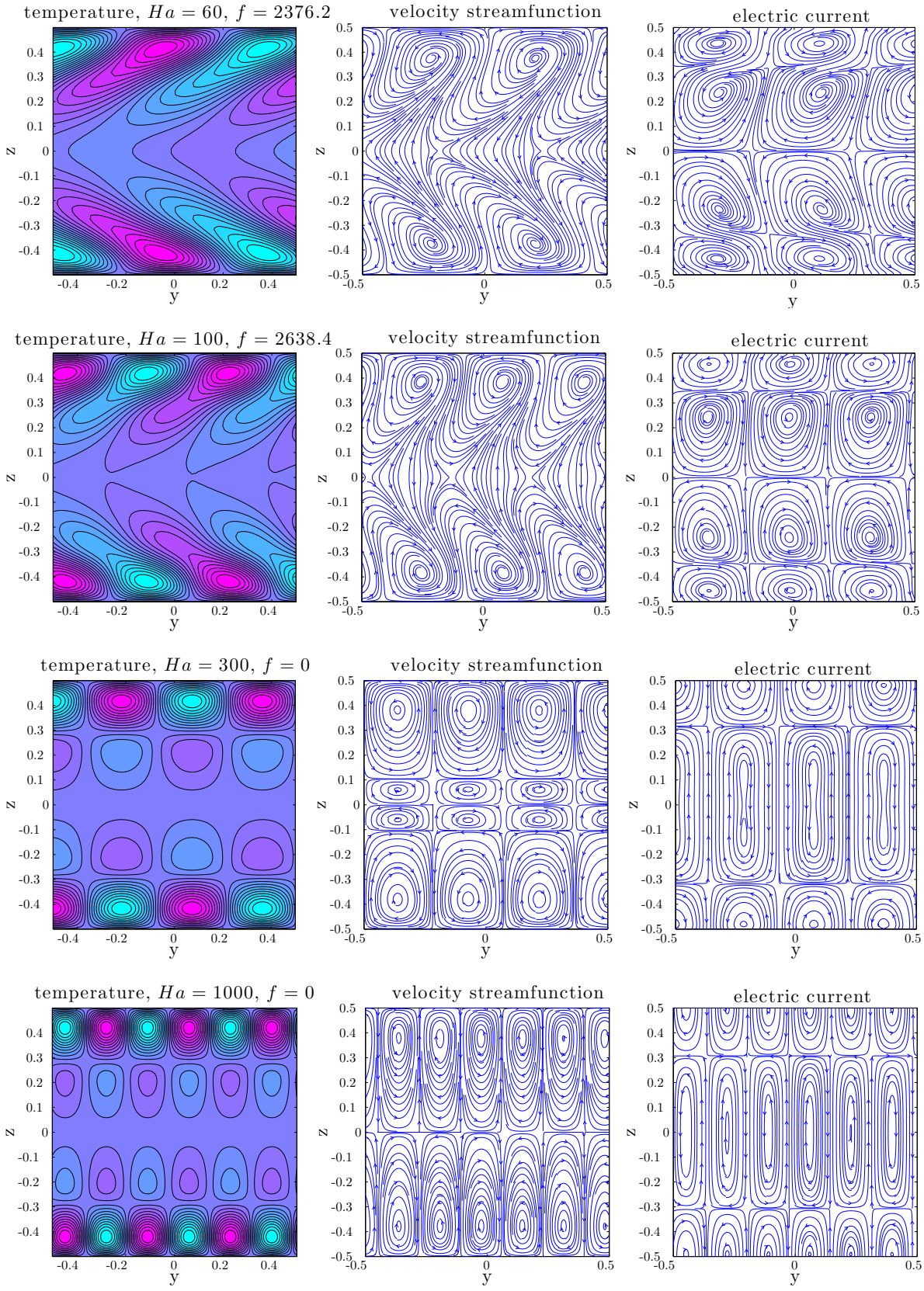

Figure 5.12: Longitudinal modes contour plots of disturbance isotherms (left), disturbed velocity streamlines (center) and electric current streamlines (right) for the thermally and electrically conducting walls; high Ha

5.2.3 Longitudinal modes, thermally insulating boundaries

5.2.3.1 Longitudinal modes, thermally insulating and electrically insulating boundaries

In the case of thermally insulating boundaries, with no thermal modes of instabilities, the results for both electrical boundary conditions are relatively similar (Fig. 5.13). For the longitudinal oscillatory mode, changing thermal boundary conditions from conducting to insulating shifts the onset of instability to much lower Grashof numbers, though this mode is more quickly stabilised and disappears at $Ha \simeq 21$.

Longitudinal stationary curves for both thermally conducting and thermally insulating horizontal boundaries are relatively close to one another, with the insulating case mode being slightly more dangerous for $Ha < 14$ and the conducting case mode for $Ha > 14$.

In the case of three-dimensional oscillatory mode, the wavenumber is roughly three times lower for the thermally insulating case and reaches its maximum $k_y \simeq 0.96$ at $Ha \simeq 17$.

The longitudinal oscillatory mode occurs here at lower frequency than in the case of thermally conducting boundaries.

Thermal boundary conditions do not strongly affect the dominant fluctuating thermal energy balance (Table 5.5) for the oscillatory instabilities and similar conclusions can be drawn as for the cases of thermally conducting boundaries. The secondary fluctuating kinetic energy balance is here less affected by the magnetic field than for the thermally conducting walls cases.

For the stationary longitudinal instabilities of dynamical origin, the thermal energy balances strongly depend on the thermal boundary conditions. For the thermally insulating walls, the horizontal temperature transport $\bar{\Theta}_2$ is the only destabilizing effect, growing with the increasing Hartmann number Ha. The vertical temperature transport $\bar{\Theta}_1$ serves here as a weak stabilizing contribution, becoming more pronounced at the higher values of Ha.

The dominant kinetic fluctuating energy balance is here very similar to the case of thermally conducting and electrically insulating boundaries. The kinetic contributions are here slightly more influenced by the magnetic field strength,

with the stronger respective stabilizing and destabilizing terms.

The contour plots with side views of disturbed temperature isotherms, velocity streamlines and electric current streamlines are presented in Fig. 5.14.

Ha	$\bar{K}_f$	$\bar{K}_b$	$\bar{K}_m$	$\bar{\Theta}_1$	$\bar{\Theta}_2$	R_{dt}
oscillatory instabilities						
2	0.49	0.60	-0.09	-0.07	1.07	0.29
6	0.69	1.00	-0.69	-0.14	1.14	0.24
10	0.90	1.71	-1.61	-0.29	1.29	0.21
stationary instabilities						
2	1.00	0.01	-0.01	-0.08	1.08	5.69
6	1.07	0.01	-0.08	-0.08	1.08	4.87
10	1.14	0.01	-0.15	-0.10	1.10	3.97
25	1.29	0.02	-0.31	-0.14	1.14	3.18
60	1.39	0.02	-0.41	-0.19	1.19	2.98
100	1.43	0.02	-0.45	-0.22	1.22	3.04

Table 5.5: Longitudinal modes, energy balances for the thermally insulating and electrically insulating walls.

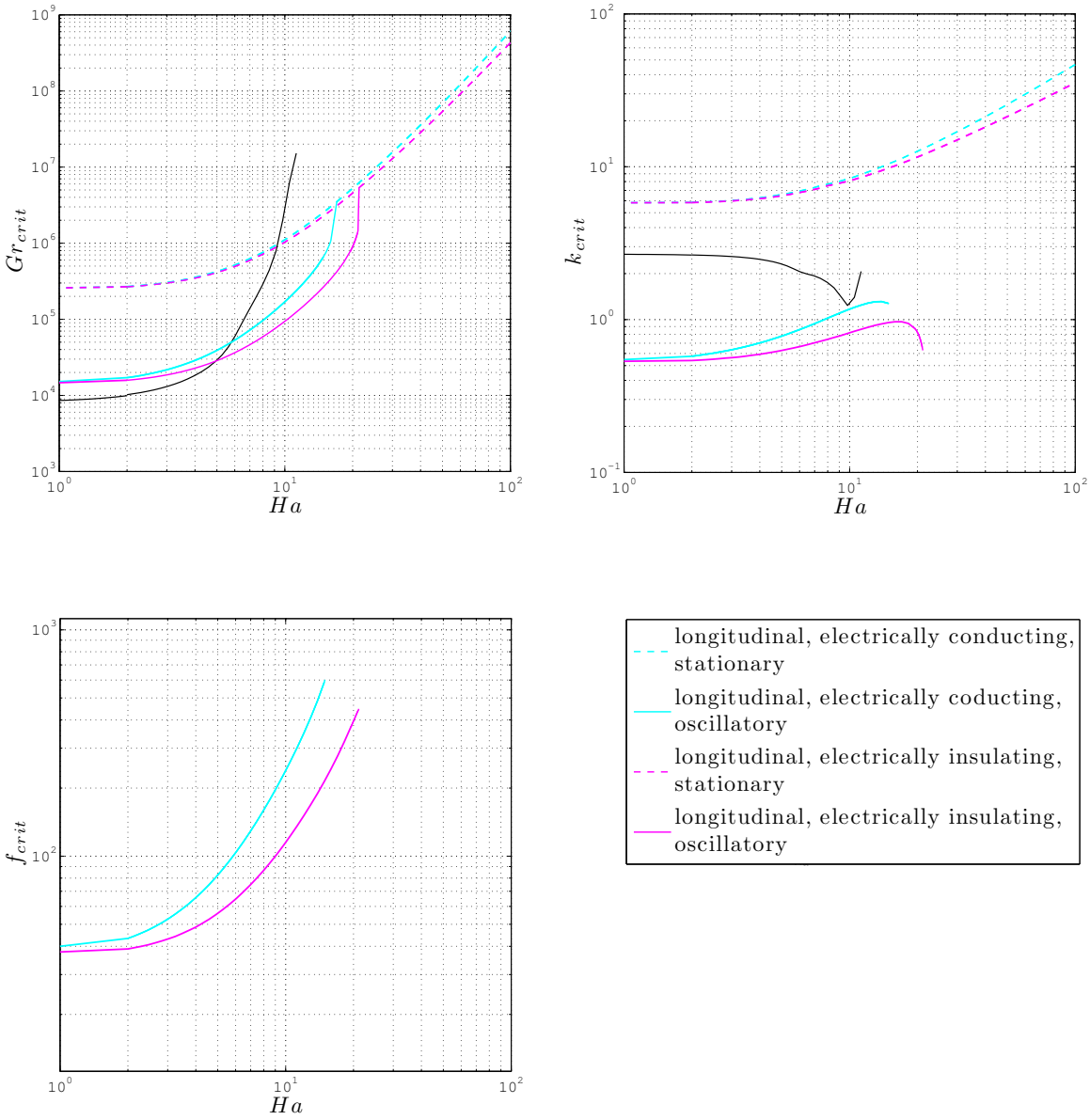

Figure 5.13: Longitudinal modes critical values of parameters for the thermally insulating boundaries; additional black lines represent respective curves for transverse modes

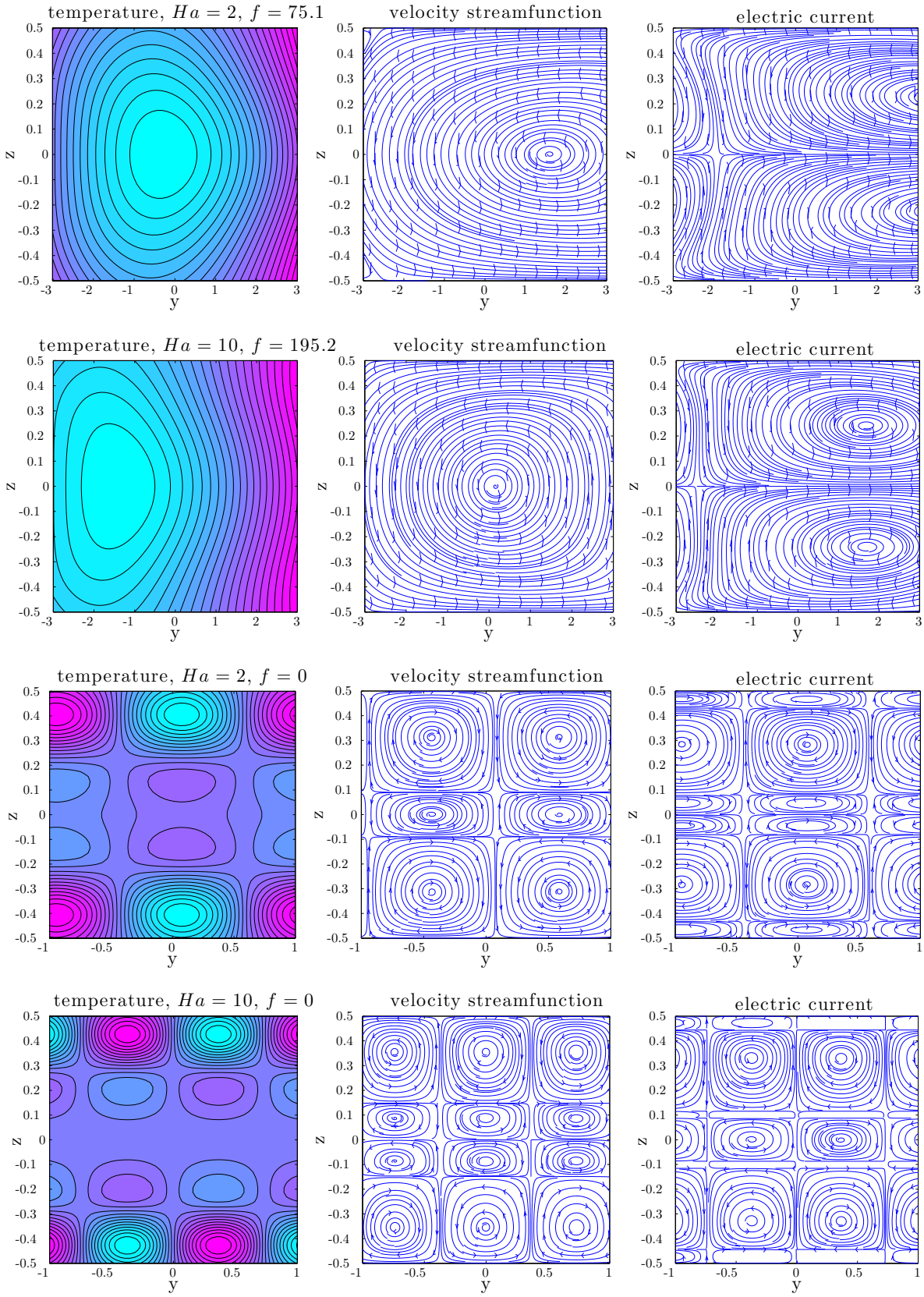

Figure 5.14: Longitudinal modes contour plots of disturbance isotherms (left), disturbed velocity streamlines (center) and electric current streamlines (right) for the thermally and electrically insulating walls

5.2.3.2 Longitudinal modes, thermally insulating and electrically conducting boundaries

The results for electrically conducting walls show, as in the previous subsections, a more stabilizing effect on the longitudinal modes (Fig.5.13). The three-dimensional oscillatory instability reaches here its limit in Ha value and disappears at $Ha \simeq 17.1$. The longitudinal stationary mode, identical for both electrical conductivities of the boundaries at the lowest values of Hartmann number, becomes clearly more stable for electrically conducting boundary conditions at $Ha > 5$.

The wavenumber curves for the electrically conducting case lie again above the same curves in the case of electrically insulating boundaries. The wavenumber of the longitudinal oscillatory mode increases slowly reaching the maximum $k_y \simeq 1.3$ at $Ha \simeq 13.85$. The longitudinal stationary mode wavenumber increases more quickly for the electrically conducting case, indicating faster decrease of the marginal cells with increasing magnetic field intensity. The oscillatory longitudinal mode occurs here at higher frequencies for the electrically conducting boundaries.

As mentioned before, thermal boundary conditions do not strongly affect the fluctuating energy balances (Table 5.6) for the oscillatory instabilities of thermal origin, while the stationary instabilities of dynamical origin strongly depend on the electromagnetic and thermal boundary conditions.

The ratio R_{dt} for the case of thermally insulating and electrically conducting boundaries increases with the increasing magnetic field strength, indicating the increasing influence of dynamical effects. For all the other boundary conditions combinations, the ratio R_{dt} decreases.

The contour plots with side views of disturbed temperature isotherms, velocity streamlines and electric current streamlines are presented in Fig. 5.15.

Ha	$\bar{K}_f$	$\bar{K}_b$	$\bar{K}_m$	$\bar{\Theta}_1$	$\bar{\Theta}_2$	R_{dt}
oscillatory instabilities						
2	0.60	0.56	-0.16	-0.08	1.08	0.30
6	1.44	0.74	-1.18	-0.17	1.17	0.29
10	2.49	1.17	-2.65	-0.35	1.35	0.22
stationary instabilities						
2	1.01	0.01	-0.02	-0.08	1.08	5.72
6	1.10	0.01	-0.11	-0.08	1.08	4.96
10	1.21	0.01	-0.22	-0.10	1.10	4.11
25	1.47	0.01	-0.48	-0.15	1.15	3.65
60	1.71	0.01	-0.72	-0.20	1.20	4.06
100	1.81	0.01	-0.82	-0.22	1.22	4.68

Table 5.6: Longitudinal modes, energy balances for the thermally insulating and electrically conducting walls.

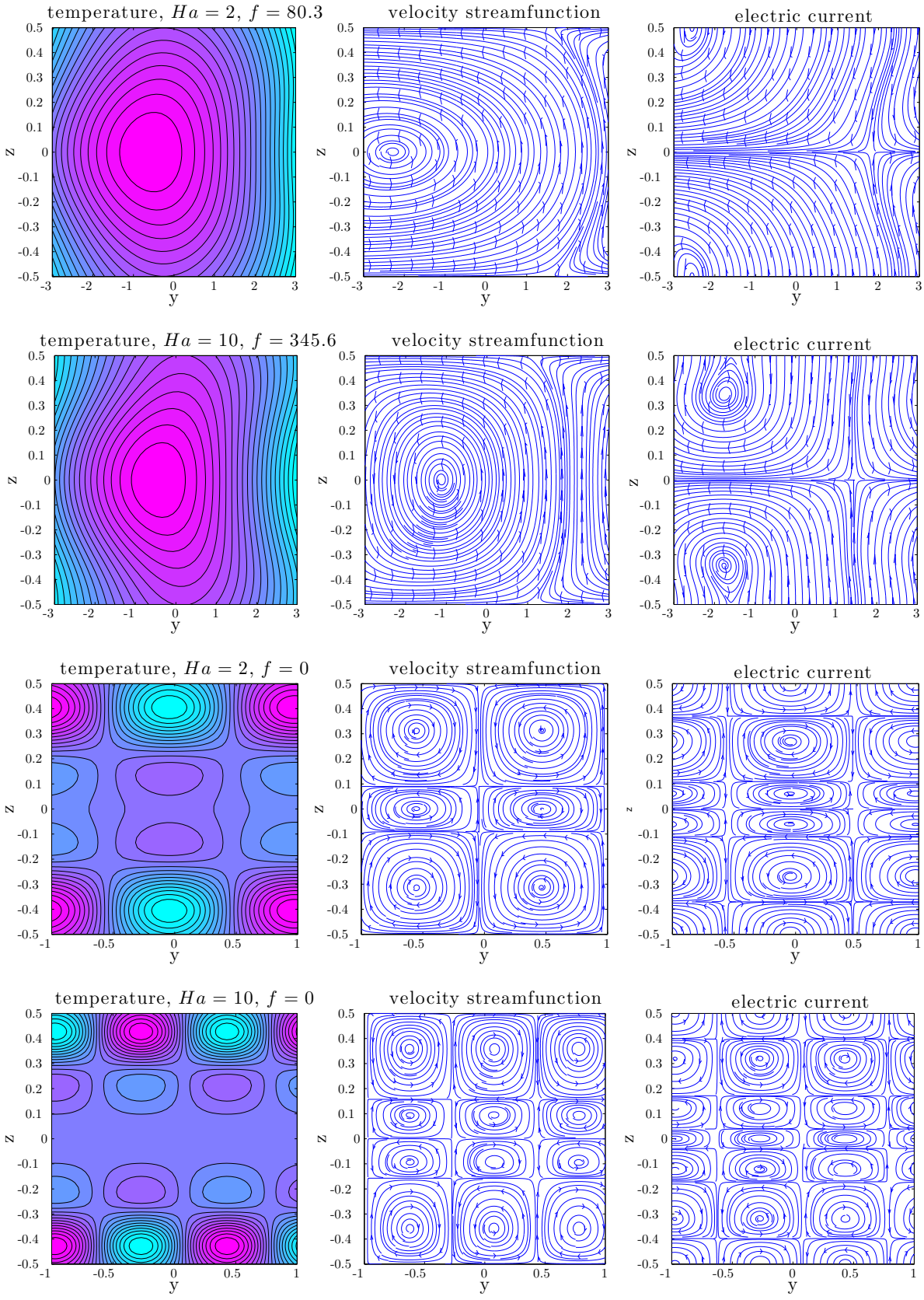

Figure 5.15: Longitudinal modes contour plots of disturbance isotherms (left), disturbed velocity streamlines (center) and electric current streamlines (right) for the thermally and insulating and electrically conducting walls

5.2.4 Summary

It has been found that in the case of electrically conducting boundaries, the magnetic field stabilises the longitudinal oscillatory modes more efficiently in both cases of thermal boundary conditions. Thermally conducting walls seem to cause most dangerous instabilities in almost all ranges of the Hartmann number. Critical values of parameters for the most dangerous modes for all the boundary conditions combinations considered are presented in Tables 5.7-5.10.

type of instability	Ha	Gr_{crit}	k_{crit}
transverse stationary	2	$9.903 \cdot 10^3$	2.65
transverse stationary	6	$4.058 \cdot 10^4$	2.12
longitudinal oscillatory	10	$4.313 \cdot 10^5$	2.41
longitudinal stationary	40	$2 \cdot 10^7$	15.3
transverse oscillatory	100	$7.65 \cdot 10^7$	11.3
transverse oscillatory	400	$7.827 \cdot 10^8$	24.4
transverse oscillatory	1000	$4.5 \cdot 10^9$	38.2

Table 5.7: The most dangerous modes for thermally and electrically conducting boundaries

type of instability	Ha	Gr_{crit}	k_{crit}
transverse stationary	2	$9.903 \cdot 10^3$	2.65
transverse stationary	6	$4.058 \cdot 10^4$	2.12
longitudinal oscillatory	10	$3.839 \cdot 10^5$	2.28
longitudinal stationary	40	$1.868 \cdot 10^7$	21.7
longitudinal oscillatory	100	$7.092 \cdot 10^7$	16.6
transverse oscillatory	400	$7.827 \cdot 10^8$	24.4
transverse oscillatory	1000	$4.5 \cdot 10^9$	38.2

Table 5.8: The most dangerous modes for thermally conducting and electrically insulating boundaries

type of instability	Ha	Gr_{crit}	k_{crit}
transverse stationary	2	$1.023 \cdot 10^4$	2.65
longitudinal oscillatory	6	$5.375 \cdot 10^4$	0.86
longitudinal oscillatory	10	$1.696 \cdot 10^5$	1.17
longitudinal stationary	40	$3.573 \cdot 10^7$	21.3
longitudinal stationary	100	$6.095 \cdot 10^8$	46.7

Table 5.9: The most dangerous modes for thermally insulating and electrically conducting boundaries

type of instability	Ha	Gr_{crit}	k_{crit}
transverse stationary	2	$1.023 \cdot 10^4$	2.65
longitudinal oscillatory	6	$3.664 \cdot 10^4$	0.67
longitudinal oscillatory	10	$9.385 \cdot 10^4$	0.82
longitudinal stationary	40	$2.842 \cdot 10^7$	18.2
longitudinal stationary	100	$4.296 \cdot 10^8$	35.5

Table 5.10: The most dangerous modes for thermally and electrically insulating boundaries

5.3 $Pr_m \neq 0$ linear stability results

The inductionless approximation is confirmed to be valid for Pr_m up to $Pr_m = 10^{-4}$ for the range of Ha considered here. Further increase of Pr_m will cause a divergence between different modes, depending on the boundary conditions, and on the values of critical parameters.

Here only the results for transverse modes with $k_y = 0$ are presented. The detailed analysis of inductionless approximation presented in Section 5.2 confirmed, that these are the most dangerous instabilities for most ranges of the Hartmann number. A brief inspection of the longitudinal modes showed, that with the increase of Pr_m, only small deviations of no significance can be observed and no new longitudinal instabilities have been found.

For $Pr_m \to 0$ the electrical boundary conditions show no effect on the transverse instabilities. The magnetic field stabilises these modes very efficiently shifting the onset of instabilities to higher Grashof numbers. At the higher values of Ha, instabilities appear mainly as a result of potentially unstable thermal stratification zones near the horizontal boundaries and exist only for thermally conducting cases.

An increase of the value of magnetic Prandtl numbers results in a divergence between the two cases of electromagnetic boundary conditions. All the instability modes, described in the previous subsections for $Pr_m \to 0$, have their counterparts for the nonzero Pr_m values considered here. The influence of Pr_m on the respective modes can be described by the following common characteristics.

The stationary low Hartmann number branches, for all the boundary conditions, lie very closely to one another for different magnetic Prandtl numbers, with the lower Pr_m modes disappearing at slightly lower Ha values. The increased Pr_m values shifts the critical wavenumbers towards lower values, which is apparent for the thermally insulating cases (Fig. 5.16 and 5.20; notice that all the modes in these figures are stationary), causing the increase of the marginal cells sizes.

For the oscillatory thermal branches, present at higher Ha values, in the cases of thermally conducting walls, the increase of the magnetic Prandtl number Pr_m has a stabilising effect for both cases of electromagnetic boundary conditions.

The wavenumber decreses here, causing again the increase of the marginal cells sizes.

In both cases the frequency curves experience very similar behaviour: the higher Pr_m modes, appearing at higher critical frequencies, after a characteristic Ha values, switch to the lowest frequencies.

In the cases of electrically insulating boundaries there are new most dangerous instabilities appearing for the whole range of Ha considered. These will be discussed in details in the following subsections.

5.3.1 Transverse modes, thermally insulating and electrically conducting walls

The stationary low Ha modes are the only instabilities present for these boundary conditions, giving a pattern for the respective branches in the other boundary conditions cases (Fig. 5.16).

The energy analysis results (Table 5.7) show, that, while increasing magnetic Prandtl number up to $Pr_m = 10^{-4}$ show no effect on the neutral stability curves, slight changes in the fluctuating energy balances can be noticed. The ratio R_{dt} is here lower than in the inductionless approximation case, suggesting weaker dominance of the dynamical effects. In the thermal energy balance, the production of fluctuating thermal energy by the vertical transport of temperature $\bar{\Theta}_1$ increases here quicker with the increasing Hartmann number. In the very weak fluctuating magnetic energy balance, the only remaining contribution balancing dissipation is the term corresponding to stretching of magnetic field lines along the field, $\bar{M}_{s3}$.

The increase of magnetic Prandtl number up to $Pr_m = 10^{-2}$ does not change significantly the thermal and kinetic energy balances, while the weakest fluctuating magnetic energy balance is modified. The main destabilizing term $\bar{M}_{s3}$ weakens here with the increasing magnetic field strength, and other destabilizing contributions, corresponding to advection $\bar{M}_{ad}$ and stretching of magnetic field lines along the flow $\bar{M}_{s2}$, increase. The fluctuating magnetic energy production by shear of mean flow $\bar{M}_{s1}$ serves as a weak stabilizing contribution at the lowest Hartmann numbers, turning into a destabilizing term just before the instability

Ha	$\bar{K}_f$	$\bar{K}_b$	$\bar{K}_m$	$\bar{\Theta}_1$	$\bar{\Theta}_2$	$\bar{M}_{ad}$	$\bar{M}_{s1}$	$\bar{M}_{s2}$	$\bar{M}_{s3}$	R_{dt}	R_{dm}	R_{tm}
$Pr_m = 10^{-4}$ stationary instabilities												
2	1.11	-0.06	-0.05	0.17	0.83	0	0	0	1	10.9	20.6	1.89
6	1.73	-0.42	-0.31	0.65	0.35	0	0	0	1	1.69	3.19	1.89
9	2.02	-0.74	-0.28	0.94	0.06	0	0	0	1	0.16	3.52	22.3
$Pr_m = 10^{-2}$ stationary instabilities												
2	1.11	-0.06	-0.05	0.17	0.83	0.02	-0.02	0.06	0.94	10.8	18.4	1.70
6	1.83	-0.47	-0.36	0.73	0.27	0.09	-0.05	0.15	0.81	1.44	2.48	1.73
9	2.08	-0.76	-0.32	0.97	0.03	0.28	0.20	0.15	0.31	0.20	1.11	5.62
$Pr_m = 10^{-1}$ stationary instabilities												
2	1.14	-0.06	-0.08	0.17	0.83	0.24	0.01	0.46	0.29	10.2	6.53	0.64
6	1.60	-0.36	-0.24	0.52	0.48	0.24	0.43	0.27	0.06	1.91	0.36	0.19
9	-0.84	-0.16	2.00	0.60	0.40	0.41	1.49	-1.15	0.25	0.51	0.34	0.66
$Pr_m = 10^{0}$ stationary instabilities												
2	0.40	-0.03	0.63	0.22	0.78	0.16	1.20	-0.46	0.10	14.0	0.55	0.04
6	-0.69	-0.02	1.71	0.10	0.90	2.29	2.75	-4.42	0.38	1.68	1.08	0.64
9	-0.45	-0.01	1.46	0.01	0.99	3.94	2.41	-5.77	0.42	0.64	1.00	1.56

Table 5.11: Transverse modes, energy balances for the thermally insulating and electrically conducting walls

disappearance.

Further increase of Pr_m show significant changes in the fluctuating energy balances. For $Pr_m = 10^{-1}$, in the dominant fluctuating kinetic energy balance, all the contributions increase slowly with Ha and just before disappearance of the instability, the term corresponding to production of fluctuating energy by shear of mean flow $\bar{K}_f$ changes from destabilizing, to stabilizing, while the contribution corresponding to magnetic forces $\bar{K}_m$, changes from stabilizing to destabilizing.

The thermal fluctuating energy balance is here less affected by the magnetic field strength. In the magnetic energy balance, all the contributions balancing dissipation (advection $\bar{M}_{ad}$, stretching of magnetic field lines by shear of mean flow $\bar{M}_{s1}$, along the flow $\bar{M}_{s2}$ and along the magnetic field $\bar{M}_{s3}$) are destabilizing first, and the term corresponding to stretching of magnetic field lines along the flow $\bar{M}_{s2}$ becomes stabilizing just before the instability disappearance. The ratio R_{tm} shows the dominance of magnetic effects over thermal.

For the highest value of magnetic Prandtl number considered here, $Pr_m = 10^0$, the ratio R_{dm} shows, that the magnetic effects gain importance and dominate together with the dynamic contributions. In the kinetic energy balance, the contribution corresponding to magnetic forces $\bar{K}_m$ is destabilizing, while the shear of mean flow term $\bar{K}_f$ serves as a destabilizing contribution for the lowest Ha values and quickly changes to a stabilizing contribution. The buoyancy forces contribution $\bar{K}_b$ here is negligible.

In the magnetic energy balance, the contribution by stretching of magnetic field lines along the flow $\bar{M}_{s2}$ is a strong stabilizing term, while all the other contributions are destabilizing. In the secondary thermal energy balance, the horizontal transport of temperature $\bar{\Theta}_2$ destabilizes the flow, while the vertical transport of temperature $\bar{\Theta}_1$ becomes negligible with the increased Ha.

The side views of temperature disturbance isotherms, disturbed velocity streamlines and disturbed magnetic field lines are presented in Fig. 5.17, showing the influence of the magnetic Prandtl number on the instability cross-sections. These results confirm, that while the slight increase of Pr_m does not affect transverse modes significantly, $Pr_m = 10^{-1}$ seems to be a transition value between the purely dynamical originated instabilities (low Pr_m) and the instabilities dominated by the magnetic induction.

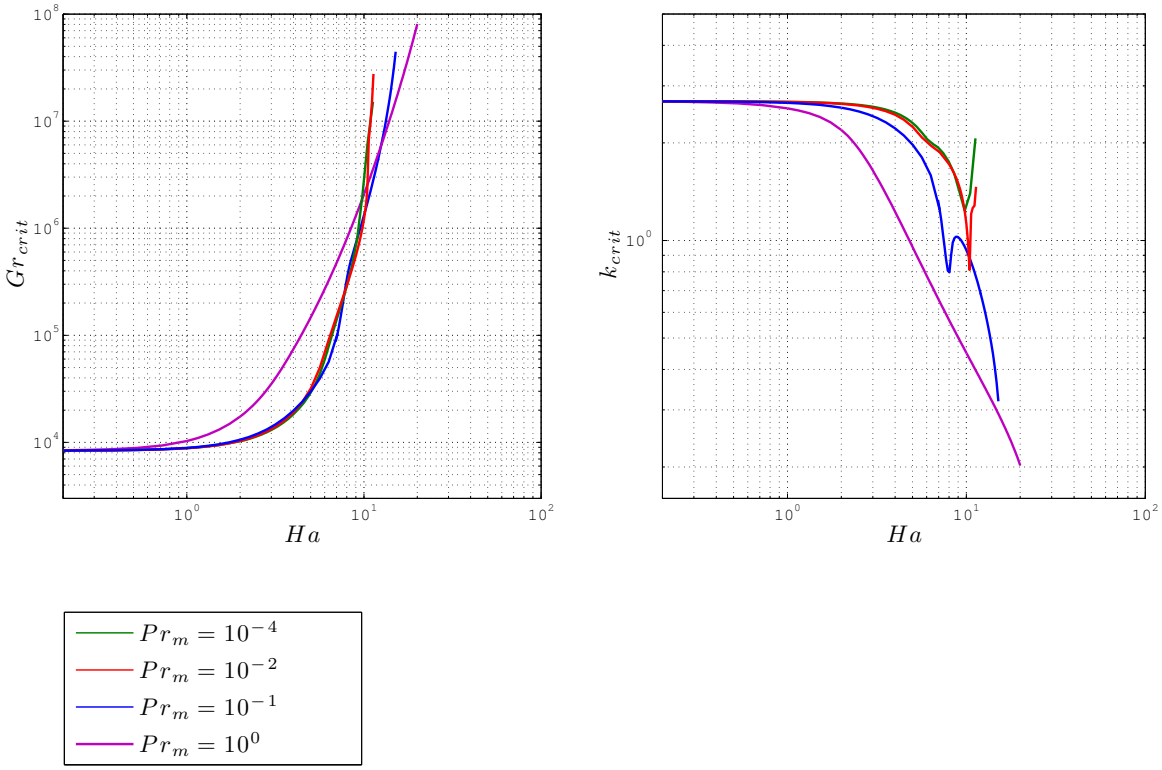

Figure 5.16: Critical values of parameters, thermally insulating & electrically conducting walls

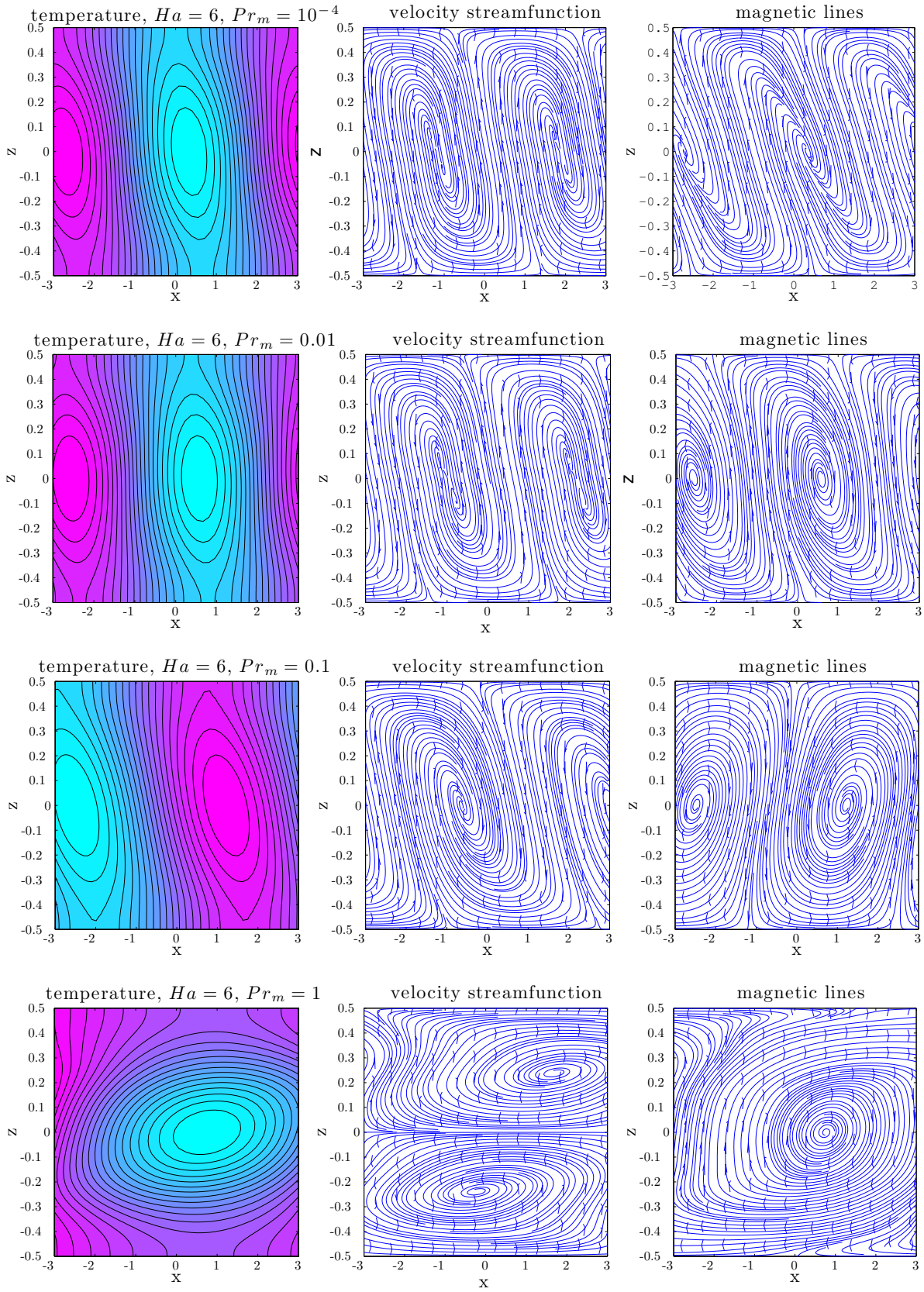

Figure 5.17: Transverse modes contour plots of disturbance isotherms (left), disturbed velocity streamlines (center) and disturbed magnetic field lines (right) for the thermally insulating and electrically conducting walls

5.3.2 Transverse modes, thermally conducting and electrically conducting walls

Here the instability modes experience common behavior patterns for the respective branches, described above. The neutral stability curves (Fig. 5.18) for $Pr_m = 10^{-4}$ repeat the inductionless approximation results, both for the low Hartmann stationary instabilities and for the high Hartmann number oscillatory thermal instabilities. The results for $Pr_m = 10^{-3}$ show small deviations, while further increase up to $Pr_m = 10^{-2.5}$ results in a significant shift towards lower oscillatory mode wavenumbers. An interesting change is observed at the onset of the oscillatory instability for $Pr_m = 10^{-2.5}$, occurring at much higher Grashof number and higher frequency.

The energy analysis results show that the kinetic and thermal fluctuating energy balances for $Pr_m = 10^{-4}$ are identical with the inductionless approximation case for the stationary instabilities of dynamical origin, while small deviation for the oscillatory instabilities may be considered negligible. In the very weak magnetic energy balance, again the only component balancing a weak magnetic dissipation is the contribution corresponding to stretching of magnetic field lines along the field, $\bar{M}_{S3}$.

For $Pr_m = 10^{-3}$, the energy balances for low Hartmann number stationary instabilities remain unchanged. In the case of oscillatory instabilities of thermal origin, the kinetic energy balance is more affected by the changing magnetic field, with the stronger stabilizing contributions due to magnetic forces $\bar{K}_m$ and shear of mean flow $\bar{K}_f$, and stronger destabilizing contribution due to buoyancy effects $\bar{K}_b$. The thermal energy balance remains here very similar to the inductionless approximation case, with a slightly weaker vertical transport of temperature term $\bar{\Theta}_1$ and slightly stronger horizontal transport of temperature term $\bar{\Theta}_2$. In the magnetic energy balance, contributions corresponding to advection $\bar{M}_{ad}$ and stretching of magnetic field lines due to shear of mean flow $\bar{M}_{S1}$ remain negligible, the stretching of magnetic field lines along the field term $\bar{M}_{S3}$ remain the main destabilizing contribution, while the effect of stretching of magnetic field lines along the flow $\bar{M}_{S2}$ serves as a small stabilizing contributions at the low Ha values and as a small destabilizing contribution for the higher Ha.

For $Pr_m = 10^{-2.5}$, in the case of low Hartmann stationary instabilities, the kinetic energy balance is slightly more affected by the increased Ha, while the thermal energy balance remains unchanged. In the fluctuating magnetic energy balance, all the deviations from the inductionless approximations are negligible for the lowest Ha values, while the contribution due to stretching of magnetic field lines along the flow $\bar{M}_{S2}$ serves as an additional small destabilizing effect just before the instability disappearance.

For the high Hartmann number oscillatory instabilities in the case of $Pr_m = 10^{-2.5}$, the dominant thermal fluctuating energy balance is more affected by the magnetic field strength and for $Ha > 100$ the term corresponding to the horizontal transport transport of temperature $\bar{\Theta}_2$ gains importance as an additional destabilizing term. In the fluctuating kinetic energy balance, the only destabilizing contribution due to buoyancy forces $\bar{K}_b$ is much stronger here and balanced by strong stabilizing effects of magnetic field $\bar{K}_m$ and the secondary stabilizing contribution due to shear of mean flow $\bar{K}_f$.

In the magnetic energy balance for $Pr_m = 10^{-2.5}$, the contribution corresponding to stretching of magnetic field lines due to shear of mean flow $\bar{M}_{S1}$ remains negligible. The stretching of magnetic field lines along the field $\bar{M}_{S3}$ serves as a weak destabilizing contribution at the onset of this instability, increases with increasing Ha and becomes the only destabilizing effect at high Ha values. The contribution due to stretching of magnetic field lines along the flow $\bar{M}_{S2}$ is the main destabilizing contribution at the instability onset, then decreases and becomes negligible at high Ha values. The magnetic contribution corresponding to advection $\bar{M}_{ad}$ serves first as a small destabilizing effect and for $Ha > 500$ also becomes negligible.

The side views of temperature disturbance isotherms, velocity streamlines and magnetic field lines (Fig. 5.19) show that for the magnetic Prandtl number increased up to $Pr_m = 10^{-2.5}$, previously weak magnetic field disturbances, gain importance and significantly deform the instability modes.

Ha	$\bar{K}_f$	$\bar{K}_b$	$\bar{K}_m$	$\bar{\Theta}_1$	$\bar{\Theta}_2$	$\bar{M}_{ad}$	$\bar{M}_{s1}$	$\bar{M}_{s2}$	$\bar{M}_{s3}$	R_{dt}	R_{dm}	R_{tm}
$Pr_m = 10^{-4}$ stationary ostabilities												
2	1.08	-0.03	-0.05	0.06	0.94	0	0	0	1	25.5	20.5	0.81
6	1.48	-0.11	-0.37	0.14	0.86	0	0	0	1	6.66	2.70	0.41
10	1.87	-0.54	-0.33	0.73	0.27	0	0	0	1	0.53	3.01	5.71
oscillatory instabilities												
60	-1.00	4.47	-2.47	0.98	0.02	0	0	0	1	0.04	0.41	9.18
100	-1.78	9.32	-6.54	0.92	0.08	0	0	-0.01	1.01	0.03	0.15	5.22
500	-0.40	23.8	-22.4	0.95	0.05	0	0	-0.02	1.02	0.01	0.05	3.12
10^3	-0.10	29.0	-27.9	0.97	0.03	0	0	-0.02	1.02	0.01	0.04	3.04
$Pr_m = 10^{-3}$ stationary instabilities												
2	1.08	-0.03	-0.05	0.06	0.94	0	0	0.01	0.99	25.5	20.3	0.80
6	1.48	-0.10	-0.38	0.14	0.86	0	0	0.01	0.99	6.58	2.65	0.40
10	1.90	-0.55	-0.35	0.73	0.27	0	0	0.04	0.96	0.51	2.75	5.43
oscillatory instabilities												
60	-1.58	5.47	-2.89	0.96	0.04	0.05	0	0.23	0.72	0.03	0.33	10.4
100	-2.69	9.91	-6.22	0.88	0.12	0.02	0	-0.01	0.99	0.03	0.16	6.02
500	-1.20	29.3	-27.1	0.89	0.11	0.01	0	-0.15	1.14	0.01	0.04	2.86
10^3	-0.60	36.1	-34.5	0.91	0.09	0.01	0	-0.15	1.14	0.01	0.03	2.78
$Pr_m = 10^{-2.5}$ stationary instabillities												
2	1.08	-0.03	-0.05	0.06	0.94	0.01	-0.01	0.02	0.98	25.4	19.8	0.78
6	1.50	-0.11	-0.39	0.14	0.86	0.01	-0.01	0.03	0.97	6.41	2.54	0.40
10	1.93	-0.56	-0.37	0.74	0.26	0.16	-0.04	0.14	0.74	0.50	2.10	4.21
oscillatory instabilities												
60	-1.52	8.13	-5.61	0.98	0.02	0.22	0.02	0.61	0.15	0.01	0.16	25.1
100	-2.74	9.49	-5.75	0.87	0.13	0.18	0.01	0.34	0.47	0.02	0.16	10.7
500	-2.20	39.0	-35.8	0.67	0.33	0.02	0	-0.19	1.17	0.01	0.03	2.73
10^3	-1.40	54.2	-51.8	0.68	0.32	0	0	-0.26	1.26	0.01	0.02	2.39

Table 5.12: Transverse modes, energy balances for the thermally and electrically conducting walls

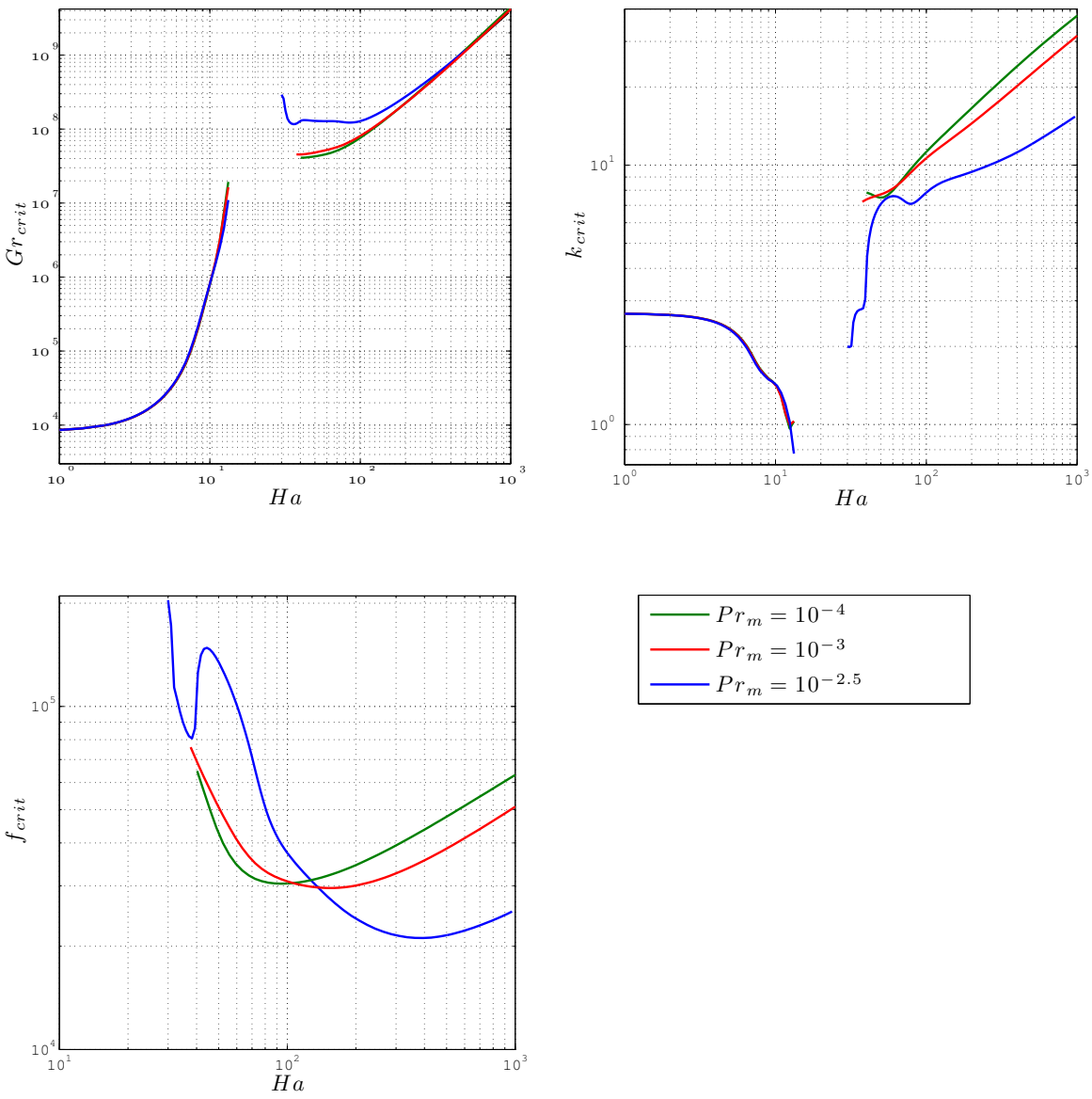

Figure 5.18: Critical values of parameters, thermally conducting & electrically conducting walls

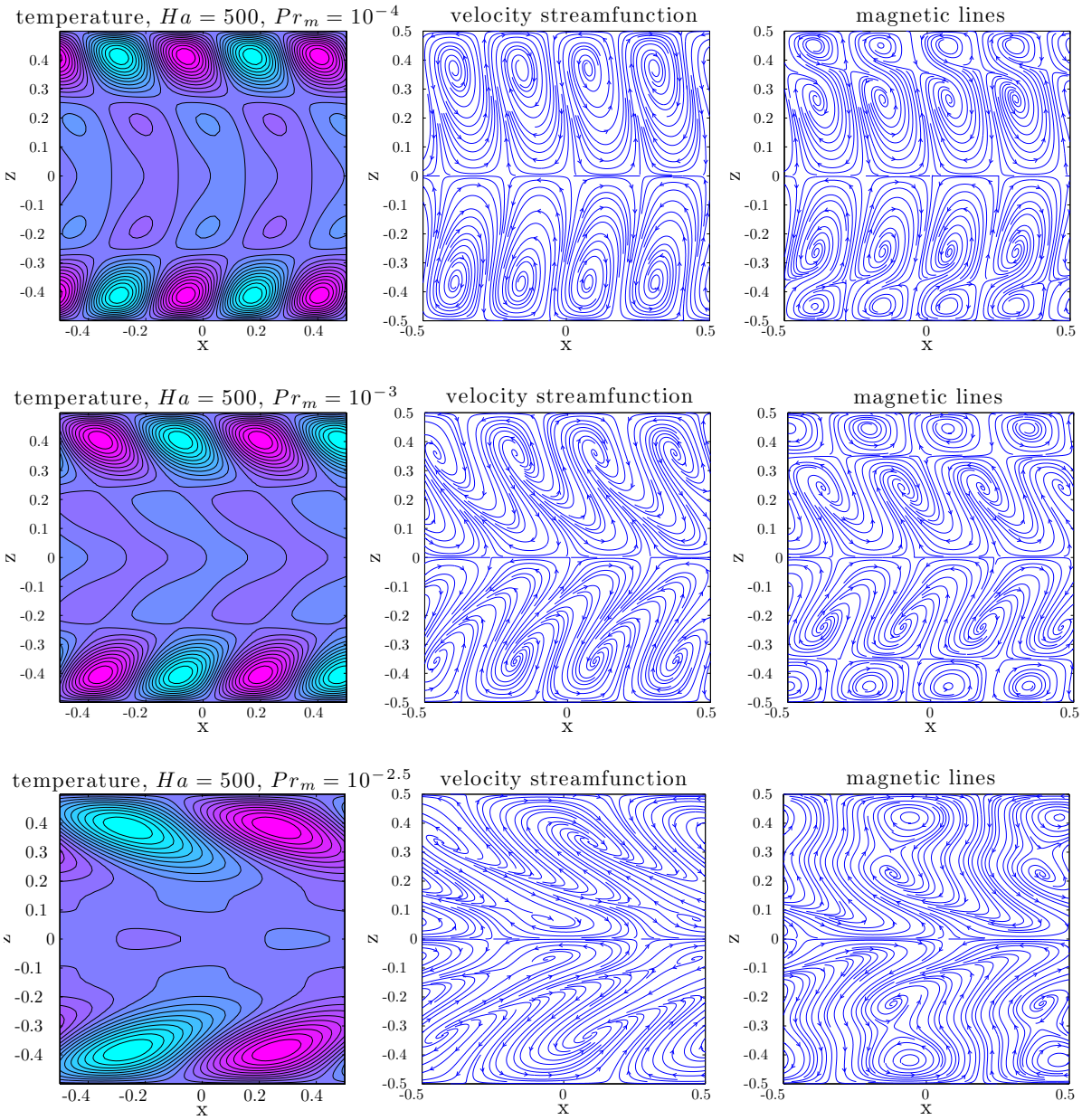

Figure 5.19: Transverse modes contour plots of disturbance isotherms (left), disturbed velocity streamlines (center) and disturbed magnetic field lines (right) for the thermally and electrically conducting walls

5.3.3 Transverse modes, thermally insulating and electrically insulating walls

The stationary instability of dynamical origin both thermally and electrically insulating walls show common behavior patterns with the case of the thermally insulating and electrically conducting walls, for different values of Pr_m considered.

A new stationary instability, with no counterpart in the inductionless approximation case, is observed here for a very small range of the magnetic Prandtl number at around $Pr_m = 10^{-1}$. The onset of this new stationary instability, $Ha \simeq 5.3$, corresponds to a small minimum in the critical wavenumber curve of the initial instability. The new instability becomes most dangerous and persists up to high Hartmann numbers.

For $Ha > 70$ the critical Grashof number values reach asymptotic relation $Gr_{crit} = 118Ha^2$, while the critical wavenumber remains constant, $k_{crit} = 1.68$.

The energy analysis results (Table 5.9), show that for $Pr_m = 10^{-4}$, the energy balances are identical with the case of thermally insulating and electrically conducting boundaries. For $Pr_m = 10^{-2}$, the fluctuating thermal and magnetic energy balances remain very similar, while in the kinetic energy balance the only destabilizing contribution, due to shear of mean flow $\bar{K}_f$, is weaker here and, with the unchanged stabilizing buoyancy effects $\bar{K}_b$, balanced by a weaker magnetic contribution $\bar{K}_m$.

Interestingly, the energy balances obtained for $Pr_m = 10^0$ are very similar for both cases of electromagnetic boundary conditions.

The energy analysis of the low Hartmann number stationary instability for $Pr_m = 10^{-1}$ show several indications of the possibility of a new instability appearance here. The thermal energy balance, similar to the electrically conducting boundaries case at the lowest Hartmann number values and just before the instability disappearance, differ in the vicinity of the new instability onset. The fluctuating thermal energy production by the vertical transport of temperature $\bar{\Theta}_1$ reaches here an unexpected maximum, exceeding the horizontal temperature transport term $\bar{\Theta}_2$ by approximately three times. The ratios R_{dt} and R_{tm} show stronger dominance of the magnetic over thermal effects and decreasing importance of the dynamic effects.

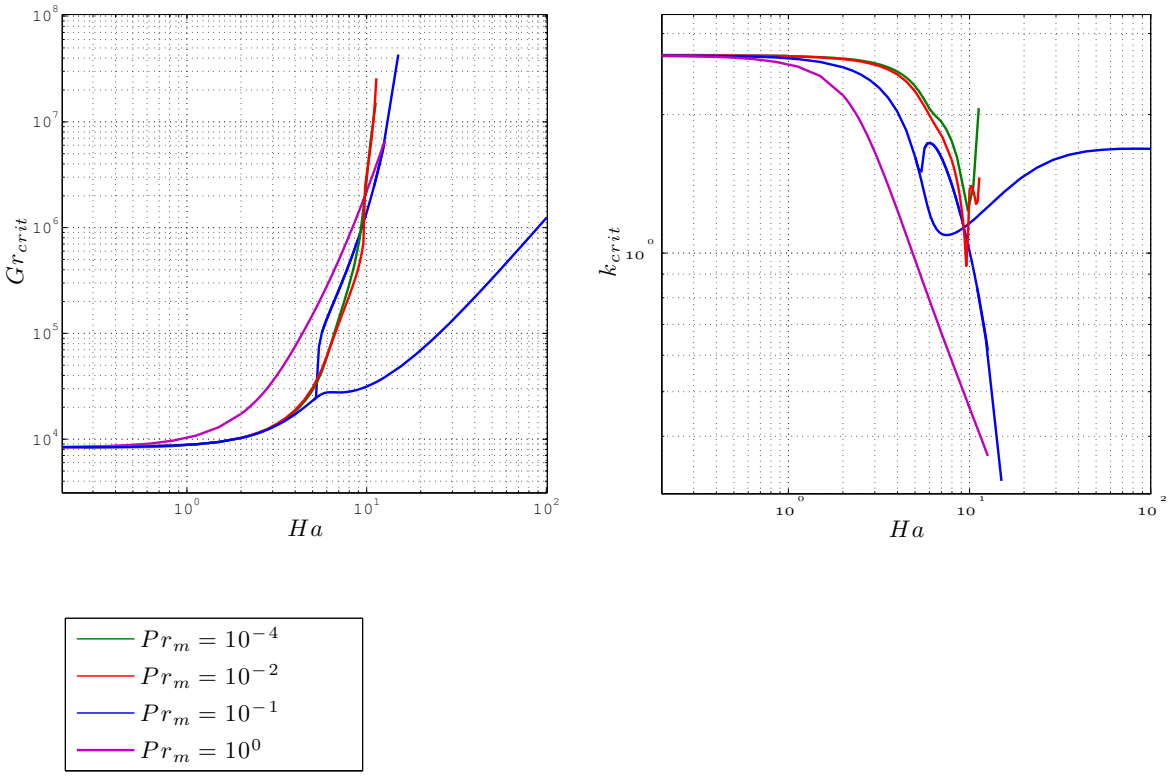

Figure 5.20: Critical values of parameters, thermally insulating & electrically insulating walls

Also the fluctuating magnetic energy balance experience a significant modification for this instability. The magnetic contribution corresponding to stretching of magnetic field lines due to shear of mean flow $\bar{M}_{S1}$ here is stronger than in the case of electrically insulating walls, while the advection contribution $\bar{M}_{ad}$ remains similar and becomes slightly stronger just before the instability disappearance. The contribution by stretching of magnetic field lines along the flow $\bar{M}_{S2}$ becomes stabilizing much sooner for this boundary conditions combinations, in the vicinity of the new instability onset. The effects of stretching of magnetic field lines along the field $\bar{M}_{S3}$ remain similar, except the Ha values around the new instability appearance.

The energy analysis results show, that the new stationary instability is of magnetic origin. With increasing strength of the magnetic field, the dynamic effects

gain importance, while the thermal effects remain least important. For $Ha > 11$ the dynamic effects weaken again and for $Ha > 16$ become least important.

In the fluctuating kinetic energy balance, the contribution due to buoyancy forces $\bar{K}_b$ stabilizes the flow, while the magnetic effects term $\bar{K}_m$ serves as the main destabilizing contribution. The fluctuating energy contribution due to shear of mean flow $\bar{K}_f$ first destabilizes the flow and in the vicinity of the minimum in the critical wavenumber stability curve, $Ha \approx 7.5$, becomes a stabilizing contribution.

The fluctuating thermal energy effects due to horizontal transport of temperature $\bar{\Theta}_2$ serve as a strong stabilizing contribution, growing with increasing magnetic field strength. The secondary stabilizing contribution corresponding to vertical transport of temperature $\bar{\Theta}_1$ becomes negligible at high Ha values.

The fluctuating magnetic energy balance at the onset of this instability and up to $Ha \approx 10.5$ show the following characteristics. The contributions due to advection $\bar{M}_{ad}$ and stretching of magnetic field lines along the flow $\bar{M}_{S2}$ are destabilizing and increase with increasing Ha. The stretching of magnetic field lines due to shear of mean flow $\bar{M}_{S1}$ serves as a decreasing destabilizing contribution, while the effects of magnetic field lines stretching along the field $\bar{M}_{S3}$ weakly stabilize the flow.

For the higher Hartmann number values, both the destabilizing advection $\bar{M}_{ad}$ contribution and the contribution due to stretching of magnetic field lines along the flow $\bar{M}_{S2}$ decrease. The effects of stretching of magnetic lines along the field $\bar{M}_{S3}$ become destabilizing while the effects of stretching due to shear of mean flow $\bar{M}_{S1}$ become a small stabilizing contribution.

The contour plots for the new instability (Fig. 5.21) illustrate the departure of temperature disturbances from the center of the flow towards horizontal boundaries with increasing magnetic field strength. The side views of disturbed velocity streamlines and magnetic field lines show the evolution of the new instability shape.

Ha	$\bar{K}_f$	$\bar{K}_b$	$\bar{K}_m$	$\bar{\Theta}_1$	$\bar{\Theta}_2$	$\bar{M}_{ad}$	$\bar{M}_{s1}$	$\bar{M}_{s2}$	$\bar{M}_{s3}$	R_{dt}	R_{dm}	R_{tm}
$Pr_m = 10^{-4}$ stationary instabilities												
2	1.11	-0.06	-0.05	0.17	0.83	0	0	0	1	10.9	20.6	1.89
6	1.73	-0.42	-0.31	0.65	0.35	0	0	0	1	1.69	3.19	1.88
9	2.02	-0.74	-0.28	0.94	0.06	0	0	0	1	0.16	3.52	22.2
$Pr_m = 10^{-2}$ stationary instabilities												
2	1.11	-0.06	-0.05	0.17	0.83	0.01	-0.02	0.07	0.94	10.8	18.6	1.72
6	1.77	-0.44	-0.33	0.67	0.33	0.06	-0.10	0.18	0.86	1.60	2.67	1.67
9	1.89	-0.80	-0.09	1.04	-0.04	0.22	0.31	0.11	0.36	0.28	1.36	4.88
$Pr_m = 10^{-1}$ stationary instabilities												
2	1.11	-0.06	-0.05	0.16	0.84	0.22	0.09	0.46	0.23	10.3	7.11	0.69
5	1.08	-0.21	0.13	0.26	0.74	0.25	0.38	0.34	0.03	2.93	0.89	0.30
6	1.25	-0.31	0.06	0.78	0.22	0.24	0.78	-0.18	0.16	1.18	0.25	0.21
7	0.28	-0.22	0.94	0.72	0.28	0.27	1.06	-0.53	0.20	0.92	0.27	0.30
9	-1.29	-0.15	2.44	0.57	0.43	0.47	1.66	-1.37	0.24	0.45	0.34	0.74
new stationary instabilities												
6	0.66	-0.32	0.66	0.26	0.74	0.26	0.47	0.37	-0.10	1.85	0.81	0.44
7	0.23	-0.33	1.10	0.20	0.80	0.29	0.44	0.50	-0.23	1.58	1.01	0.64
9	-0.14	-0.29	1.43	0.13	0.87	0.33	0.14	0.70	-0.17	1.43	1.18	0.83
10	-0.22	-0.28	1.50	0.11	0.89	0.33	0.01	0.73	-0.07	1.36	1.14	0.83
11	-0.28	-0.27	1.55	0.10	0.90	0.31	-0.10	0.73	0.06	1.30	1.04	0.80
16	-0.38	-0.27	1.65	0.06	0.94	0.23	-0.27	0.62	0.42	1.01	0.57	0.57
20	-0.38	-0.29	1.67	0.05	0.95	0.20	-0.27	0.57	0.50	0.83	0.38	0.46
100	-0.11	-1.53	2.64	0.04	0.96	0.15	-0.24	0.50	0.59	0.14	0.04	0.28
$Pr_m = 10^{0}$ stationary instabilities												
2	0.41	-0.04	0.63	0.22	0.78	0.16	1.20	-0.46	0.10	14.1	0.55	0.04
6	-0.71	-0.02	1.73	0.10	0.90	2.33	2.77	-4.48	0.38	1.65	1.08	0.66
9	-0.47	-0.01	1.48	0.01	0.99	4.04	2.44	-5.90	0.42	0.62	1.01	1.62

Table 5.13: Transverse modes, energy balances for the thermally and electrically insulating walls

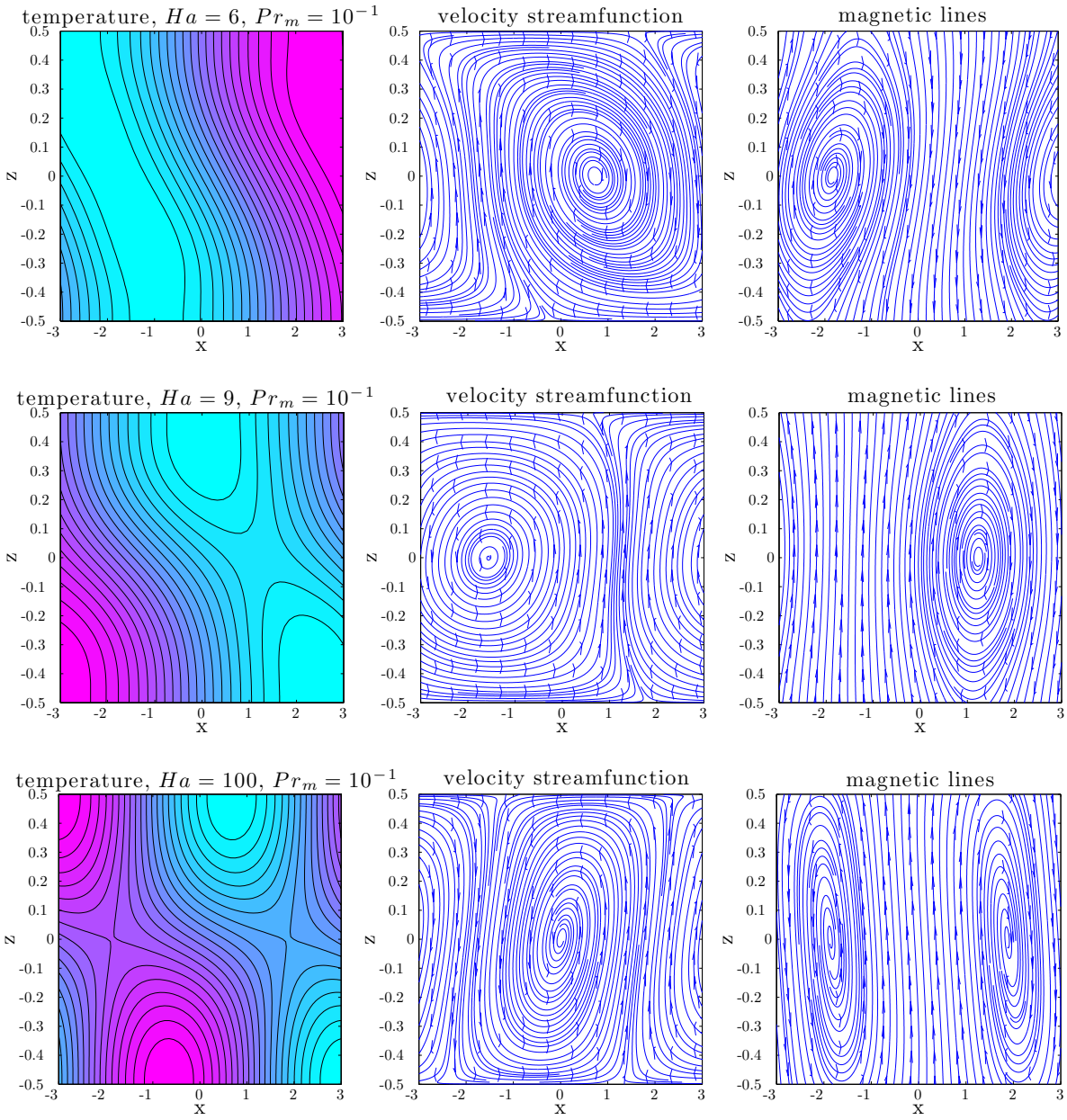

Figure 5.21: Transverse modes contour plots of disturbance isotherms (left), disturbed velocity streamlines (center) and disturbed magnetic field lines (right) for the thermally and electrically insulating walls, the new instability

5.3.4 Transverse modes, thermally conducting and electrically insulating walls

In the case of thermally conducting and electrically insulating walls, for $Pr_m = 10^{-4}$ and for $Pr_m = 10^{-3}$ the low Hartmann number stationary and the high Hartmann number oscillatory instabilities experience common behavior patterns with their counterparts of the thermally and electrically conducting boundaries case. Further increase of the magnetic Prandtl number leads to major differences between the two cases.

For for $Pr_m = 10^{-2.5}$, the oscillatory instability appears at slightly higher Ha, with lower critical Grashof number, critical wavenumber and frequency than the repsective instability in the case of thermally and electrically conducting walls.

For the boundary conditions consisting of a combination of thermally conducting and electrically insulating walls, two kinds of new instability appear at very narrow ranges of Pr_m, namely a new oscillatory instability for $Pr_m = 10^{-2.5}$ and a stationary instability for $Pr_m = 10^{-2}$, which originatess from the low Ha stationary mode.

The energy analysis results show that the stationary instabilities energy balances for $Pr_m = 10^{-4}$ and for $Pr_m = 10^{-3}$ are identical with the inductionless approximation case, except just before the instabilities disappearance, where small fluctuating energy deviations are negligible. For oscillatory modes appearing at higher Ha, fluctuating thermal and magnetic energy balances for $Pr_m = 10^{-4}$ and for $Pr_m = 10^{-3}$ are again the same as in the inductionless approximation case. The kinetic energy balance for $Pr_m = 10^{-4}$ is slightly more affected here for $Ha > 500$, while for $Pr_m = 10^{-3}$ all the kinetic contributions are stronger over the whole instability range.

The energy results for $Pr_m = 10^{-2.5}$ show, that for the low Ha stationary instability, again slight deviations form the inductionless approximation case occur only just before the instability disappearance. For the oscillatory instability, in the dominant thermal energy balance, the secondary destabilizing effects of horizontal temperature transport $\bar{\Theta}_2$ are here stronger, while the contribution corresponding to vertical transport of temperature $\bar{\Theta}_1$ is weaker here than in the inductionless approximation case. In the kinetic energy balance, terms corre-

sponding to the buoyancy $\bar{K}_b$ and magnetic $\bar{K}_m$ effects are stronger here destabilizing and stabilizing, respectively. The magnetic energy balance shows, that the effects of stretching of magnetic field lines along the field $\bar{M}_{S3}$ are weakly stabilizing at the instability onset, gaining importance with the increase of Ha. Both the advection $\bar{M}_{ad}$ and stretching of magnetic lines due to shear of mean flow $\bar{M}_{S1}$ contributions are slightly destabilizing at the instability onset and soon become negligible. Stretching of magnetic field lines along the flow $\bar{M}_{S2}$ is the main destabilizing effect at the beginning of the instability. It decreases with increased Ha and switches no negative values for higher magnetic field strength.

The ratios R_{dm} and R_{tm} indicate increasing importance of the magnetic effects with increasing Pr_m.

The new oscillatory instability for $Pr_m = 10^{-2.5}$ appears at $Ha \approx 19$ and is the most dangerous for a small range of Ha, just after its onset. After the appearance of the high Ha instability originated from the inductionless approximation, it soon becomes the most stable. This instability has lower frequency and much lower wavenumber than other oscillatory instabilities discussed above. There is no indication of possible asymptotic behavior for high Hartmann numbers.

The energy analysis for this new instability shows that in the dominant thermal energy balance, the effects of vertical transport of temperature $\bar{\Theta}_1$ serve here as main destabilizing contribution, with the secondary stabilizing effects of horizontal transport of temperature $bar\Theta_2$. In the fluctuating magnetic energy balance, advection $\bar{M}_{ad}$ serves as a small stabilizing contribution for all the instability range, while the contribution due to stretching of magnetic field lines along the flow $\bar{M}_{S2}$ becomes destabilizing soon after the instability onset. The effect of stretching of magnetic field lines due to shear of mean flow $\bar{M}_{S1}$ is the main destabilizing contribution at the instability onset but it decreases with increasing Ha. At the same time the destabilizing effects due to stretching of magnetic lines along the field $\bar{M}_{S3}$, first negligible, become significant at larger Ha. In the least important fluctuating kinetic energy balance, the magnetic term $\bar{K}_m$ is the main destabilizing contribution at the onset. It decreases with increasing magnetic field strength and stabilizes the flow at higher Ha. The buoyancy forces term $\bar{K}_b$, stabilizing at the beginning, soon becomes an increasing destabilizing contribution. The kinetic contribution due to shear of mean flow $\bar{K}_f$, stabilizing

at the instability onset, quickly switches to positive values, and back to negative for higher Ha values.

The side views of temperature disturbance isotherms, velocity streamlines and magnetic field lines (Fig. 5.23) show the new oscillatory instability evolution with increasing magnetic field strength, particularly the appearance of disturbance isotherms structures near horizontal boundaries and changes in the velocity streamlines towards more regular modes.

The stationary instability for $Pr_m = 10^{-2}$ continues from the inductionless approximation originated mode at relatevely low critical Grashof numbers, becoming the most dangerous of all the instabilities discussed above. The critical wavenumber decreases quickly for the original instability and instead of disappearing, reaches its minimum $k_{crit} = 0.53$ at $Ha \approx 15.1$, increases with increasing magnetic field strength up to $k_{crit} = 1.47$ at $Ha \approx 225$, and remains constant at higher values of the Hartmann number.

The energy balances for this instability, similar to the cases of lower Pr_m for $Ha < 9$, change significantly and for $Ha > 10$ the dynamical effects loose the dominance and the instability becomes thermal. In the dominant fluctuating thermal energy balance, the contribution corresponding to horizontal transport of temperature $\bar{\Theta}_2$ remains the main destabilizing term, while $\bar{\Theta}_1$ serves as the secondary stabilizing contribution. The energy analysis shows major differences in the fluctuating kinetic energy balance, where, while the effects of buoyancy forces $\bar{K}_b$ remain stabilizing and increase with Ha, the term due to shear of mean flow $\bar{K}_f$ becomes an increasing stabilizing contribution, while the magnetic effects $\bar{K}_m$ strongly destabilize the flow at increased values of Ha. In the magnetic energy balance, the effects of magnetic field lines stretching along the field $\bar{M}_{S3}$ remain the main stabilizing contribution, decreasing slightly at higher Ha. The term corresponding to stretching of magnetic field lines along the flow $\bar{M}_{S2}$ serves as an increasing secondary destabilizing contribution, while the advection contribution $\bar{M}_{ad}$ additionally weakly stabilizes the flow. Stabilizing effects of stretching of magnetic field lines due to shear of mean flow $\bar{M}_{S1}$ become less significant with increasing magnetic field strength.

The contour plots (Fig. 5.24) show the new stationary instability evolution with increasing Ha, where the disturbance isotherms move towards horizontal

boundaries and again the velocity streamlines appear as more regular modes.

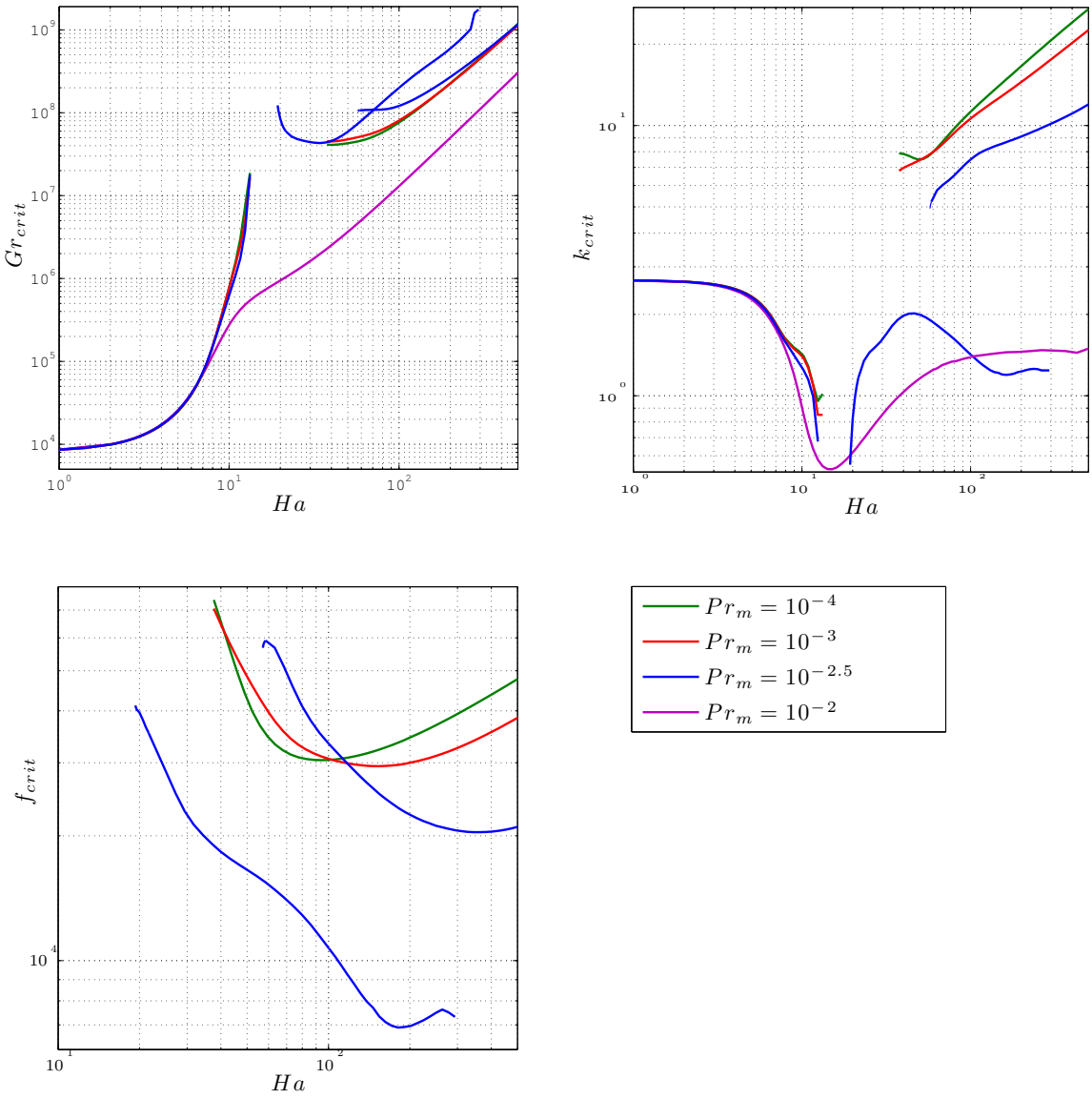

Figure 5.22: Critical values of parameters, thermally conducting & electrically insulating walls

Ha	$\bar{K}_f$	$\bar{K}_b$	$\bar{K}_m$	$\bar{\Theta}_1$	$\bar{\Theta}_2$	$\bar{M}_{ad}$	$\bar{M}_{S1}$	$\bar{M}_{S2}$	$\bar{M}_{S3}$	R_{dt}	R_{dm}	R_{tm}
$Pr_m = 10^{-4}$ stationary ostabilities												
2	1.08	-0.03	-0.05	0.06	0.94	0	0	0	1	25.5	20.5	0.80
6	1.48	-0.11	-0.37	0.14	0.86	0	0	0	1	6.66	2.69	0.40
10	1.87	-0.54	-0.33	0.73	0.27	0	0	0	1	0.53	2.99	5.66
oscillatory instabilities												
60	-1.00	4.48	-2.48	0.98	0.02	0	0	0	1	0.04	0.40	9.16
100	-1.78	9.33	-6.55	0.92	0.08	0	0	-0.01	1.01	0.03	0.15	5.18
500	-0.40	24.3	-22.9	0.95	0.05	0	0	-0.02	1.02	0.01	0.04	3.05
10^3	-0.20	31.4	-30.2	0.97	0.03	0	0	-0.02	1.02	0.01	0.03	2.94
$Pr_m = 10^{-3}$ stationary instabilities												
2	1.08	-0.03	-0.05	0.06	0.94	0	0	0.01	0.99	25.5	20.3	0.80
6	1.48	-0.10	-0.38	0.14	0.86	0	0	0.01	0.99	6.59	2.65	0.40
10	1.89	-0.55	-0.34	0.72	0.28	0.02	-0.05	0.06	0.97	0.53	2.84	5.34
oscillatory instabilities												
60	-1.53	5.51	-2.98	0.96	0.04	0.04	-0.01	0.25	0.72	0.03	0.32	10.0
100	-2.70	10.0	-6.30	0.88	0.12	0.01	0	0	0.99	0.03	0.16	5.93
500	-1.30	30.1	-27.8	0.89	0.11	0	0	-0.14	1.14	0.01	0.04	2.79
10^3	-0.70	40.2	-38.5	0.91	0.09	0	0	-0.14	1.14	0.01	0.03	2.68
$Pr_m = 10^{-2.5}$ stationary instabillities												
2	1.08	-0.03	-0.05	0.06	0.94	0	0	0.02	0.98	25.4	19.8	0.78
6	1.50	-0.11	-0.39	0.14	0.86	0.01	-0.01	0.03	0.97	6.45	2.56	0.40
10	1.84	-0.56	-0.28	0.65	0.35	0.10	-0.11	0.16	0.85	0.62	2.50	4.01
oscillatory instabilities												
60	-0.76	7.09	-5.33	0.98	0.02	0.12	0.13	0.55	0.20	0.01	0.13	14.96
100	-3.0	10.3	-6.30	0.86	0.14	0.08	0.01	0.41	0.50	0.01	0.14	9.46
500	-2.30	41.4	-38.1	0.67	0.33	-0.01	0	-0.13	1.14	0.01	0.03	2.60
10^3	-1.70	69.4	-66.7	0.69	0.31	-0.02	0	-0.21	1.23	0.01	0.01	2.26
new oscillatory instabilities												
20	-2.39	-1.29	4.68	0.93	0.07	-0.04	1.14	-0.09	-0.01	0.01	0.06	6.28
40	0.69	0.27	0.04	0.93	0.07	-0.06	0.62	0.31	0.13	0.03	0.06	2.25
60	0.51	3.88	-3.39	0.97	0.03	-0.03	0.38	0.36	0.29	0.01	0.05	3.99
100	-1.28	5.25	-2.97	0.88	0.12	-0.08	0.33	0.30	0.45	0.01	0.06	4.85
$Pr_m = 10^{-2}$ stationary instabillities												
2	1.08	-0.03	-0.05	0.06	0.94	0.02	-0.02	0.06	0.94	25.3	18.5	0.73
6	1.51	-0.11	-0.40	0.14	0.86	0.04	-0.07	0.13	0.90	6.17	2.34	0.38
10	1.48	-0.40	-0.08	0.28	0.72	0.17	-0.19	0.27	0.75	0.94	1.63	1.73
20	-0.77	-0.69	2.46	0.12	0.88	0.21	-0.63	0.32	1.10	0.21	0.79	3.69
40	-1.67	-1.46	4.13	0.10	0.90	0.15	-0.44	0.31	0.98	0.11	0.17	1.53
60	-1.43	-2.34	4.77	0.11	0.89	0.14	-0.35	0.36	0.85	0.08	0.09	1.10

Table 5.14: Transverse modes, energy balances for the thermally conducting and electrically insulating walls

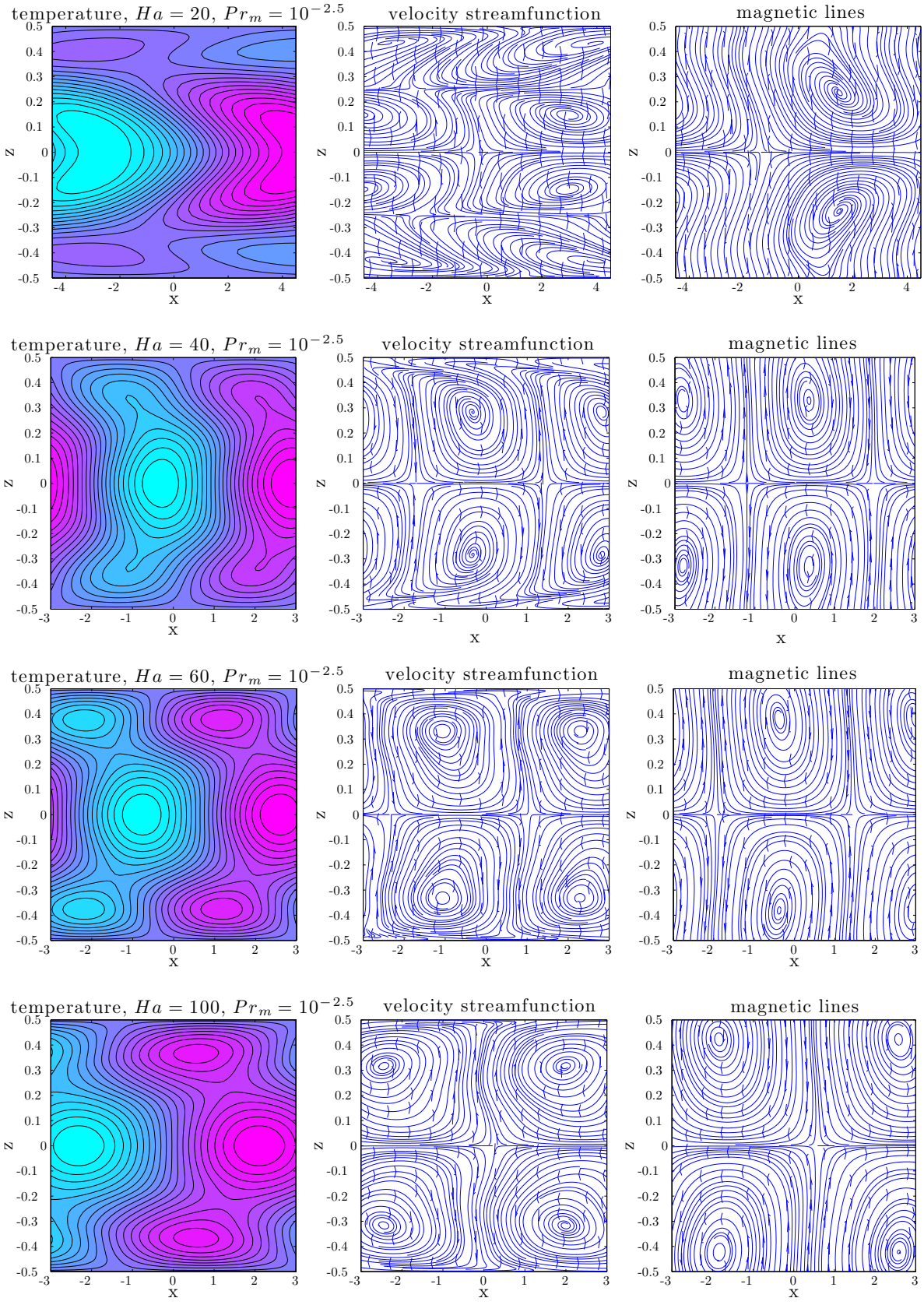

Figure 5.23: Transverse modes contour plots of disturbance isotherms (left), disturbed velocity streamlines (center) and disturbed magnetic field lines (right) for the thermally conducting and electrically insulating walls, the new instability for $Pr_m = 10^{-2.5}$

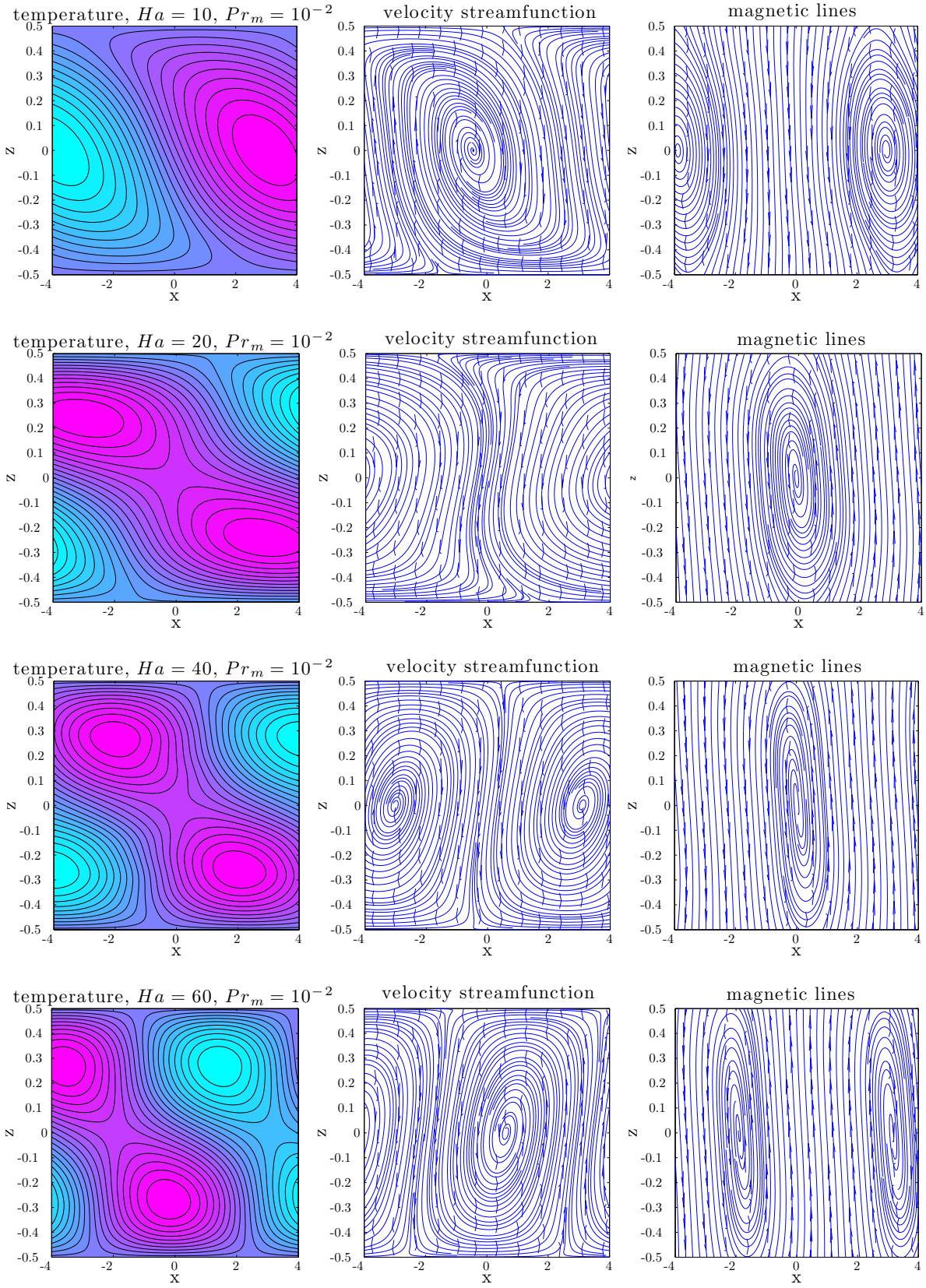

Figure 5.24: Transverse modes contour plots of disturbance isotherms (left), disturbed velocity streamlines (center) and disturbed magnetic field lines (right) for the thermally conducting and electrically insulating walls, the new instability for $Pr_m = 10^{-2}$

Chapter 6

Vertical channel with internal heating sources

6.1 Problem formulation

Consider the problem of linear stability of an infinite vertical fluid layer with uniformly distributed internal heat sources $Q = 1$, as shown in Fig. 6.1. The two parallel vertical rigid boundaries are maintained at constant and equal temperatures, and it is assumed that the horizontal extension of the plates is large. The flow, subject to a uniform magnetic field $\mathbf{B}_0 = \mathbf{e}_z$ is studied in the presence of gravity $\mathbf{g} = \mathbf{e}_x$.

The problem, considered in the inductionless approximation, has a steady flow solution (Fig. 6.2), whereby the base velocity profile $\mathbf{u}_0 = [u_0(z), 0, 0]$ and the basic temperature profile $T_0(z)$ are governed, as follows from (2.35)-(2.37), by the following set of equations:

$$u_0''' - Ha^2 u_0' - GrT_0' = 0 \ , \tag{6.1}$$

$$T_0'' + PrQ = 0 \ . \tag{6.2}$$

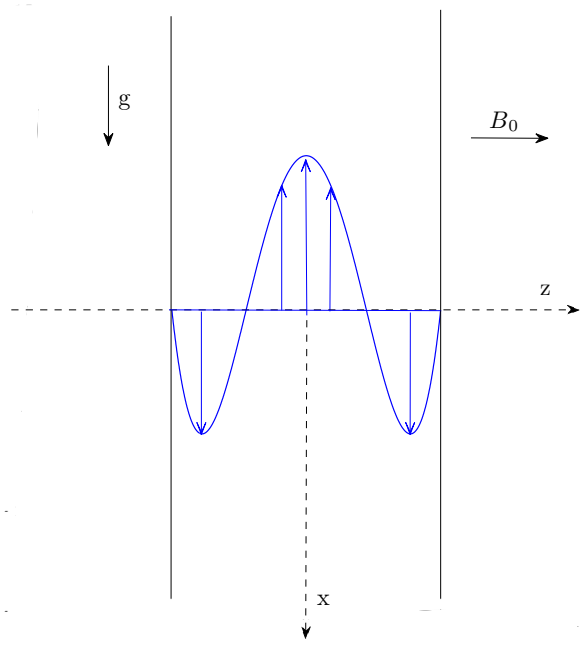

Figure 6.1: Schematic diagram of the vertical fluid layer with side walls of equal temperatures

The analytical expressions for basic velocity $u_0(z)$ and temperature $T_0(z)$ profiles are:

$$u_0 = \frac{PrGrQ}{2Ha^2}\left\{z^2 + \frac{2Ha\cosh(Haz) - 6\sinh(0.5Ha) + Ha\cosh(0.5Ha)}{24\sinh(0.5Ha) - 12Ha\cosh(0.5Ha)}\right\}, \tag{6.3}$$

$$T_0 = \frac{1}{2}PrQ\left\{-z^2 + \frac{1}{4}\right\} . \tag{6.4}$$

The temperature profile does not depend on the Hartmann number, thus, being independent of the magnetic field B_0, is identical with the case of natural convection in the absence of the magnetic field [59]. The basic electric potential for both electrically conducting and electrically insulating walls is constant and can be set to zero:

$$\phi_0 = 0 . \tag{6.5}$$

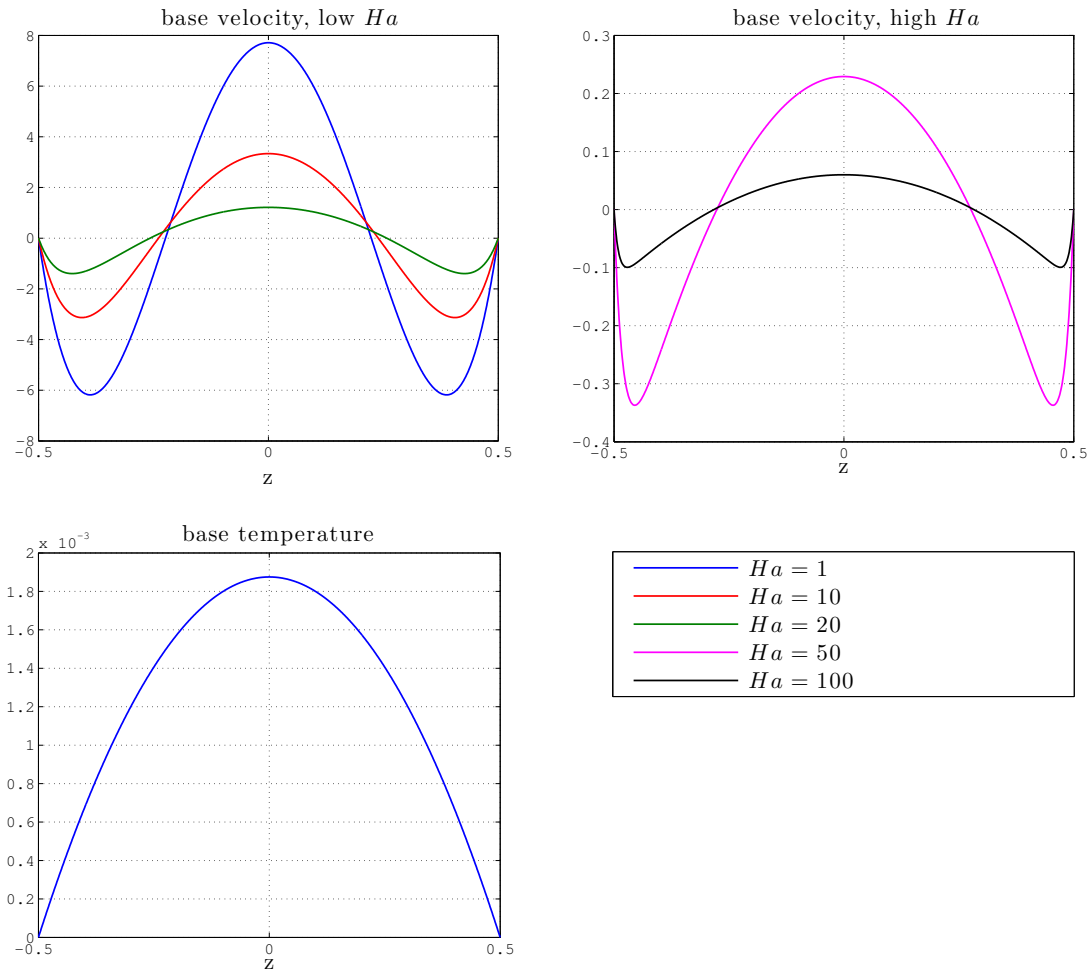

Figure 6.2: Base velocity and temperature profiles for $Pr = 0.015$ and $Gr = 10^6$

The disturbance equations derived in Chapter 3 apply here with a number of simplifications, namely:

$$\{\mathbf{D}^4 - u_0 ik_x \mathbf{D}^2 + u_0'' ik_x - Ha^2 \partial_z^2\}\hat{w} + Grik_x \partial_z \hat{\theta} = \lambda \mathbf{D}^2 \hat{w} \ , \tag{6.6}$$

$$\{\mathbf{D}^2 - u_0 ik_x - Ha^2\}\hat{\omega}_z + u_0' ik_y \hat{w} - Ha^2 k^2 \hat{\phi} + Grik_y \hat{\theta} = \lambda \hat{\omega}_z \ , \tag{6.7}$$

$$\{\frac{1}{Pr}\mathbf{D}^2 - u_0 ik_x\}\hat{\theta} - T_0' \hat{w} = \lambda \hat{\theta} \ . \tag{6.8}$$

Here, similarly to Chapter 5.2, the electric potential ϕ is related to the vorticity $\underline{\omega}$ through (2.46), which leads to the following disturbance equation:

$$\hat{\omega}_z = \mathbf{D}^2\hat{\phi} \,, \tag{6.9}$$

with the following boundary conditions for the disturbed electric potential:

$\hat{\phi} = 0$ at $z = \pm 0.5$ for electrically conducting walls,
$\partial_z\hat{\phi} = 0$ at $z = \pm 0.5$ for electrically insulating walls.

Hereafter, following the reasoning presented in [59] for $Ha = 0$, only transverse modes with $k_y = 0$ are considered. In order to examine the effect of a uniform magnetic field applied along the $z-$ axis on the stability of convective flow in the vertical channel, the numerical stability results have been obtained for $Pr = 0.015$. As in previous chapters, the critical Grashof number is defined by minimization along the wavenumber k_x.

The appropriate boundary conditions for disturbances are applied, as specified in Section 3.2. Since the vertical walls are held and constant temperatures, only thermally conducting boundary conditions for disturbed temperature are considered.

6.2 Linear stability results

It has been already shown in [59], that in the absence of externally applied magnetic field, for $Ha = 0$, the transverse oscillatory instability modes are observed. The dependence of critical Grashof number, critical wavenumber and critical frequency for different values of Pr are shown in Fig.6.3. These results are in agreement with the findings in [59] and serve as a starting point for the investigation of the effects of an externally applied magnetic field on the problem.

The linear stability analysis has been performed for the cases of electrically conducting and electrically insulating side walls. The results show (Fig. 6.4), that the electrical boundary conditions have no effect on the instabilities. For $Ha \to 0$ the instability tends to a unique limit $Gr_{crit} = 3.616 \cdot 10^6$, $k_{crit} = 4.14$ and $f_{crit} = 38$.

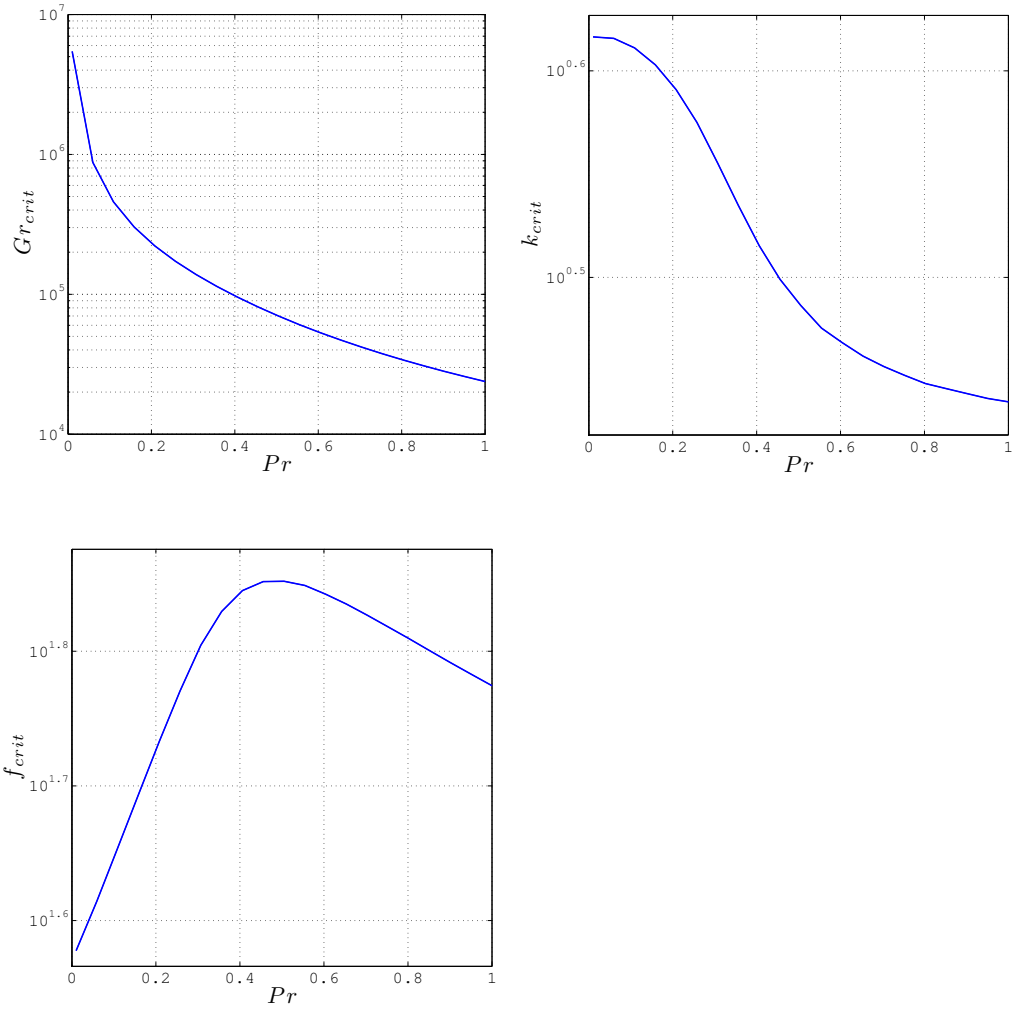

Figure 6.3: Critical values of parameters for $Ha = 0$

With the increased magnetic field strength, the critical values of these parameters increase slowly up to $Ha \approx 9.3$, where the critical wavenumber reaches its maximum $k_{crit} \approx 4.4$. For $Ha > 9.3$, the magnetic field stabilizes the flow very quickly, shifting the critical Grashof number and the critical frequency towards high values. For $40 < Ha < 100$, the following behavior of the neutral stability curves has been observed: $Gr_{crit} = 172Ha^{4.3}$, $k_{crit} = 10.6Ha^{-0.3}$, $f_{crit} = 0.14Ha^{2.6}$. The instability then disappears and no new branches have been

found for $Ha > 100$.

The energy analysis has been performed to establish the perturbation energy balances and to identify the instability mechanisms. In the fluctuating thermal energy balance, the contribution corresponding to horizontal transeptrt of temperature $\bar{\Theta}_2$ does not exist as the basic temperature profile is here independent of the $x-$ direction. The only contribution balancing the dissipation is the energy production by vertical transport of temperature $\bar{\Theta}_1$, and the fluctuating thermal energy balance reads $\bar{\Theta}_1 = \bar{\Theta}_d = 1$.

The energy results (Table 6.1) show, that the comparison ratio R_{dt} is large, $R_{dt} \gg 1$, indicating the strong dominance of the dynamical effects and negligible importance of the thermal contributions. The kinetic energy balance is strongly influenced by the magnetic field, which stabilizes the instability very efficiently. The increasing stabilizing magnetic contribution $\bar{K}_m$ is balanced by the destabilizing buoyancy effects $\bar{K}_b$ and the energy production by shear of mean flow $\bar{K}_f$.

The contour plots illustrating side views of temperature disturbance isotherms and disturbed velocity streamlines are presented for different values of Ha in Fig. 6.5.

Ha	$\bar{K}_f$	$\bar{K}_b$	$\bar{K}_m$	R_{dt}
0.1	0.98	0.02	0	5983
2	1.02	0.02	-0.04	5410
5	1.17	0.02	-0.19	3410
10	1.58	0.06	-0.64	1152
30	2.92	1.03	-2.95	85.9
80	0.20	11.8	-11.0	38.1

Table 6.1: Energy balances for the vertical channel problem

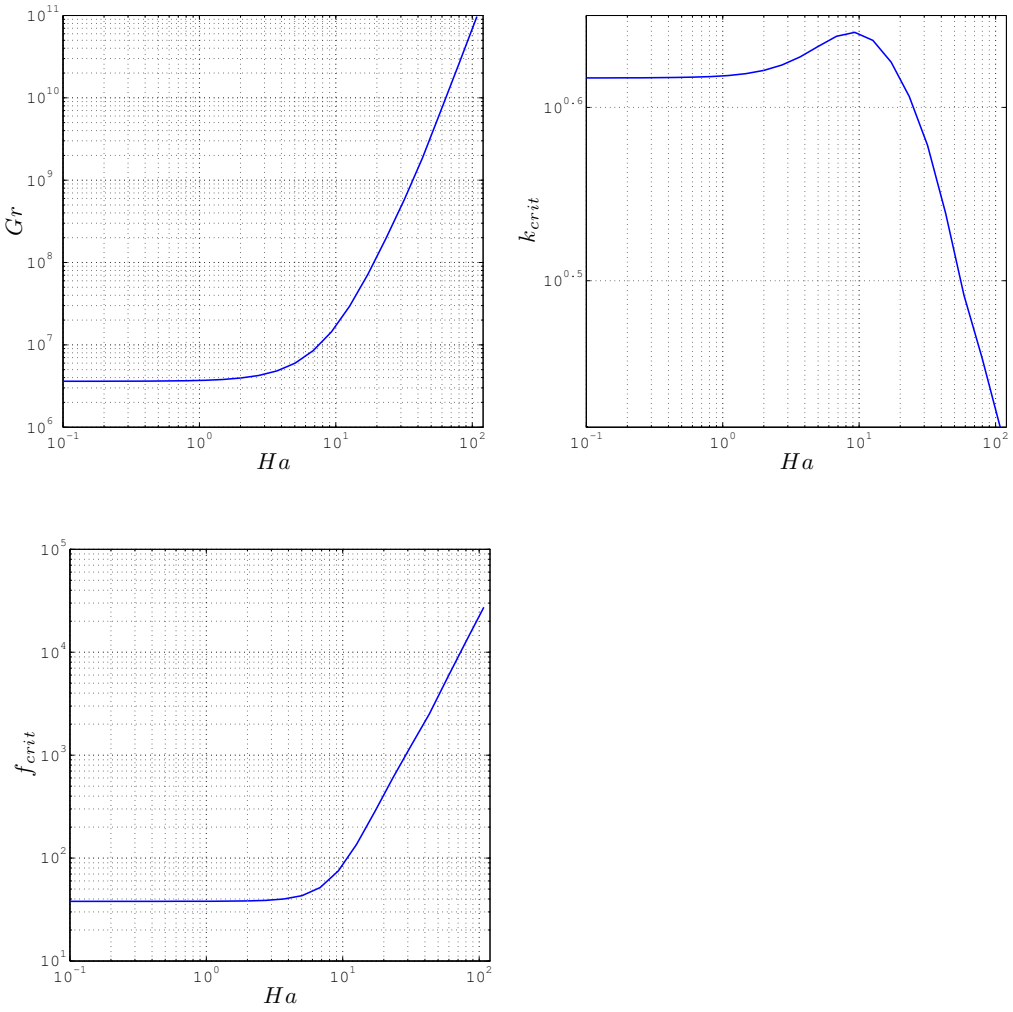

Figure 6.4: Critical values of parameters for the vertical channel problem

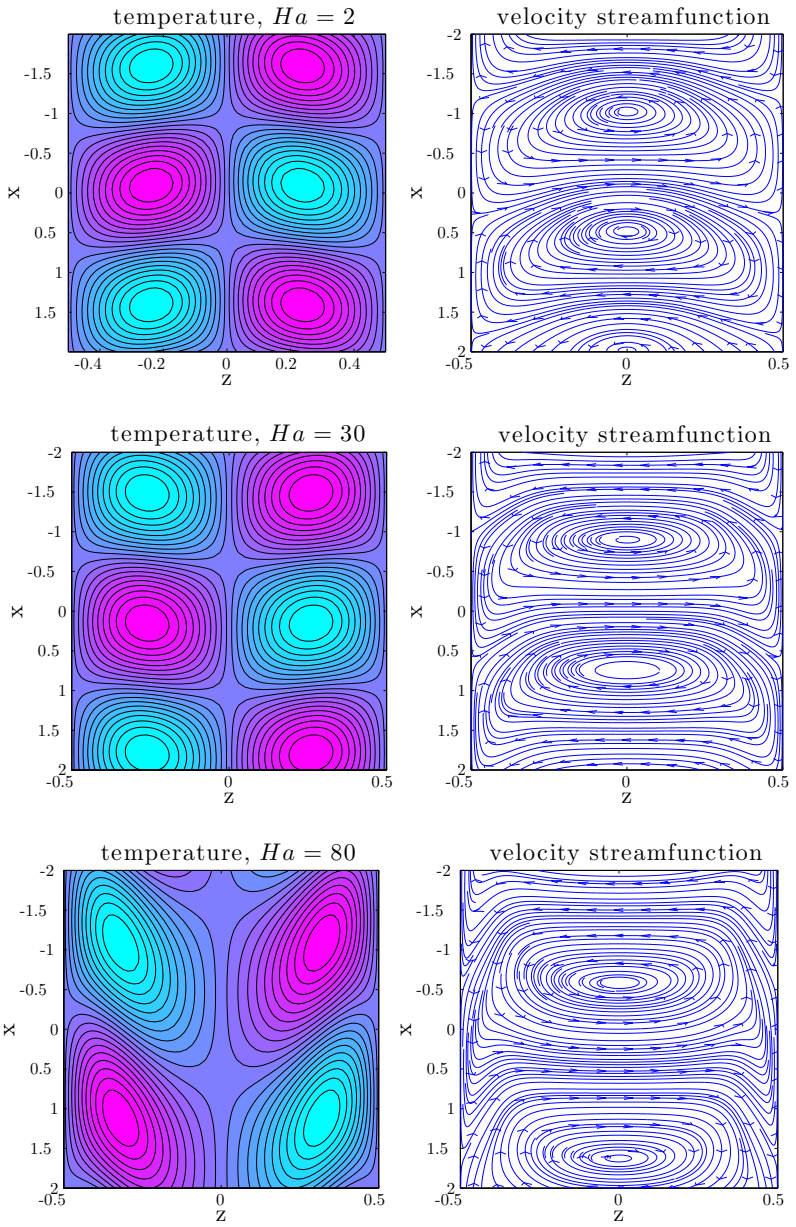

Figure 6.5: Contour plots of disturbance isotherms (left) and disturbed velocity streamlines (right)

Chapter 7

Conclusions

The present study has addressed the problem of the stability of buoyant convective flows in horizontal layers and vertical channels. A number of configurations has been considered, including the Rayleigh-Bénard problem, the horizontal layer with longitudinal temperature gradient and the vertical channel with internal heating sources.

The effect of an externally applied magnetic field on the onset of instability has been studied numerically. The numerical method has been verified by a convergence study and by a comparison with the results for the simplified problems available in literature.

The preset study allowed to verify the validity of the inductionless approximation by comparing the neutral stability results for small but non-zero magnetic Prandtl numbers with the results obtained in the approximation of $Pr_m = 0$.

Patterns of steady state flows and their stability have been investigated for the Prandtl number $Pr = 0.015$, corresponding to the liquid metal or semiconductor properties in the relevant applications, and for the wide range of the Hartmann number, sometimes up to $Ha = 10^5$. The results obtained for the high values of the applied magnetic field allowed to deduce asymptotic relations for the critical parameters for high Ha.

This study successfully allowed to identify the nature of instabilities considered. Additionally, for each configuration, the perturbation energy analysis has been performed for better understanding of the instability mechanisms. The main results can be summarized as follows.

The problem of Rayleigh-Bénard convection with the stabilizing effect of a vertical magnetic field has been investigated in Chapter 4. The results show that for the considered range of Ha, the inductionless approximation is valid for $Pr_m \leq 10^{-2}$. The linear stability results have been obtained for the two cases of electromagnetic boundary conditions: perfectly conducting and perfectly insulating. Two types of instabilities have been identified, namely the stationary mode present both in the inductionless approximation and for the non-zero magnetic Prandtl number, and the oscillatory mode observed for $Pr_m > 10^{-2}$.

For the Hartmann numbers lower than a certain critical value, dependent on Pr_m, the instability sets in a stationary mode, and above that value, the instability sets in an oscillatory mode. It has been shown that the electrical conductivity of the walls has no effect on the stationary instability, but the transition from stationary to oscillatory mode takes place at higher Ha for the case of electrically conducting boundaries. For the highest values of Ha considered, the asymptotic relations have been obtained for the stationary and oscillatory modes. These results are in good agreement with the asymptotic expansions for $Ha \gg 1$.

The problem of the horizontal layer with longitudinal temperature gradient and vertical magnetic field has been considered in Chapter 5, first in the inductionless approximation, and then for the non-zero magnetic Prandtl number. Linear stability results have been obtained for the following cases of the boundary conditions: both thermally and electrically conducting walls, thermally conducting and electrically insulating walls, both thermally and electrically insulating walls, and for thermally insulating and electrically conducting walls.

Here four main types of instabilities have been identified: the low-Hartmann number stationary transverse instabilities of hydrodynamical origin, the high-Hartmann number transverse oscillatory instabilities of thermal origin, the low-Hartmann number longitudinal oscillatory instabilities of thermal origin and the high-Hartmann number longitudinal instabilities of thermal origin.

The inductionless approximation results show that, in contrast to the previous notion, the transverse modes are most dangerous for almost all ranges of the Hartmann number. For the cases of thermally insulating boundaries, the magnetic field stabilizes instability modes, longitudinal and transverse, very efficiently. Thermally conducting walls cause the most dangerous instabilities at

the higher values of Ha, appearing as a result of unstable thermal stratification zones.

It has been shown that the inductionless approximation is valid for the values of magnetic Prandtl number up to $Pr_m = 10^{-4}$ for the range of Ha considered here. Further increase of Pr_m will cause a divergence between different modes, depending on the boundary conditions, and on the values of critical parameters. For $Pr_m \to 0$ the electrical boundary conditions show no effect on the transverse instabilities, but an increase of the value of magnetic Prandtl number results in a divergence between the two cases of electromagnetic boundary conditions.

For the case of electrically insulating boundaries there are new transverse instabilities appearing for small ranges of Pr_m. These new instabilities, with no counterparts in the inductionless approximation, are shown to be the most dangerous up to high values of Ha. Specifically, for the case of both thermally and electrically insulating boundaries, a new transverse stationary instability of magnetic origin is observed for $Pr_m = 10^{-1}$. For the case of thermally conducting and electrically insulating walls, two kinds of new instabilities appear at very narrow ranges of Pr_m: a new oscillatory instability for $Pr_m = 10^{-2.5}$ and a stationary instability for $Pr_m = 10^{-2}$, which originates from the low Ha stationary mode.

The main conclusion for the convective flow in a vertical layer with internal heating, considered in Chapter 6, is that the origin of the instability is two inflection points in the basic velocity profile. These instabilities clearly have a hydrodynamic origin and smoothly extend up to $Ha = 100$. Further investigation is required to determine the behavior of the flow for $Ha > 100$, as this may involve the instabilities of the Hartmann layers at the walls perpendicular to the magnetic field. This will most probably occur at much higher values of the critical Grashof number. On the other hand it may also happen that these instabilities are fully suppressed by a high magnetic field, as the basic velocity decreases here in amplitude Ha^{-2}.

The present study has highlighted a number of topics on which further research would be beneficial. Further studies need to address the problem of internal heating sources in different configurations and the analysis of the validity of inductionless approximation in systems with different orientations of the externally applied magnetic field.

The initial goal of this work was to show the evidence of Alfvén wave propagation in liquid metals. The results obtained suggest that the Alfvénic oscillations appear for the values of Pr_m above the range for liquid metals. However, there is a number of additional research areas for exploring the possibility of Alfvén wave propagation even for very small Pr_m. These include the cases of horizontal magnetic field applied along the flow.

The present study involves an infinite fluid layer, which allows very accurate analysis of instabilities from the fundamental point of view. The natural direction for future research includes more realistic configurations. Hence, further investigation needs to address the flows in finite cavities, as the sidewall regions strongly modify the problem.

Much research remains to be done on topics with reference to liquid metal blankets for a fusion reactor. Particularly, the problem of linear stability of a vertical fluid layer with horizontal temperature gradient and internal heating sources needs to be considered both in the inductionless approximation and for non-zero magnetic Prandtl numbers.

Bibliography

[1] H. Fredriksson and U. Akerlind. *Solidification and Crystallization Processing in Metals and Alloys*. J. Wiley & Sons, 2012. 2

[2] Hiroyuki Ozoe. *Magnetic Convection*. Imperial College Press, 2005. 2

[3] M.G. Braunsfurth, A.C. Skeldon, A. Juel, T. Mullin, and D.S. Riley. Free convection in liquid gallium. *Journal of Fluid Mechanics*, 342:295–314, 7 1997. 2

[4] S. Molokov, R. Moreau, and H.K. Moffatt. *Magnetohydrodynamics. Historical Evolution and Trends*. Springer, 2007. 2, 4

[5] D.T.J. Hurle. *Crystal Pulling from the Melt*. Springer, 1993. 2

[6] G. Dhanaraj, K. Byrappa, V. Prasad, and M. Dudley. *Springer Handbook of Crystal Growth*. Springer, 2010. 2

[7] J.P. Garandet and T. Alboussiere. Bridgman growth: Modelling and experiments. *Progress in Crystal Growth and Characterization of Materials*, 38(1-4):133–159, 1999. 2

[8] D. Henry, A. Juel, H. Ben Hadid, and S. Kaddeche. Directional effect of a magnetic field on oscillatory low-prandtl-number convection. *Physics of Fluids*, 181(034104), 2008. 2

[9] R.W. Series and D.T.J. Hurle. The use of magnetic fields in semiconductor crystal growth. *Journal of Crystal Growth*, 113(1-2):305–328, 1991. 3

[10] V. Bojarevics. Buoyancy driven flow and its stability in a horizontal rectangular channel with an arbitrary oriented transversal magnetic field. *Magnetohydrodynamics*, 31:245–253, 1995. 3, 6, 7

[11] T. Alboussiere, A.C. Neubrand, J.P. Garandet, and R. Moreau. Segregation during horizontal bridgman growth under an axial magnetic field. *Journal of Crystal Growth*, 181(1-2):133 – 144, 1997. 3, 6

[12] H. Ben Hadid, D. Henry, and S. Kaddeche. Numerical study of convection in the horizontal bridgman configuration under the action of a constant magnetic field. part 1. two-dimensional flow. *Journal of Fluid Mechanics*, 333:23–56, 2 1997. 3, 6

[13] H. Ben Hadid and D. Henry. Numerical study of convection in the horizontal bridgman configuration under the action of a constant magnetic field. part 2. three-dimensional flow. *Journal of Fluid Mechanics*, 333:57–83, 2 1997. 3, 6, 7

[14] S. Kaddeche, H. Ben Hadid, and D. Henry. Macrosegregation and convection in the horizontal bridgman configuration i. dilute alloys. *Journal of Crystal Growth*, 135:341–353, 1994. 3

[15] S. Aleksandrova. *Buoyant convection in cavities in a strong magnetic field.* Ph.D. Thesis, Coventry University, 2001. 3

[16] S. Aleksandrova and S. Molokov. Three-dimensional buoyant convection in a rectangular cavity with differentially heated walls in a strong magnetic field. *Fluid Dynamics Research*, 35(1):37 – 66, 2004. 3, 6, 7

[17] L. Buhler, C. Mistrangelo, J. Konys, R. Bhattacharyay, Q. Huang, D. Obukhov, S. Smolentsev, and M. Utili. Facilities, testing program and modeling needs for studying liquid metal magnetohydrodynamic flows in fusion blankets. *Fusion Engineering and Design*, 2014. 4

[18] L. Morgan and J. Pasley. Tritium breeding control within liquid metal blankets. *Fusion Engineering and Design*, 88(3):107 – 112, 2013. 4

[19] L. Barleon, U. Burr, K.J. Mack, and R. Stieglitz. Heat transfer in liquid metal cooled fusion blankets. *Fusion Engineering and Design*, 5152(0):723 – 733, 2000. 4

[20] S. Chandrasekhar. *Hydrodynamic and Hydromagnetic Stability*. Dover Books on Physics Series. Dover Publications, 1961. 4, 39, 40, 44

[21] G.Z. Gershuni and E.M. Zhukhovitskii. *Convective Stability of Incompressible Fluids*. I.P.S.T., 1976. 4, 44

[22] M. Takashima, M. Hirasawa, and H. Nozaki. Buoyancy-driven instability in a horizontal layer of electrically conducting fluid in the presence of a vertical magnetic field. *International Journal of Heat and Mass Transfer*, 42(9):1689–1706, 1999. 6, 27, 39, 40, 43

[23] J.E. Hart. Stability of thin non-rotating Hadley circulations. *Journal of Atmospheric Sciences*, 29:687–697, May 1972. 6

[24] A.E. Gill. A theory of thermal oscillations in liquid metals. *Journal of Fluid Mechanics*, 64:577–588, 7 1974. 6

[25] D.T.J. Hurle, E. Jakeman, and C.P. Johnson. Convective temperature oscillations in molten gallium. *Journal of Fluid Mechanics*, 64:565–576, 7 1974. 6

[26] H.P. Kuo and S.A. Korpela. Stability and finite amplitude natural convection in a shallow cavity with insulated top and bottom and heated from a side. *Physics of Fluids*, 31(1), 1988. 6

[27] P. Laure and B. Roux. Linear and non-linear analysis of the hadley circulation. *Journal of Crystal Growth*, 97(1):226–234, 1989. 6, 36

[28] M. Lappa. *Thermal Convection: Patterns, Evolution and Stability*. Wiley, 2009. 9, 10, 11, 15, 18, 22, 36, 40, 44, 66

[29] P.H. Roberts. *An introduction to magnetohydrodynamics*. American Elsevier Pub. Co., 1967. 9, 10, 11, 12, 13, 19, 20, 27

[30] R.J. Moreau. *Magnetohydrodynamics*. Springer, 1990. 9, 11, 12, 13, 41

[31] J.F. Gerbeau, C.L. Bris, and T. Lelièvre. *Mathematical Methods for the Magnetohydrodynamics of Liquid Metals*. Clarendon Press, 2006. 9, 10, 13, 14, 19, 21, 23

[32] V.C.A. Ferraro and C. Plumpton. *An introduction to magneto-fluid mechanics*. Oxford University Press, 1966. 10

[33] I.G. Currie. *Fundamental Mechanics of Fluids, Third Edition*. Dekker Mechanical Engineering. Taylor & Francis, 2002. 10, 11

[34] A. V. Getling. *Rayleigh-Benard Convection: Structures and Dynamics*. World Scientific, 1998. 11, 39

[35] T. Cebeci. *Convective Heat Transfer*. Horizons Publishing, 2002. 11, 12

[36] E. Blums, I.U.A. Mikhailov, and R. Ozols. *Heat and Mass Transfer in MHD Flows*. Series in theoretical and applied mechanics. World Scientific, 1987. 12, 13, 14

[37] U. Müller and L. Bühler. *Magnetofluiddynamics in Channels and Containers*. Springer, 2001. 12, 15, 41

[38] J.A. Shercliff. Thermoelectric magnetohydrodynamics. *Journal of Fluid Mechanics*, 91:231–251, 3 1979. 13

[39] J. Mao, S. Aleksandrova, and S. Molokov. Joule heating in magnetohydrodynamic flows in channels with thin conducting walls. *International Journal of Heat and Mass Transfer*, 51(17-18):4392 – 4399, 2008. 14

[40] J. Lahjomri, K. Zniber, A. Oubarra, and A. Alemany. Heat transfer by laminar hartmann's flow in thermal entrance region with uniform wall heat flux: the graetz problem extended. *Energy Conversion and Management*, 44(1):11–34, 2003. 14

[41] N.F. Cramer. *The Physics of Alfven Waves*. Wiley, 2011. 14

[42] M. Kaviany. *Principles of Convective Heat Transfer*. Mechanical Engineering Series. Springer, 2001. 14

[43] H.K. Moffatt. *Magnetic Field Generation in Electrically Conducting Fluids*. Cambridge Monographs on Mechanics. Cambridge University Press, 1978. 14

[44] S. Kaddeche, D. Henry, and H. Ben Hadid. Magnetic stabilization of the buoyant convection between infinite horizontal walls with a horizontal temperature gradient. *Journal of Fluid Mechanics*, 480:185–216, 4 2003. 15, 18, 28, 66, 67

[45] J. Priede, S. Aleksandrova, and S. Molokov. *Stability of buoyant convection in laterally heated liquid metal layer subject to transverse magnetic field*. Proceedings of the 7th PAMIR Conference, France, 2008. 15, 66, 74

[46] W.O. Criminale, T.L. Jackson, and R.D. Joslin. *Theory and Computation of Hydrodynamic Stability*. Cambridge Monographs on Mechanics. Cambridge University Press, 2003. 21, 22, 24, 35, 67

[47] C. Canuto, Y. Hussaini, A. Quarteroni, and T.A. Zang. *Spectral Methods: Fundamentals in Single Domains*. Springer-Verlag, 2007. 31

[48] J.P. Boyd. *Chebyshev and Fourier Spectral Methods: Second Revised Edition*. Dover Publications, 2001. 31

[49] P.J. Roache. *Fundamentals of Computational Fluid Dynamics*. Hermosa Publishers, 1998. 31

[50] L.N. Trefethen. *Spectral Methods in MATLAB*. Software, Environments, and Tools. Society for Industrial and Applied Mathematics, 2000. 31

[51] J.A. Weideman and S.C. Reddy. A matlab differentiation matrix suite. *ACM TOMS*, 26(4):465–519, 2000. 31, 32, 33

[52] S.A. Orszag. Accurate solution of the orr sommerfeld stability equation. *Journal of Fluid Mechanics*, 50:689–703, 12 1971. 35

[53] L.C. Burmeister. *Convective Heat Transfer*. A Wiley-Interscience publication. Wiley, 1993. 35

[54] J. Hart. A note on the stability of low-prandtl-number hadley circulations. *Journal of Fluid Mechanics*, 132:271–281, 7 1983. 36

[55] U. Burr and U. Muller. Rayleighbenard convection in liquid metal layers under the influence of a vertical magnetic field. *Physics of Fluids*, 13(11):3247–3257, 2001. 39, 40, 43, 45

[56] P.C. Matthews. Asymptotic solutions for nonlinear magnetoconvection. *Journal of Fluid Mechanics*, 387:397–409, 5 1999. 44

[57] R.D. Gibson. Overstability in the magnetohydrodynamic bénard problem at large hartmann numbers. *Mathematical Proceedings of the Cambridge Philosophical Society*, 62:287–299, 4 1966. 44

[58] J.P. Garandet, T. Alboussiere, and R. Moreau. Buoyancy driven convection in a rectangular enclosure with a transverse magnetic field. *Int. Journal of Heat and Mass Transfer*, 35(4):741–748, 1992. 62

[59] M. Takashima. The stability of natural convection in a vertical fluid layer with internal heat generation. *Journal of the Physical Society of Japan*, 52(7):2364–2370, 1983. 118, 120

List of Figures

Appendix A: Nomenclature

(x, y, z)	Cartesian coordinates
$\nabla = [\partial x, \partial y, \partial z,]$	nabla operator

Vector variables and constants

$\mathbf{B}_0$	external magnetic field
$\mathbf{B}$	total magnetic field
$\mathbf{b}_0$	induced magnetic field
$\mathbf{B}_w$	magnetic field inside a solid wall
$\mathbf{D}$	electric induction
$\mathbf{E}$	electric field
$\hat{e}_g$	unit vector in the gravity direction
$\hat{e}_x, \hat{e}_y, \hat{e}_z$	unit vectors in the $x-$, $y-$ and $z-$ directions
$\mathbf{f}$	density of body forces
$\mathbf{f}_m$	body forces per unit mass
$\mathbf{f}_V$	body forces per unit volume
$\mathbf{g}$	gravity
$\mathbf{H}$	magnetic field intensity

$\mathbf{h}$ heat conduction vector

$\mathbf{I}$ unity tensor

$\mathbf{j}$ electric current density

$\mathbf{n}$ unit vector normal to the wall

π stress tensor

τ tangential unit vector

$\mathbf{v}$ fluid velocity

Dimensional scalar variables and constants

a adiabatic speed of sound

c speed of light in vacuum

c_p specific heat at constant pressure

d characteristic length

p pressure

q charge density

s entropy per unit mass

t time

T temperature

T_0 reference temperature

ΔT characteristic temperature difference

v_0 characteristic velocity

β thermal expansion coefficient

ϵ volumetric internal heat sources

ε_0 vacuum electric permittivity

ε_r relative permittivity of a material

η magnetic diffusivity

κ thermal diffusivity

λ_T thermal conductivity

μ_0 vacuum magnetic permeability

μ_r relative permeability of a material

ν kinematic viscosity

ρ fluid density

ρ_0 reference density at T_0

σ electric conductivity

ϕ electric potential

Dimensionless variables and constants

Gr Grashof number

Ha Hartmann number

Lu Lundquist number

Pe Peclet number

Pr Prandtl number

Pr_m magnetic Prandtl number

Q dimensionless internal heat sources

Ra Rayleigh number

Re_m magnetic Reynolds number

Appendix B: Matlab code

```
global Gr Pr Ha N kx ky z zv D1 D2 aas D2c D3 D3t D4c D4 I freq bc...
    Prm no asym D1t D2t D1c V Lam mgr ind k_crit induction Q

% bc 1 thermal conducting + electrical conducting + longitudinal
% bc 2 thermal conducting + electrical conducting + transverse
% bc 3 thermal insulating + electrical conducting + longitudinal
% bc 4 thermal insulating + electrical conducting + transverse
% bc 5 thermal insulating + electrical insulating + longitudinal
% bc 6 thermal insulating + electrical insulating + transverse
% bc 7 thermal conducting + electrical insulating + longitudinal
% bc 8 thermal conducting + electrical insulating + transverse
% bc 9 RB ellectrically insulating
% bc 10 RB electrically conducting
% bc 12 vertical thermal conducting + electrical conducting + transv
% bc 18 vertical thermal conducting + electrical insulating + transv
induction = 0 % induction = 0 = inductionless approximation
              % induction = 1 = induction eq. included
% values
```

```
asym = 400 ; Pr = 0.015 ; Q = 1 ; Prm = 10^(-1) ; N = 56 ; bc = 12 ;
% guess
Gr = 90*10^4 ; k_crit0  =  2.2 ;
%range
pocz = 1 ; kon = 3; points = 10 ; delta = (kon-pocz)/points; no = 0 ;

for j = pocz:delta:kon
Ha = 10^j ; no = no+1 ;
[z,D] = chebdif(N,4); % size (DM = M);
D1 =  D(:,:,1); D2 =  D(:,:,2); D3 =  D(:,:,3); D4 =  D(:,:,4);
[zzz, D4c] = cheb4c(N);
pion = diag(zeros(N-2)); poz = diag(zeros(N)); poz = poz';
if induction == 1
if      bc==1 || bc==3 || bc==4 || bc==5 || bc==6 || bc==7 ...
        || bc==8 || bc==9
        I = eye(N);
        D4c = horzcat(pion,D4c,pion); D4c = vertcat(poz,D4c,poz);
elseif  bc == 10 || bc == 2
        D1 = D1(2:N-1,2:N-1); D2 = D2(2:N-1,2:N-1);
        D3 = D3(2:N-1,2:N-1);
        z = z(2:N-1); I = eye(N-2) ;
end
elseif induction == 0
if      bc==3 || bc==4 || bc==5 || bc==6 || bc==7 || bc==8
        I = eye(N);
        D4c = horzcat(pion,D4c,pion); D4c = vertcat(poz,D4c,poz);
```

```
elseif  bc == 1 || bc == 2 || bc == 11 || bc == 12
        D1 = D1(2:N-1,2:N-1); D2 = D2(2:N-1,2:N-1);
        z = z(2:N-1); I = eye(N-2);
end
end

zv = z ;          % VECTOR
z = diag(z);      % MATRIX
if bc == 2 || bc == 4 || bc == 6 || bc ==8 || bc == 9 || bc == 10 ...
    || bc == 12
ky = 0;   %  TRANSVERSE
elseif bc == 1 || bc == 3 || bc == 5 || bc ==7 || bc == 11
kx = 0;     % LONGITUDINAL
end

 k_crit            = fminsearch('fun_kx',k_crit0);
 k_crit0           = k_crit;
 ki_array(no)      = k_crit
 Ha_array(no)      = Ha
 Gr_crit_array(no) = Gr
 freq_array(no)    = freq;
 end
```

```
function Gr_crit = fun_kx(k1)

global Gr Pr Ha N kx ky z zv D1 D2  aas D2c D3 D3t D4c D4 I freq ...
    bc Prm no asym D1t D2t D1c V Lam mgr ind k_crit induction Q
if bc == 2 || bc == 4 || bc == 6 || bc ==8 || bc == 9 || bc == 10 ...
        || bc == 12 || bc == 18
kx = k1;   % TRANSVERSE
elseif bc == 1 || bc == 3 || bc == 5 || bc ==7
ky = k1;     % LONGITUDINAL
end

Gr_crit_1 = Gr;
Gr_crit = fzero('eigenvalue',Gr_crit_1);
Gr = Gr_crit;
```

```
function ev = eigenvalue(Gr1)

global Gr Pr Ha N kx ky z zv D1 D2 aas D2c D3 D3t D4c D4 I freq bc ...
    Prm no asym D1t D2t D1c V Lam mgr ind k_crit induction Q
Gr = Gr1;
if  Gr == Inf
    Gr = 100000000000;
else
    Gr = Gr;
end
        k2 = ky*ky + kx*kx; kk = sqrt(k2);
        g = [kk,1,0;-kk,1,0]; [xt,D2t,D1t,D3t,phip,phim]=cheb2bc(N,g);
        gd = [0,1,0;0,1,0]; [xtd,D2td,D1td,D3td,phipd,phimd]=cheb2bc(N,gd);
        gv = [1,1,0;1,1,0]; [xtv,D2tv,D1tv,D3tv,phipv,phimv]=cheb2bc(N,gv);

if induction == 1
if bc==1 || bc==3 || bc==4 || bc==5 || bc==6 || bc==7 || bc==8 || bc==9
        I1 = I(2:N-1,2:N-1); pion = diag(zeros(N-2)); poz = diag(zeros(N));
        poz = poz';  I1 = horzcat(pion,I1,pion); I1 = vertcat(poz,I1,poz);
        D1c = I1*D1*I1 ; D2c = I1*D2*I1; D3c = I1*D3*I1 ;
        DD = -1*k2*I + D2 ; DDc = -1*k2*I + D2c ;
        DDtd = -1*k2*I + D2td ; DDt = -1*k2*I + D2t  ;
        DD4c = D4c - 2*k2*D2c + k2*k2*I ; DD4  = D4c - 2*k2*D2 + k2*k2*I  ;
elseif  bc == 10 || bc == 2
        DD = -1*k2*I + D2 ;
        DD4c = D4c - 2*k2*D2 + k2*k2*I ; DD4  = D4c - 2*k2*D2 + k2*k2*I  ;
```

```
end
elseif induction == 0
if bc==3 || bc==4 || bc==5 || bc==6 || bc==7 || bc==8 || bc == 18
        I1 = I(2:N-1,2:N-1); pion = diag(zeros(N-2)); poz = diag(zeros(N));
        poz = poz'; I1 = horzcat(pion,I1,pion); I1 = vertcat(poz,I1,poz);
        D1c = I1*D1*I1 ; D2c = I1*D2*I1; D3c = I1*D3*I1 ;
        DD = -1*k2*I + D2 ; DDc = -1*k2*I + D2c  ;
        DDtd = -1*k2*I + D2td ; DDt = -1*k2*I + D2t ;
        DD4c = D4c - 2*k2*D2c + k2*k2*I ; DD4  = D4c - 2*k2*D2 + k2*k2*I  ;
elseif bc == 1 || bc == 2 || bc == 11 || bc == 12
         DD = -1*k2*I + D2  ; DD4  = D4c - 2*k2*D2 + k2*k2*I  ;
end
end
% basic flow profiles
ep = exp(Ha*(zv-diag(I))) ; em = exp(-Ha*(zv+diag(I))) ; b = 1/(sinh(Ha)) ;
if Ha <= asym
    if bc==1 || bc==2 || bc==7 || bc==8 || bc==9 || bc==10 || bc==11 ...
            || bc==12
    Dtemp = (1/6)*diag(I) - (1/(Ha*Ha))*diag(I) ;
    elseif bc == 3 || bc == 4 || bc ==5 || bc == 6  || bc == 18
    Dtemp = 0.5*diag(I) - ((cosh(Ha))/(Ha*sinh(Ha)))*diag(I) ;
    end
B1_short = 0.5*diag(I) - 0.5*zv.^2 + ...
    (1/(Ha*sinh(Ha)))*(cosh(Ha*zv)-cosh(Ha)*diag(I)) ;
u_short = zv - b*sinh(Ha*zv) ;
dzu_short = diag(I) - b*Ha*cosh(Ha*zv) ;
```

```
dz2u = -Gr* b* sinh(Ha*zv) ;
dz2u_short = - b* sinh(Ha*zv) ;
dzto_short=  ( (1/Ha)*b*cosh(Ha*zv) - 0.5*zv.^2 + Dtemp );
dzto_short = diag(dzto_short);
else
    if bc==1 || bc==2 || bc==7 || bc==8 || bc==9 || bc==1 || bc ==10 ...
            || bc==11 || bc==12
    Dtemp = (1/6)*diag(I) - (1/(Ha*Ha))*diag(I) ;
    elseif bc == 3 || bc == 4 || bc ==5 || bc == 6    || bc == 18
    Dtemp = 0.5*diag(I) - (1/Ha)*diag(I) ;
    end
B1_short = ((ep+em)/(Ha)) + 0.5*diag(I) - 0.5*zv.^2 - (1/Ha) ;
u_short =  zv + em - ep ;
dzu_short = diag(I) -Ha*em - Ha*ep ;
dz2u = -Gr* (ep - em) ;
dz2u_short = -(ep - em) ;
dzto_short = -0.5*zv.^2 +(1/Ha)*(ep+em) + Dtemp ;
dzto_short = diag(dzto_short);
end
dxto = -I;
B1_short = diag(B1_short) ; u_short = diag(u_short);
dzu_short = diag(dzu_short) ;  dz2u = diag(dz2u) ;
dz2u_short = diag(dz2u_short) ; dzto = Pr*(Gr/(Ha*Ha)) * dzto_short ;
Ha2Prm = Ha*Ha*Prm ;
u = (Gr/(Ha*Ha))*u_short; dzu = (Gr/(Ha*Ha))*dzu_short;
if bc==11 || bc==12 || bc == 18
```

```
    if Ha <= asym
    To = -0.5*Pr*Q*zv.^2 + diag(I) +0.5*Pr*Q*diag(I)  ;
    To = diag(To) ; dzTov = -Pr*Q*zv ; dzTov = diag(dzTov) ;
    C4=0 ; C3 = (Gr/Ha)*(Pr/Ha)*Q ; si = sinh(Ha) ; co = cosh(Ha) ;
    C5 = (C3/6)*(3*si-Ha*co)/(Ha*co-si) ;
    C2 = Ha*(Ha/co)*(Ha/4)*(C3+2*C5) ; C1 = -C2 ;
uov = (C1/(Ha*Ha*Ha))*exp(Ha*zv) - (C2/(Ha*Ha*Ha))*exp(-Ha*zv) + ...
    0.5*C3*zv.^2 + C4*zv + C5*diag(I) ; uov = diag(uov) ;
dzuov = (C1/(Ha*Ha))*exp(Ha*zv) + (C2/(Ha*Ha))*exp(-Ha*zv) + C3*zv + ...
    C4*diag(I) ; dzuov = diag(dzuov) ;
    dz2uov = (C1/(Ha))*exp(Ha*zv) - (C2/(Ha))*exp(-Ha*zv) + C3*diag(I) ;
    dz2uov = diag(dz2uov) ;
    else
    To = -0.5*Pr*Q*zv.^2 + diag(I) +0.5*Pr*Q*diag(I) ; To = diag(To) ;
    dzTov = -Pr*Q*zv ; dzTov = diag(dzTov) ;
    C4=0 ; C3 = (Gr/Ha)*(Pr/Ha)*Q ; C5 = ((3-Ha)/(6*Ha-6))*C3 ;
    C2 = Ha*Ha*Ha*Ha*C3*(1/(3*Ha-3))*(1/exp(Ha)) ; C1 = -C2 ;
    uov = (C1/(Ha*Ha*Ha))*exp(Ha*zv) - (C2/(Ha*Ha*Ha))*exp(-Ha*zv) + ...
        0.5*C3*zv.^2 + C4*zv + C5*diag(I) ; uov = diag(uov) ;
    dzuov = (C1/(Ha*Ha))*exp(Ha*zv) + (C2/(Ha*Ha))*exp(-Ha*zv) + ...
        C3*zv + C4*diag(I) ; dzuov = diag(dzuov) ;
    dz2uov = (C1/(Ha))*exp(Ha*zv) - (C2/(Ha))*exp(-Ha*zv) + C3*diag(I) ;
    dz2uov = diag(dz2uov) ;

    end
end
```

```
% generalized eigenvalue A*V=lambda*B*V

if induction ==1

if  bc == 1

A11 =  ( DDc ) ;

A12 = I1*( dzu_short*1i*ky ) ;

A13 =  Prm *I1*( 1i*ky*u_short ) ;

A14 =  (D1td);

A15 = zeros(N);

B11 = I;

A21 = zeros(N)  ;

A22 = DD4c ;

A23 = ( (D3c-k2*D1c)) ;

A24 = zeros(N);

A25 = -(Gr) * ( k2 *I) ;

B22 = DDc ;

A31 = zeros(N)   ;

A32 = Ha*Ha*D1 ;

A33 = DDc ;

A34 = zeros(N) ;

A35 = zeros(N) ;

B33 = Prm*I ;

A41 = Ha*Ha*( D1 ) ;

A42 = - (Prm*Ha*Ha)*I1*( 1i*ky*u_short ) ;

A43 = -(Prm) *I1*( 1i*ky*dzu_short )  ;

A44 =  ( -1*I*k2 + D2td )  ;

A45 =  zeros(N);
```

```
B44 = Prm*I;

A51 = -(Gr/(Ha*Ha))*  ( 1i*(ky/k2)*I1*dxto*I1 ) ;

A52 = - ( I1*dzto*I1 ) ;

A53 = zeros(N);

A54 = zeros(N);

A55 = ( (1/Pr)*DDc )  ;

B55 = I1;

elseif  bc == 2

A22 = ( DD4 ) +1i*kx*Gr*(-(1/(Ha*Ha))*u_short*DD + dz2u_short );

A23 = (Gr/(Ha*Ha))*1i*kx *I*( B1_short*DD + dzu_short ) +...

    (1/Prm)*((D3-k2*D1)) ;

A25 = -(Gr) * ( k2*I ) ;

B22 = DD ;

A32 = Gr*Prm*1i*kx*I*B1_short + Ha*Ha*( D1 ) ;

A33 = (1/Prm)*DD - (Gr/(Ha*Ha))*1i*kx*u_short ;

A35 = zeros(N-2) ;

B33 = I ;

A52 = - (I*dzto ) - 1i*(1/kx)*dxto*D1 ;

A53 = zeros(N-2);

A55 = ( (1/Pr)*DD ) - (Gr/(Ha*Ha))*1i*kx*I*u_short ;

B55 = I;

elseif  bc == 3

A11 =  ( DDc ) ;

A12 = ( dzu_short*1i*ky ) ;

A13 =  ( 1i*ky*u_short ) ;

A14 =  Ha*Ha*I1*(D1td);
```

```
A15 = zeros(N);

B11 = I;

A21 = zeros(N)  ;

A22 = DD4c ;

A23 = (1/Prm)*((D3c-k2*D1c)) ;

A24 = zeros(N);

A25 = -(Gr/(Ha*Ha)) * ( k2 *I1) ;

B22 = DDc ;

A31 = zeros(N)   ;

A32 = Ha*Ha*D1 ;

A33 = (1/Prm)*DDc ;

A34 = zeros(N) ;

A35 = zeros(N) ;

B33 = I ;

A41 = ( D1 ) ;

A42 = - (Prm)*I*( 1i*ky*u_short ) ;

A43 = -(1/(Ha*Ha)) *I*( 1i*ky*dzu_short )  ;

A44 =  ( -1*I*k2 + D2td )  ;

A45 =  zeros(N);

B44 = Prm*I;

A51 = -(Gr)* ( 1i*(ky/k2)*dxto ) ;

A52 = - Pr*Gr*( dzto_short) ;

A53 = zeros(N);

A54 = zeros(N);

A55 = ( (1/Pr)*DDtd )  ;

B55 = I;
```

```
elseif  bc == 4

A21 = zeros(N)  ;

A22 = ( DD4c ) +1i*kx*( -(Gr/(Ha*Ha))*u_short*DDc + dz2u ) ;

A23 = Prm*Gr*1i*kx*( B1_short*DDc + dzu_short ) + (Ha*Ha)*((D3c-k2*D1c)) ;

A24 = zeros(N);

A25 = -(Gr) * ( k2*I1 ) ;

B22 = DDc ;

A31 = zeros(N)   ;

A32 = Gr*Prm*1i*kx*B1_short + Ha*Ha*( D1c ) ;

A33 = Ha*Ha*DDc - Gr*Prm*1i*kx*u_short ;

A34 = zeros(N) ;

A35 = zeros(N) ;

B33 = Ha2Prm*I ;

A51 = zeros(N) ;

A52 = - ( I1*dzto ) - 1i*(1/kx)*dxto*D1c ;

A53 = zeros(N);

A54 = zeros(N);

A55 = ( (1/Pr)*DDtd ) - (Gr/(Ha*Ha))*1i*kx*u_short ;

B55 = I;

elseif  bc == 5

A11 =  ( DDc ) ;

A12 = ( dzu_short*1i*ky) ;

A13 =  I1*( 1i*ky*u_short ) ;

A14 =  Ha*Ha*(D1c);

A15 = zeros(N);

B11 = I;
```

```
A21 = zeros(N)  ;

A22 = Prm*DD4c ;

A23 = I1*(1/Prm)*( (D3t-k2*D1t)) ;

A24 = zeros(N);

A25 = -(Gr/(Ha*Ha)) * ( k2 *I1) ;

B22 = Prm*DDc ;

A31 = zeros(N)   ;

A32 = Ha*Ha*D1c ;

A33 = (1/Prm)*DDt ;

A34 = zeros(N) ;

A35 = zeros(N) ;

B33 = I ;

A41 = ( D1c ) ;

A42 = - (Prm)*( 1i*ky*u_short ) ;

A43 = -(1/(Ha*Ha)) *I1*( 1i*ky*dzu_short )  ;

A44 =  ( -1*I*k2 + D2c )  ;

A45 =  zeros(N);

B44 = Prm*I;

A51 = -(Gr)*  I1*( 1i*(ky/k2)*I*dxto ) ;

A52 = - Pr*Gr*( I1*dzto_short ) ;

A53 = zeros(N);

A54 = zeros(N);

A55 = ( 1/Pr)*DDtd   ;

B55 = I;

elseif  bc == 6

A21 = zeros(N)  ;
```

```
A22 = ( DD4c ) +1i*kx*( -(Gr/(Ha*Ha))*u_short*DDc + dz2u ) ;

A23 = Prm*Gr*1i*kx *( B1_short*I1*DDt + I1*dzu_short ) +...

    (Ha*Ha)*(I1*(D3t-k2*D1t)) ;

A24 = zeros(N);

A25 = -(Gr) * ( k2*I1 ) ;

B22 = DDc ;

A31 = zeros(N)   ;

A32 = Gr*Prm*1i*kx*I1*B1_short + Ha*Ha*( D1c ) ;

A33 = Ha*Ha*DDt - Gr*Prm*1i*kx*u_short ;

A34 = zeros(N) ;

A35 = zeros(N) ;

B33 = Ha2Prm*I ;

A51 = zeros(N) ;

A52 = - ( I1*dzto ) - 1i*(1/kx)*dxto*D1c ;

A53 = zeros(N);

A54 = zeros(N);

A55 = ( (1/Pr)*DDtd ) - (Gr/(Ha*Ha))*1i*kx*u_short ;

B55 = I;

elseif  bc == 7

A11 =  ( DDc ) ;

A12 = ( dzu_short*1i*ky ) ;

A13 =  Prm *I1*( 1i*ky*u_short ) ;

A14 =  D1c ;

A15 = zeros(N);

B11 = I;

A21 = zeros(N)  ;
```

```
A22 = DD4c ;

A23 = ( I1*(D3t-k2*D1t)) ;

A24 = zeros(N);

A25 = -(Gr) * ( k2 *I1) ;

B22 = DDc ;

A31 = zeros(N)   ;

A32 = Ha*Ha*D1c ;

A33 = D2t - k2*I ;

A34 = zeros(N) ;

A35 = zeros(N) ;

B33 = Prm*I ;

A41 = Ha*Ha*( D1c ) ;

A42 = - (Prm*Ha*Ha)*( 1i*ky*u_short ) ;

A43 = -(Prm) *I1*( 1i*ky*dzu_short )  ;

A44 =  DDc ;

A45 =  zeros(N);

B44 = Prm*I;

A51 = -(Gr/(Ha*Ha))*( 1i*(ky/k2)*I1*dxto*I1 ) ;

A52 = - ( I1*dzto*I1 ) ;

A53 = zeros(N);

A54 = zeros(N);

A55 = ( (1/Pr)*DDc )  ;

B55 = I1;

elseif  bc == 8

A22 = ( DD4c ) +1i*kx*( -(Gr/(Ha*Ha))*u_short*DDc + dz2u ) ;

A23 = Prm*Gr*(1/(Ha*Ha))*1i*kx *( B1_short*I1*DDt + I1*dzu_short ) + ...
```

```
    (I1*(D3t-k2*D1t)) ;
A25 = -(Gr) * ( k2*I ) ;
B22 = DDc ;
A32 = Gr*Prm*1i*kx*I*B1_short + Ha*Ha*( D1 ) ;
A33 = DDt - Gr*Prm*(1/(Ha*Ha))*1i*kx*u_short ;
A35 = zeros(N) ;
B33 = Prm*I ;
A52 = - ( I1*dzto ) - 1i*(1/kx)*dxto*D1c ;
A53 = zeros(N);
A55 = ( (1/Pr)*DDc ) - (Gr/(Ha*Ha))*1i*kx*I1*u_short ;
B55 = I1;
elseif  bc == 9
A21 = zeros(N)  ;
A22 = (1/(Ha*Ha))*( DD4c ) ;
A23 =   I1*(D3t-k2*D1t) ;
A24 = zeros(N);
A25 = - ( k2*I1 ) ;
B22 = (1/(Ha*Ha))*DDc ;
A31 = zeros(N)   ;
A32 =  ( D1) ;
A33 = DDt;
A34 = zeros(N) ;
A35 = zeros(N) ;
B33 = (Prm)*I ;
A51 = zeros(N) ;
A52 = (Gr/(Ha*Ha))*I ;
```

```
A53 = zeros(N);

A54 = zeros(N);

A55 = ( (1/Pr)*DDc );

B55 = I ;

elseif  bc == 10

A21 = zeros(N-2)  ;

A22 = (1/(Ha*Ha))*( DD4 ) ;

A23 =   ((D3-k2*D1)) ;

A24 = zeros(N-2);

A25 = -( k2*I ) ;

B22 = (1/(Ha*Ha))*DD ;

A31 = zeros(N-2)   ;

A32 = ( D1 ) ;

A33 = DD;

A34 = zeros(N-2) ;

A35 = zeros(N-2) ;

B33 = Prm*I ;

A51 = zeros(N-2) ;

A52 = (Gr/(Ha*Ha))*I;

A53 = zeros(N-2);

A54 = zeros(N-2);

A55 = ( (1/Pr)*DD );

B55 = I;

end

if bc==1 || bc==8 || bc==3 || bc==4 || bc==5 || bc==6 || bc==7 || bc==9

B12 = zeros(N) ; B13 = zeros(N) ; B14 = zeros(N) ; B15 = zeros(N) ;
```

```
B21 = zeros(N) ; B23 = zeros(N) ; B24 = zeros(N) ; B25 = zeros(N) ;
B31 = zeros(N) ; B32 = zeros(N) ; B34 = zeros(N) ; B35 = zeros(N) ;
B41 = zeros(N) ; B42 = zeros(N) ; B43 = zeros(N) ; B45 = zeros(N) ;
B51 = zeros(N) ; B52 = zeros(N) ; B53 = zeros(N) ; B54 = zeros(N) ;
elseif bc == 10 || bc == 2
B12 = zeros(N-2) ; B13 = zeros(N-2) ; B14 = zeros(N-2) ; B15 = zeros(N-2);
B21 = zeros(N-2) ; B23 = zeros(N-2) ; B24 = zeros(N-2) ; B25 = zeros(N-2);
B31 = zeros(N-2) ; B32 = zeros(N-2) ; B34 = zeros(N-2) ; B35 = zeros(N-2);
B41 = zeros(N-2) ; B42 = zeros(N-2) ; B43 = zeros(N-2) ; B45 = zeros(N-2);
B51 = zeros(N-2) ; B52 = zeros(N-2) ; B53 = zeros(N-2) ; B54 = zeros(N-2);
end
if bc == 2 || bc == 4 || bc == 6 || bc ==8 || bc == 9 || bc == 10
A = [ A22, A23, A25 ;  A32, A33, A35 ;  A52, A53, A55 ] ;
B = [ B22, B23, B25 ;  B32, B33, B35 ;  B52, B53, B55 ] ;
elseif bc == 1 || bc == 3 || bc == 5 || bc ==7
A = [A11, A12, A13, A14, A15; A21, A22, A23, A24, A25; A31, A32, ...
    A33, A34, A35; A41, A42, A43, A44, A45; A51, A52, A53, A54, A55];
B = [B11, B12, B13, B14, B15; B21, B22, B23, B24, B25; B31, B32, ...
    B33, B34, B35; B41, B42, B43, B44, B45; B51, B52, B53, B54, B55];
end
elseif induction == 0
if bc == 1
A11 = DD - Ha*Ha*I -Ha*Ha*k2*inv(DD);
A12 = 1i*ky*dzu_short*I;
A22 = DD4 - Ha*Ha*D2;
A23 = -Gr*k2*I;
```

```
A31 = Pr*Gr*I*((1i)/(ky));

A32 = -Pr*Pr*Gr*I*dzto_short;

A33 = Ha*Ha*DD;

B11 = I;

B22 = DD;

B33 = Ha*Ha*Pr*I;

A13 = zeros(N-2) ; A21 = zeros(N-2) ; B12 = zeros(N-2) ; B13 = zeros(N-2);

B21 = zeros(N-2) ; B23 = zeros(N-2) ; B31 = zeros(N-2) ; B32 = zeros(N-2);

A = [A11, A12, A13; A21, A22, A23; A31, A32, A33];

B = [B11, B12, B13; B21, B22, B23; B31, B32, B33];

elseif bc == 2

A11=  DD -u*1i*kx*I - Ha*Ha*D2*inv(DD);

A12 = zeros(N-2);

A13 = zeros(N-2);

A21 = zeros(N-2);

A22 = DD4 - Ha*Ha*D2 - u*1i*kx*DD +  1i*kx*dz2u*I ;

A23 = -Gr*k2*I;

A31 = zeros(N-2);

A32 = -I*dzto - dxto*((1i*kx)/(k2))*D1;

A33 = -1i*u*kx*I + (1/Pr)*DD;

B11 = I;

B22 = DD;

B33 = I;

B12 = zeros(N-2) ; B13 = zeros(N-2) ;  B21 = zeros(N-2);

B23 = zeros(N-2) ;  B31 = zeros(N-2) ; B32 = zeros(N-2);

A = [A11, A12, A13; A21, A22, A23; A31, A32, A33] ;
```

```
B = [B11, B12, B13; B21, B22, B23; B31, B32, B33] ;

elseif bc == 3;

A11 = DDc - Ha*Ha*D2c*inv(DDc);

A12 = 1i*ky*dzu*I;

A13 =  zeros(N);

A21 = zeros(N);

A22 = DD4c - Ha*Ha*D2c;

A23 = -Gr*k2*I;

A23 = A23(2:N-1,2:N-1);

A23 = horzcat(pion,A23,pion);

A23 = vertcat(poz,A23,poz);

A31 = -I*dxto*((1i*ky)/(k2));

A32 = -I*dzto;

A33 = (1/Pr)*DDt;

B11 = I;

B22 = DDc;

B33 = I;

B12 = zeros(N) ; B13 = zeros(N) ; B21 = zeros(N);

B23 = zeros(N) ; B31 = zeros(N) ; B32 = zeros(N);

A = [A11, A12, A13; A21, A22, A23; A31, A32, A33];

B = [B11, B12, B13; B21, B22, B23; B31, B32, B33];

elseif  bc == 4

A00 = Ha*Ha*D2c*inv(DDc) ; A00 = A00(2:N-1,2:N-1);

A00 = horzcat(pion,A00,pion) ; A00 = vertcat(poz,A00,poz) ;

A11 =  DDc -u*1i*kx*I - A00;

A12 = zeros(N);
```

```
A13 =  zeros(N);
A21 = zeros(N);
A22 = DD4c - Ha*Ha*D2c - u*1i*kx*DDc +  1i*kx*dz2u*I ;
A23 = -Gr*k2*I;
A23 = A23(2:N-1,2:N-1);
A23 = horzcat(pion,A23,pion);
A23 = vertcat(poz,A23,poz);
A31 = zeros(N);
A32 = -I*dzto - dxto*((1i*kx)/(k2))*D1;
A33 = -1i*u*kx*I + (1/Pr)*DDt;
B11 = I;
B22 = DDc;
B33 = I;
B12 = zeros(N) ; B13 = zeros(N) ; B21 = zeros(N);
B23 = zeros(N) ; B31 = zeros(N) ; B32 = zeros(N);
A = [A11, A12, A13; A21, A22, A23; A31, A32, A33];
B = [B11, B12, B13; B21, B22, B23; B31, B32, B33];
elseif  bc == 5
A00 = Ha*Ha*D2td*inv(DDtd) ; A00 = A00(2:N-1,2:N-1) ;
A00 = horzcat(pion,A00,pion) ; A00 = vertcat(poz,A00,poz);
A11 = DDc - A00;
A12 = 1i*ky*dzu*I;
A13 =  zeros(N);
A21 = zeros(N);
A22 = DD4c - Ha*Ha*D2c;
A23 = -Gr*k2*I;
```

```
A23 = A23(2:N-1,2:N-1);

A23 = horzcat(pion,A23,pion);

A23 = vertcat(poz,A23,poz);

A31 = -I*dxto*((1i*ky)/(k2));

A32 = -I*dzto;

A33 = (1/Pr)*DDt;

B11 = I;

B22 = DDc;

B33 = I;

B12 = zeros(N) ; B13 = zeros(N) ; B21 = zeros(N);

B23 = zeros(N) ; B31 = zeros(N) ; B32 = zeros(N);

A = [A11, A12, A13; A21, A22, A23; A31, A32, A33];

B = [B11, B12, B13; B21, B22, B23; B31, B32, B33];

elseif  bc == 6

A00 = Ha*Ha*D2td*inv(DDtd) ; A00 = A00(2:N-1,2:N-1);

A00 = horzcat(pion,A00,pion) ; A00 = vertcat(poz,A00,poz);

A11 =  DDc -u*1i*kx*I - A00 ;

A12 = zeros(N) ;

A13 =  zeros(N) ;

A21 = zeros(N);

A22 = DD4c - Ha*Ha*D2c - u*1i*kx*DDc +  1i*kx*dz2u*I ;

A23 = -Gr*k2*I ;

A23 = A23(2:N-1,2:N-1) ;

A23 = horzcat(pion,A23,pion) ;

A23 = vertcat(poz,A23,poz) ;

A31 = zeros(N) ;
```

```
A32 = -I*dzto - dxto*((1i*kx)/(k2))*D1 ;

A33 = -1i*u*kx*I + (1/Pr)*DDt ;

B11 = I;

B22 = DDc;

B33 = I;

B12 = zeros(N) ; B13 = zeros(N) ; B21 = zeros(N);

B23 = zeros(N) ; B31 = zeros(N) ; B32 = zeros(N);

A = [A11, A12, A13; A21, A22, A23; A31, A32, A33];

B = [B11, B12, B13; B21, B22, B23; B31, B32, B33];

elseif  bc == 7

A11 = DDc -  Ha*Ha*I1*D2td*inv(DDtd)*I1 ;

A12 = 1i*ky*dzu*I ;

A13 =  zeros(N) ;

A21 = zeros(N) ;

A22 = DD4c - Ha*Ha*D2c ;

A23 = -Gr*k2*I ;

A31 = -I1*dxto*((1i*ky)/(k2)) ;

A32 = -I1*dzto ;

A33 = (1/Pr)*DDc ;

B11 = I ;

B22 = DDc;

B33 = I1;

B12 = zeros(N) ; B13 = zeros(N) ; B21 = zeros(N);

B23 = zeros(N) ; B31 = zeros(N) ; B32 = zeros(N);

A = [A11, A12, A13; A21, A22, A23; A31, A32, A33];

B = [B11, B12, B13; B21, B22, B23; B31, B32, B33];
```

```
elseif  bc == 8

A00 = Ha*Ha*D2td*inv(DDtd) ; A00 = A00(2:N-1,2:N-1);

A00 = horzcat(pion,A00,pion) ; A00 = vertcat(poz,A00,poz);

A11 =  DDc -u*1i*kx*I - A00 ;

A12 = zeros(N) ;

A13 =  zeros(N) ;

A21 = zeros(N);

A22 = DD4c - Ha*Ha*D2c - u*1i*kx*DDc +  1i*kx*dz2u*I ;

A23 = -Gr*k2*I ;

A31 = zeros(N) ;

A32 = -I1*dzto - dxto*((1i*kx)/(k2))*D1c ;

A32 = A32(2:N-1,2:N-1) ;

A32 = horzcat(pion,A32,pion) ;

A32 = vertcat(poz,A32,poz) ;

A33 = -1i*u*kx*I1 + (1/Pr)*DDc ;

B11 = I;

B22 = DDc;

B33 = I1;

B12 = zeros(N) ; B13 = zeros(N) ; B21 = zeros(N);

B23 = zeros(N) ; B31 = zeros(N) ; B32 = zeros(N);

A = [A11, A12, A13; A21, A22, A23; A31, A32, A33];

B = [B11, B12, B13; B21, B22, B23; B31, B32, B33];

elseif bc == 12

A11=  DD -uov*1i*kx*I - Ha*Ha*D2*inv(DD) ;

A12 = zeros(N-2) ;

A13 = zeros(N-2) ;
```

```
A21 = zeros(N-2) ;
A22 = DD4 - Ha*Ha*D2 - uov*1i*kx*DD +  1i*kx*dz2uov*I ;
A23 = +Gr*1i*kx*D1 ;
A31 = zeros(N-2) ;
A32 = -I*dzTov ;
A33 = -1i*uov*kx*I + (1/Pr)*DD ;
B11 = I ;
B22 = DD ;
B33 = I ;
B12 = zeros(N-2) ; B13 = zeros(N-2) ; B21 = zeros(N-2) ;
B23 = zeros(N-2) ; B31 = zeros(N-2) ; B32 = zeros(N-2) ;
A = [A11, A12, A13; A21, A22, A23; A31, A32, A33];
B = [B11, B12, B13; B21, B22, B23; B31, B32, B33];
elseif bc == 18
A00 = Ha*Ha*D2td*inv(DDtd) ; A00 = A00(2:N-1,2:N-1) ;
A00 = horzcat(pion,A00,pion) ; A00 = vertcat(poz,A00,poz) ;
A11=  DDc -uov*1i*kx*I - A00;
A12 = zeros(N) ;
A13 = zeros(N) ;
A21 = zeros(N) ;
A22 = DD4c - Ha*Ha*D2c - uov*1i*kx*DDc +  1i*kx*dz2uov*I ;
A23 = +Gr*1i*kx*D1c ;
A31 = zeros(N) ;
A32 = -I1*dzTov ;
A33 = -1i*uov*kx*I1 + (1/Pr)*DDc ;
B11 = I ;
```

```
B22 = DDc ;
B33 = I1 ;
B12 = zeros(N) ; B13 = zeros(N) ; B21 = zeros(N) ;
B23 = zeros(N) ; B31 = zeros(N) ; B32 = zeros(N);
A = [A11, A12, A13; A21, A22, A23; A31, A32, A33];
B = [B11, B12, B13; B21, B22, B23; B31, B32, B33];
end
end
[V,Lam] = eig(A,B) ;
re = real(diag(Lam)) ; im = imag(diag(Lam)) ; [mgr,ind] = max(re);
ee = diag(Lam) ; [ereal,is] = sort(-real(ee)) ;
es = ee(is) ; esmax = es(1) ;
freq1 = imag(esmax) ; freq1 = abs(freq1) ;
if freq1 == Inf
    freq = 10000000000;
else
    freq = freq1;
end
ev1 = max(re);
if ev1 == Inf
    ev = 100000000000;
else
    ev = ev1;
end
```